Alma Mater Studiorum – Università di Bologna
in cotutela con
Università Claude Bernard Lyon1

DOTTORATO DI RICERCA IN

CHIMICA

Ciclo XXVI

Settore Concorsuale di afferenza: **03/C2**

Settore Scientifico disciplinare: **CHIM/04**

A chemical-loop approach for the generation of hydrogen by means of ethanol reforming

Presentata da: **Cristian Trevisanut**

Coordinatore Dottorato   Relatore

Chiar.mo Prof. Aldo Roda   **Prof. Fabrizio Cavani**

                                                                      Relatore

                                                        Dr. Jean-Marc M. Millet

Esame finale anno 2014

Hydrogen production

Steam iron process

Thermochemical cycles

Ethanol reforming

Ferrite mixed oxide

Mössbauer spectroscopy

DRIFT-MS

ABSTRACT

Pollution and global warming, linked to the increasing of the world's population and, therefore the energy demand, had in the last decades highlighted the necessity of finding new sources of renewable energies. However it will be also important to find a new way to carry the energy and hydrogen is one of the most eco-efficient solutions. Devices, like fuel cells, allow to obtain electricity from the hydrogen without the production of pollutant, however they requires high purity of hydrogen in order to maintain a good lifetime. The work investigates the feasibility of a new process aimed at the production of hydrogen with inherent separation of carbon oxides. The process consists in a cycle in which, in the first step, a mixed metal oxide is reduced by ethanol (obtained from biomasses). The reduced metal is then contacted with steam in order to split the water and sequestrating the oxygen into the looping material's structure. The oxides used to run this thermochemical cycle, also called "steam-iron process" are mixed ferrites in the spinel structure $MeFe_2O_4$ (Me = Fe, Co, Ni or Cu).

To understand the reactions involved in the anaerobic reforming of ethanol, diffuse reflectance spectroscopy (DRIFTS) was used, coupled with the mass analysis of the effluent, to study the surface composition of the ferrites during the adsorption of ethanol and its transformations during the temperature program. This study was paired with the tests on a laboratory scale plant and the characterization through various techniques such as XRD, Mössbauer spectroscopy, elemental analysis... on the materials as synthesized and at different reduction degrees

In the first step it was found that besides the generation of the expected CO, CO_2 and H_2O, the products of ethanol anaerobic oxidation, also a large amount of H_2 and coke were produced. The latter is highly undesired, since it affects the second step, during which water is fed over the pre-reduced spinel at high temperature. The behavior of the different spinels was affected by the nature of the divalent metal cation; magnetite was the oxide showing the slower rate of reduction by ethanol, but on the other hand it was that one which could perform the entire cycle of the process more efficiently. Still the problem of coke formation remains the greater challenge to solve.

The thesis has been carried out in co-tutelle between the "ALMA MATER STUDIORUM" University of Bologna and the University "Claude Bernard" Lyon 1 and it was part of the Enerbio project, financed by the Tuck Foundation.

SUMMARY

1. INTRODUCTION

Environmental problems such as climate change and pollution have become more and more important over the past few years. It is well known and scientifically demonstrated that they are mainly caused by the high consumption of energy of humanity life-style. Energy production is one of the main problems for climate change because of both the massive utilization of fossil-fuels derived raw materials, that implies both high CO2 emissions (CO_2 is considered as the main greenhouse gas responsible for the global warming effect) and the use of these sources in low-efficiency systems (i.e., in internal combustion engines typically used for transportation and in stationary systems for power production). These problems, together with the continuous increase of energy demand, has pushed the human being to search for new approaches in order to satisfy the world energy demand. Many solutions have been proposed both from the scientific community and from the policy world, but the main problem for the application of these solutions still is the cost associated to the implementation of new technologies. The solutions proposed by the scientific community can be divided into different categories:

- Reduction of energy consumption by means of decrease of energy dissipation during production and usage (i.e., decrease the heat loss in buildings by incrementing thermal insulation)

- Reduction of the greenhouse gases emissions by decreasing the usage of carbon-containing fossil fuels

- Utilization of renewable energy sources and of new technologies dedicated to this new type of sources

The utilization of renewable energy sources and the development of new technologies for using these new resources are now the subject of intense investigation. In the long-term range perspective, the total amount of energy that can be obtained from renewable sources is unlimited (as also the name suggests), which may finally offer the opportunity to abandon the production of energy from fossil fuels.

However, together with the use of renewable sources, it is also important to find more efficient energy carriers. Amongst them, one of the most interesting is hydrogen. Nowadays, hydrogen is obtained predominantly by steam reforming of methane, but it is well known that hydrocarbon-based routes result in environmental problems; moreover, the energy supply is dependent on the availability of these limited resources, which are suffering from rapid depletion. Therefore, alternative processes using renewable sources like wind, solar energy and biomasses, are now being considered for the production of hydrogen.

One of these alternative technologies is derived from the so-called "steam-iron" process, which consists in the reduction of a metal-oxide by a feedstock (methane, syngas, CO, or alcohols, as in the case of the present work) followed by the re-oxidation of the reduced material with steam to produce "clean hydrogen" (the overall process is also sometimes called "water splitting", but more precisely it should be referred as water reduction, since O_2 is not produced during the process). Indeed, the overall process is a reforming of the reducing fuel, which however is split into two separate steps. This kind of thermochemical cycles (also referred as "chemical-loop" technologies) have been studied since long time, but in more recent years some important advancements, such as the development of more active materials as oxygen/electrons carriers, combined with the high potential of the chemical-loop reforming, derived from both the flexibility of the feedstock (including renewable bio-alcohols) and the fact that the purification of hydrogen could in principle be avoided, have significantly increased the interest for this research topic.

1.1. HYDROGEN

Despite hydrogen is one of the most common elements in Earth's crust, it is not significantly present in elemental form. It is mostly present in water, biomass, and fossil hydrocarbons. Hydrogen gas is a versatile energy carrier that is currently produced from a variety of primary sources such as natural gas, naphtha, heavy oil, methanol, biomass, wastes, coal, solar, wind, and nuclear. It is a clean energy carrier because the chemical energy stored in the H-H bond is released when it combines with oxygen, yielding only water as the reaction product. Hydrogen is considered as a nonpolluting, inexhaustible, efficient, and cost-attractive energy carrier for the future [1]. Accordingly, a future energy infrastructure based on hydrogen has been perceived as an ideal long-term solution to energy related environmental problems [2]. In fact, it is generally understood that the renewable energy-based processes of hydrogen production (solar photochemical and photo-biological water decomposition, electrolysis of water coupled with photovoltaic cells or wind turbines, etc.) would be unlikely to yield significant reductions in hydrogen costs in the next few years.

Each year, 48 million metric tons of hydrogen are globally generated from fossil fuels and half of this hydrogen goes into ammonia production, while the second largest amount of hydrogen is used for chemical processes such as removing sulfur from gasoline (hydrodesulphurization) and converting heavy hydrocarbons into gasoline or diesel fuel. The demand for hydrogen in the next decade, both for traditional uses, such as ammonia synthesis, and for running fuel cells, is expected to grow [3]. In fact, many car manufacturers already have produced prototype vehicles powered by hydrogen fuel cells. At least in the near future, this thirst for hydrogen will be quenched primarily using fossil fuels.

1.2. FUEL CELLS

Fuel Cells are devices aimed at the production of energy from hydrogen (or other fuels, such as natural gas, methanol, gasoline, etc.) oxidation. A fuel cells convert the chemical energy of a fuel and an oxidant (air or oxygen) into electricity. In principle, a fuel cell operates like a battery, but does not require recharging, because it will produce electricity and heat as long as the fuel and the oxidant are supplied.

1.2.1. Basic operating of Fuel Cells

In a typical fuel cell, the fuel is fed continuously to the anode (negative electrode), whereas the oxidant is fed continuously to the cathode (positive electrode). The electrochemical reactions take place at the electrodes to produce an electric current flowing through the electrolyte, while driving a complementary electric current that performs work on the load. Fuel cells are classified according to the choice of electrolyte and fuel, which in turn determine the electrode reactions and the type of ions that carry the current across the electrolyte. Though the direct use of conventional fuels in fuel cells would be desirable, most fuel cells under development today use either gaseous hydrogen, or a synthesis gas rich in hydrogen, as the fuel. Hydrogen shows a high reactivity for anode reactions, and can be produced chemically from a wide range of fossil and renewable fuels, as well as via electrolysis [4].

1.2.2. Fuel Cells types

Fuel cells are classified according to the type of electrolyte used. Today the most used fuel cells are:

- polymer electrolyte fuel cells (PEFC),
- alkaline fuel cells (AFC),
- phosphoric acid fuel cells (PAFC),

- molten carbonate fuel cells (MCFC)
- solid oxide fuel cells (SOFC)

Each one of these fuel cells types is used at specific operative conditions, due to the different chemical and physical properties of the electrolyte.

Table 1-1 summarizes the main characteristics of the various types of fuel cells.

Table 1-1. Summary of main characteristics of the different fuel cells [4]

	PEFC	AFC	PAFC	MCFC	SOFC
Electrolyte	Hydrated Polymeric Ion Exchange Membranes	Mobilized or Immobilized Potassium Hydroxide in asbestos matrix	Immobilized Liquid Phosphoric Acid in SiC	Immobilized Liquid Molten Carbonate in $LiAlO_2$	Perovskites (Ceramics)
Electrodes	Carbon	Transition metals	Carbon	Nickel and Nickel Oxide	Perovskite and perovskite / metal cermet
Catalyst	Platinum	Platinum	Platinum	Electrode material	Electrode material
Interconnect	Carbon or metal	Metal	Graphite	Stainless steel or Nickel	Nickel, ceramic, or steel
Operating Temperature	40 – 80 °C	65°C – 220 °C	205 °C	650 °C	600-1000 °C
Charge Carrier	H^+	OH^-	H^+	$CO3^=$	$O^=$
External Reformer for hydrocarbon fuels	Yes	Yes	Yes	No, for some fuels	No, for some fuels and cell designs
External shift conversion of CO to hydrogen	Yes, plus purification to remove trace CO	Yes, plus purification to remove CO and CO_2	Yes	No	No
Prime Cell Components	Carbon-based	Carbon-based	Graphite-based	Stainless-based	Ceramic
Product Water Management	Evaporative	Evaporative	Evaporative	Gaseous Product	Gaseous Product
Product Heat Management	Process Gas + Liquid Cooling Medium	Process Gas + Electrolyte Circulation	Process Gas + Liquid cooling medium or steam generation	Internal Reforming + Process Gas	Internal Reforming + Process Gas

Sometimes fuel cells are classified by the type of fuel used:

- Direct Alcohol Fuel Cells (DAFC). DAFC (or, more commonly, direct methanol fuel cells or DMFC) use alcohol without reforming. Mostly, this refers to a PEFC-type fuel cell in which methanol or another alcohol is used directly, mainly for portable applications.

- Direct Carbon Fuel Cells (DCFC). In direct carbon fuel cells, solid carbon is used in the anode, without an intermediate gasification step. Concepts with solid oxide, molten carbonate, and alkaline electrolytes are all under development. The advantage of this kind of fuel cells is that thermodynamics of the reactions allow very high efficiency conversion. Therefore, if the technology can be developed into practical systems, it could ultimately have a significant impact on coal-based power generation.

Nowadays, amongst the various types of fuel cell, most promising and used are the Polymer Electrolyte Membrane Fuel Cells (PEM-FC) and the Solid Oxides Fuel Cells (SOFC). The latter have the advantage of working with various types of stream and are very resistant to pollutants in the fuel. However, their main drawback is the high temperatures and the long time required in order to be operative, which limit their use. PEMs have the advantage of working at temperatures below 100°C, however their main drawback is that they require very high-purity hydrogen because of the poisoning effect of CO on the Pt electrode. For this reason water splitting through thermochemical cycle could be an important perspective for carbon-free hydrogen production.

1.3. H₂ PRODUCTION- STEAM REFORMING OF METHANE

At the industrial level, more than half of the hydrogen manufactured derives from Steam Reforming, where the hydrocarbons are split with steam:

$$C_nH_m + nH_2O \rightarrow nCO + (n + m/2)H_2$$
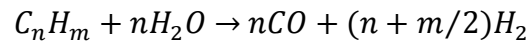
$$for\ n = 1: \Delta H^0_{298K} = +206.2\ kJ/mol$$

In processes aimed at H₂ production, Steam Reforming is followed by Water Gas Shift (WGS):

$$CO + H_2O \rightarrow CO_2 + H_2$$
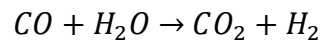
$$\Delta H^0_{298K} = -41.2\ kJ/mol$$

The optimal alkane for this reaction is methane, because it holds the greatest H/C ratio (H/C=4); in fact, the 48% of the globally produced hydrogen derives from Steam Methane Reforming (SMR). However methane is not a reactive molecule; in fact, the energy of the C-H bond is very high (439 kJ/mol) due to the sp^3 hybridization of the carbon. The process takes place in the range of temperatures of 430 − 1000°C and using a steam partial pressure of 30 bars; therefore, the catalyst has to be both active and very resistant under those conditions. The most used catalysts are based on metallic Ni; these systems are characterized by a turnover frequency (TOF) of ca. 0.5 s⁻¹ at 450°C, with a methane conversion around 10%. Thermodynamics of the process indicates that higher conversions can be obtained only at temperatures above 900°C, at which however the heat transfer coefficient of the reaction tube becomes the rate-limiting parameter [5]. One of the major problems of this reaction consists in the formation of thermodynamically favored reduced species, such as carbon - in the form of fibers and filaments -, holding a small nickel particle at their top [6]. This may lead to the breakdown of the catalyst, together with carbon deposits leading to catalysts chemical deactivation. In order to limit side reactions, water vapor is co-fed in excess. This is useful also for the second step of the process: the WGS reaction, in which CO is oxidized by steam to CO₂. The WGS reaction is moderately

exothermic (ΔH=-41.1 kJ/mol), and hence its equilibrium decreases with an increase of temperature, and high conversions are favored in the low temperatures range. Feeding water in quantities greater than the stoichiometric amount leads to an improvement of conversion; however as the reaction proceeds, the heat of the exothermal reaction increases the operating temperature, leading to a restriction of the possible conversion. In order to completely convert all the CO, two steps are typically needed: a high-temperature shift (HT), and a low-temperature shift (LT). In the HT shift, temperature is in the range 370-400°C, and catalysts used are based on chromia-supported iron. This step is thermodynamically limited, and a maximum CO conversion of 96-98% is reached. A significant improvement in the conversion of CO is then obtained in the second bed operating at the lowest temperature possible, which is dictated by the dew-point (about 200°C). The most used catalysts for this step are copper-based, with which a 99.9% CO conversion can be achieved [7].

A novel technology for the production of hydrogen from natural gas recently developed is based on a membrane reactor (MR), which promises economically sustainable small-scale hydrogen production combined with inexpensive CO_2 separation [8]. This could avoid a dedicated hydrogen infrastructure, facilitate CO_2 capture at the small scale, and thus, possibly, contribute to a more rapid decrease of greenhouse gases emissions.

1.3.1. Steam reforming of biomasses

Amongst the various sources of "renewable energy", biomass provides the largest contribution to the worldwide energy supply today. The term "biomass" indicates biological materials from living or recently living organisms that are yet not fossilized, such as wood, wastes algae and others. Biomasses are considered a renewable source of energy because the organism adsorbs the carbon dioxide generated by their combustion, thus without burdening the C cycle with additional CO_2 and theoretically providing a neutral C balance. Fuels can be produced from biomasses via either thermochemical or biological processes. Main biofuels are bioethanol, biomethanol, biodiesel, bioglycerol and biogas. Among the biochemical transformation of biomasses into fuels, the most

abundant is bioethanol [9]. The production of hydrogen from ethanol has some other advantages, such as: (1) a low toxicity of this alcohol (compared, for instance, with methanol); (2) a moderate production cost; (3) the fact that it is a relatively clean fuel in terms of composition; (4) a relatively high hydrogen content (H/C ratio=3); and (5) a large availability and ease of handling. Hydrogen can be obtained directly from ethanol by two main processes: steam reforming or partial oxidation.

1.3.1.1.Reforming of ethanol

The stoichiometry of ethanol steam reforming is the following:

$$CH_3OH + 3H_2O \rightarrow 6H_2 + 2CO_2$$
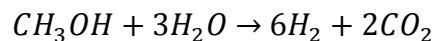
$$\Delta H^0_{298K} = +173.7\,kJ/mol$$

The process occurs in the presence of a catalyst at 550-800°C (almost the same temperature as for steam methane reforming). At these temperatures, several undesired reactions can take place (dehydration, decomposition, dehydrogenation, coking) [10]; therefore the choice of the catalyst plays a vital role in the reforming process. No industrial-scale steam ethanol reforming technologies are nowadays been used, but nevertheless this reaction is of great scientific interest. According to the literature, different metal oxide catalysts [11], metal catalysts (Ni, Co, Ni/Cu) [11–13], and noble metal catalysts (Pt, Pd, Rh) are active in ethanol reforming [14, 15].

1.4. CATALYTIC PARTIAL OXIDATION (CPO)

Differently from the steam ethanol reforming, catalytic partial oxidation can be autothermal, eliminating the need for an external heat supply. The stoichiometry of the reaction is:

$$CH_3CH_2OH + 1.5O_2 \rightarrow 3H_2 + 2CO_2$$
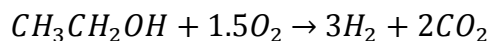
$$\Delta H^0_{298K} = -551.8 \, kJ/mol$$

Moreover, ethanol partial oxidation is much faster than catalytic steam reforming, which allows fast start-up and short response times to variation in H_2 production. The only disadvantage is that if bioethanol is used instead of ethanol, its separation from the ethanol-water mixture is expensive. Because of that, partial oxidation is usually combined with steam reforming, again leading to an autothermal process as shown in the equation if the contribution of the two reactions (the endothermal reforming and the exothermal oxidation) is properly tuned:

$$C_2H_5OH + 2H_2O + {}^1\!/_2\,O_2 \rightarrow 2CO_2 + 5H_2$$
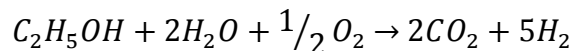
$$\Delta H^0_{298K} = -68.2 kJ/mol$$

This process has been performed at temperatures of 450-750°C using catalytic systems based on noble metals (Rh, Ru, Pd, Pt) supported on redox systems like CeO_2 and Al_2O_3 [17].

1.5. HYDROGEN FROM WATER

One of the older processes aimed at hydrogen production is water electrolysis, carried out by Nicholson and Ritter in 1800. It consists in the decomposition of water into molecular oxygen and hydrogen by means of a current passed through water. Nowadays there are two main techniques used to carry out hydrolysis: 1) high pressure electrolysis and 2) high-temperature electrolysis. However, these techniques require large amount of energy and are uncompetitive if compared with production from coal or natural gas. Even when the energy used to produce hydrogen by electrolysis comes from wind or solar power, the electricity consumed is more valuable than the hydrogen produced, so these methods are not widely used nowadays.

Another technology investigated is the thermal decomposition of water. Without a catalyst, temperatures as high as 3000°C are needed to convert 50% of the water fed into molecular hydrogen and oxygen. There are some prototypes now on stream which use either nuclear energy (Generation IV reactors) or solar energy [18].

The technologies expected to be the most efficient for large-scale hydrogen production are based on thermochemical cycles.

1.5.1. Thermochemical Cycles

A variety of materials easily react with water or acids to release molecular hydrogen. On the other hand, in order to make the process continuous, a material is needed which after reaction with water (which being a redox process has led to the oxidation of the material and the concomitant reduction of water) can be reduced back in an economically affordable way. Therefore, using a two-step cycle, these materials can be used as electrons/O^{2-} vectors for the production of pure H_2.

Thermochemical cycles were first investigated around 1970 during the first oil crisis; however, the so-called steam-iron process (which is a thermochemical cycle where a reductant is used) was already investigated and even used industrially at the beginning of

the 20th century. After the 70's, the oil price started to decrease, but nowadays with the increasing of oil price and the need to adhere the Kyoto Protocol, a new interest for thermochemical cycles has grown. The main advantages of thermochemical cycles are: 1) the possibility to obtain hydrogen separated from the product accompanying the material reduction (either O_2, in a purely thermal cycle, or CO_x in chemical cycle with a fuel as the reductant), so simplifying the process and avoiding expensive separation units; and 2) the possibility to reach relatively high efficiencies, up to 50% or more. However, since no industrial plant has yet been constructed, these efficiency values are based on small-scale tests. Most important thermochemical cycles are illustrated in Table 1-2:

Table 1-2. Thermochemical cycles currently under investigation

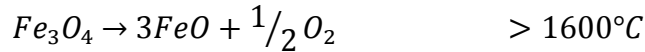| Cycle	Steps	Maximum Temperature (°C)	LHV Efficiency (%)
Sulfur cycles			
Hybrid Sulfur (Westinghouse, ISPRA Mark 11)	2	900 (1150 without catalyst)	43
Sulfur-iodine (General Atomics, ISPRA Mark 16)	3	900 (1150 without catalyst)	38
Volatile metal oxide cycles			
Zinc/zinc oxide	2	1800	45
Hybrid cadmium		1600	42
Non-volatile metal oxide cycles			
Iron oxide	2	2200	42
Cerium oxide	2	2000	68
Ferrites	2	1100-1800	43
Low-temperature cycles			
Hybrid copper chloride	4	530	39

1.5.2. The Steam-Iron process

Amongst the various materials used for thermochemical cycles, those more extensively studied are based on pure and mixed iron oxides, because of their availability, low toxicity and low cost. Cycles based on iron oxides are also known as Steam-Iron processes. This term is derived from the reaction of hot metallic iron with steam, a process already used
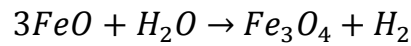
for the production of hydrogen fuel for aerostats before and during the 2nd World War [19-22].

The first complete cycle was studied by Nakamura in 1977 [23], who used magnetite (Fe_3O_4) as the oxide, first reduced thermally to wustite (FeO) and then re-oxidized with steam. Reactions involved are:

$$Fe_3O_4 \rightarrow 3FeO + \frac{1}{2}O_2 \qquad\qquad > 1600°C$$

$$\Delta H^0_{298K} = +319.5 \; kJ/mol$$

$$3FeO + H_2O \rightarrow Fe_3O_4 + H_2$$

$$\Delta H^0_{298K} = -33.6 \; kJ/mol$$

Nowadays studies are focused on reducing the temperature needed for the first step, and in using solar as the heat source.

A lowering of the temperature needed for metal oxide self-reduction can be achieved through the partial replacement of iron in Fe_3O_4 by other metals, such as Mn, Ni or Co, forming mixed metal oxides ($Fe_{1-x}M_x)_3O_4$. These mixed oxides, called ferrites, can be reduced at lower temperatures than pure Fe_3O_4, and once reduced they are capable of reducing water in the same way as FeO does.

1.5.2.1. Steam-iron process: Modified materials

Magnetite is a ferromagnetic mineral with chemical formula Fe_3O_4 that belongs to the *spinel* group whose general formula is $A^{2+}B_2^{3+}O_4^{2-}$. To be more precise, this compound presents the inverse spinel structure in which the Fe^{2+} occupies octahedral sites and the Fe^{3+} occupies both octahedral and tetrahedral sites (Figure 1-1 shows the structure of the spinel (adapted from [24]). Spinel belong to the space group $Fd3m$ and to the O_h^7 point group. The lattice is cubic, and the positions of the oxygen atoms are more or less fixed,

but the arrangement of the cations may vary considerably, although within certain limits [25].
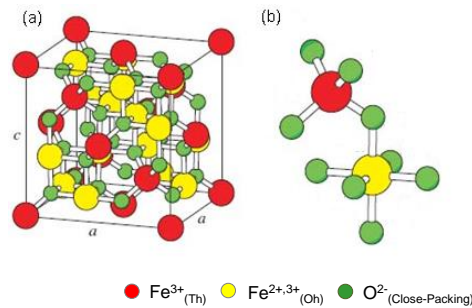
Figure 1-1. (a) Face-centered cubic spinel structure of magnetite. (b) Magnification of one tetrahedron and one adjacent octahedron sharing an oxygen atom.

1.5.2.2. Mixed-Ferrite cycles

The concept behind the steam iron cycle is to first reduce the magnetite (Fe_3O_4) to wurstite (FeO); however, this reaction takes place without reductant only at temperatures higher than 1600°C. Nevertheless, as mentioned above, if the composition is modified with other transition metals like Cu, Ni, Co, Zn, and Mn, this could help to decrease the temperature needed for this first step. These materials, holding the same structure and similar composition as magnetite, are known as *ferrites*. In most cases, the modified materials show a lower reduction temperature than magnetite; on the other hand, the re-oxidation step is more difficult than with FeO.

Figure 1-2 shows that the free energy of the oxidation and reduction of Co_3O_4, Mn_3O_4 and Fe_3O_4 are quite different [26]. In this case, Co_3O_4 is the material showing the lowest temperature for thermal reduction, but presents thermodynamic limitations for the re-oxidation step with water. The opposite is true for the Fe_3O_4. It can be inferred that in the case of mixed ferrites, the redox properties of materials are strictly related to their chemical composition.
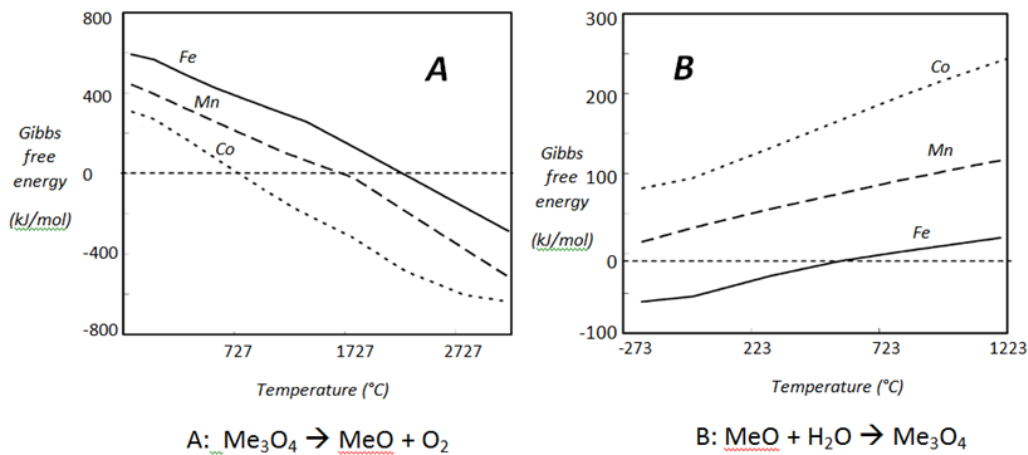
Figure 1-2. Gibbs free energy of the two reactions of the chemical loop for Co, Mn and Fe spinel-type oxides: (a) thermal reduction (b) water re-oxidation.

In the literature there are some reports about modified ferrites that present promising features for their use in chemical-loop reactions. For example, Fresno et al. [27], studied commercially available mixed oxides ($NiFe_2O_4$, $Ni_{0.5}Zn_{0.5}Fe_2O_4$, $ZnFe_2O_4$, $Cu_{0.5}Zn_{0.5}Fe_2O_4$ and $CuFe_2O_4$) by carrying out the reduction step at 1723°C; $NiFe_2O_4$ showed the lowest temperature for the thermal reduction and the highest net hydrogen production in the oxidation step [27].

Kodama et al. [28] studied the reactivity of $CoFe_2O_4/ZrO_2$ and $MnFe_2O_4/ZrO_2$. The authors performed the thermochemical cycle in an inert atmosphere, at temperatures starting from 1400°C for the reduction step, and around 1000°C for the oxidation with water. They concluded that the Co-ferrite displayed higher reactivity than the Mn-ferrite [28]. In a related paper, the performance of the Ni-ferrite was investigated under the same conditions; it was concluded that the $NiFe_2O_4/ZrO_2$ is a very promising material because its performance could be reproduced during repeated cycles with even a better performance than that obtained with $CoFe_2O_4/ZrO_2$ [29].

16

1.5.3. Thermochemical cycles using a reducing fuel

In order to further reduce the temperature of reduction of the materials, various reducing agents have been taken into consideration (Figure 1-3).
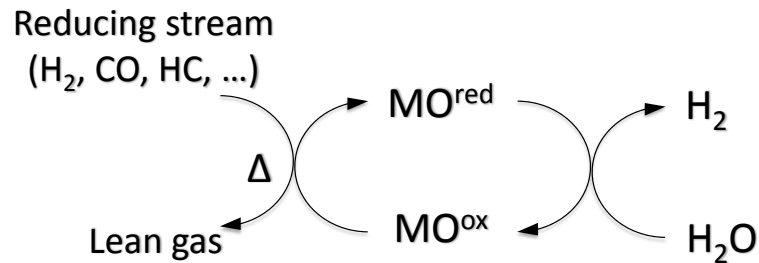
Figure 1-3. Scheme of a thermochemical cycle using a reducing fuel

Syngas produced from different sources, can be used as reducing component. Syngas can be obtained from either coal [30], biomasses [31-34], light hydrocarbons reforming [30, 31], or from pyrolysis oil gasification [37-39]. Reactions involved are:

$$MO + CO/H_2 \rightarrow M + CO_2/H_2O$$

$$M + H_2O \rightarrow MO + H_2$$
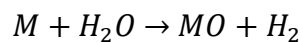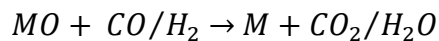
Another possible reducing fuel is methane, which use has been studied and patented by ENI company in 2004 [40]. In the process hematite is reduced to wustite with methane in a first step; in the second step, FeO is reacted with water to produce hydrogen and magnetite. Finally, in a third step air is used to further oxidize magnetite back to its starting state.

1.5.3.1.Steam-iron process: reducing fuels

The high temperatures needed for the thermal reduction are mainly due to both thermodynamic and kinetic reasons. These drawbacks can be overcome by means of a reducing agent. Amongst the various options available for the reducing compounds, the most commonly used are:

Hydrogen: The use of hydrogen in the first step is aimed at its chemical storage; the hydrogen "stored" in the reduced material can be later released in when needed. For example, the reduced material (metallic iron for instance) can be loaded in a car and then water is added to finally produce hydrogen. The practical limitation for this approach is the amount of hydrogen that can be stored (less than 4.8%) [41].

Methane: The redox cycle based on methane is as follows:

$$Me_xO_y + CH_4 \rightarrow Me_xO_{y-1} + CO + 2H_2 \ (or \ non-soichiometric, CO_2 + H_2O)$$

$$Me_xO_{y-1} + H_2O \rightarrow Me_xO_y + H_2$$
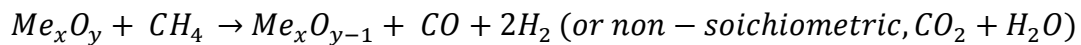
This particular process is attractive since is an alternative to the classical SMR+WGS+PSA process used for the production of high purity hydrogen [42]. Besides, as mentioned before, methane is nowadays an easily available feedstock. The drawback is that it is still hydrocarbon-bas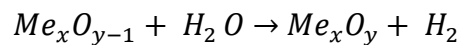ed. Other studies use syngas as the reducing stream, derived from the reforming of light hydrocarbons; this approach is similar to that one from methane because the real reducing agents are CO and H_2 obtained from methane transformation [43].

Pyrolysis oil: The use of pyrolysis oil facilitates transportation and simplifies gasification and combustion processes of the feedstock before being processed to hydrogen, as described by Bleeker et al [39]. The same authors mentioned the fact that coke deposition

on the catalyst could be a drawback, but they suggested that C could also be used as a reducing material.

Biomass gasification gas: The gasification of biomass yields the so-called biosyngas that contains various amounts of CO and H_2 depending on the applied process, oxidation medium, temperature etc, as reported by Wiebren et al [44]. On the other hand, low-temperature (<1000°C) gasification processes yield a product gas that contains significant amounts of hydrocarbons. In most cases, the biomass-derived gas produced is purified in a tar extractor and then used in the steam-iron process. There is the possibility of integrating the gasification and hydrogen production with a fuel cell, as described in [45].

BioAlcohols: Bioethanol is produced by fermentation of biomass materials. When oxygen is insufficient for normal cellular respiration, anaerobic respiration takes place by yeasts, converting glucose into ethanol and carbon dioxide. The exploitation of bioethanol and biomethanol to produce hydrogen by autothermal or steam reforming is currently an active research field [46]. The technology to produce these bioalcohols, especially ethanol, from biomass is already accessible, but it is still developing very fast; therefore, in the near future the availability of this feedstock will be even higher. The advantages of using bioethanol as feedstock include its low toxicity, ease of deliverability and its potential for production from many different sources, ranging from cellulosic biomass to algae [47]. For these reasons, in the present research work ethanol was chosen as the probe molecule.

1.6.   AIM OF THE THESIS

The work presented here is focused on the study of the feasibility of the chemical-loop reforming of ethanol, and on the understanding of the behavior of the ferrites used as looping materials (Figure 1-4).

Where X = Fe, Co, Ni, Cu
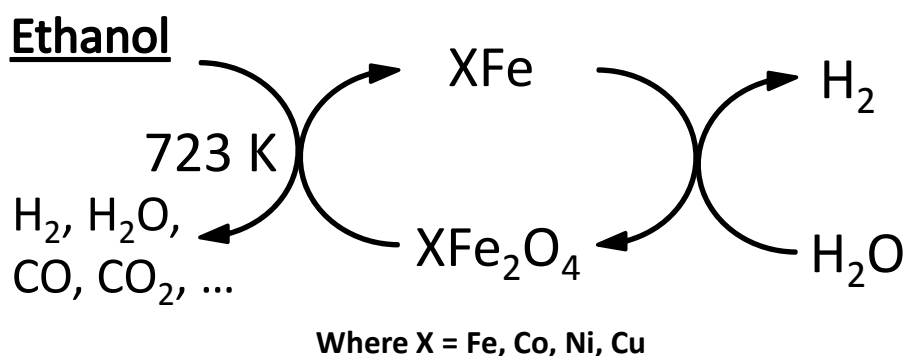
Figure 1-4. Steam-Iron process using ethanol as reducing fuel

Ethanol was chosen as the reducing agent in the cycle process for several reasons:

- The use of Bioalcohols in cycle reforming has not yet been much studied in literature;

- Ethanol can be obtained from biomasses, that might contribute to unlink the production of hydrogen from fossil fuels;

- Ethanol is a non-toxic liquid, easy to transport and handle, relatively stable at room temperature.

The aim of the work was two-fold: (a) search for materials and conditions that may allow to carry out the cycle reforming of ethanol with good yields and selectivity, and during several cycles, and (b) understand how the chemical-physical features of the materials used are modified in the course of the two steps of the chemical loop.

In the laboratory of the Dipartimento di Chimica Industriale "Toso Montanari" of Bologna University the study was focused mainly on the reactivity, while in the laboratory of the Institut de Recherches sur la Catalyse et l'Environnement de Lyon (IRCELYON – CNRS) the

research has been completed with the characterization experiments and the synthesis of materials.

References

[1]   R. M. Navarro, M. A. Peña, and J. L. G. Fierro, "Hydrogen production reactions from carbon feedstocks: fossil fuels and biomass.," *Chem. Rev.*, vol. 107, no. 10, pp. 3952–91, Oct. 2007.

[2]   J. Bockris, "The origin of ideas on a Hydrogen Economy and its solution to the decay of the environment," *Int. J. Hydrogen Energy*, vol. 27, no. 7–8, pp. 731–740, Aug. 2002.

[3]   P. Beckhaus, A. Heinzel, J. Mathiak, and J. Roes, "Dynamics of H2 production by steam reforming," *J. Power Sources*, vol. 127, no. 1–2, pp. 294–299, Mar. 2004.

[4]   Inc. EG&G Technical Services, *Fuel Cell Handbook*, 7th ed. EG&G Technical Services, Inc., 2004.

[5]   J. R. Rostrup-Nielsen, "Catalytic Steam Reforming," *Catal. Sci. Technol.*, vol. 5, pp. 1–117, 1984.

[6]   J. R. Rostrup-Nielsen, "Industrial catalysis, the science and the challenge," *Catal. Today*, vol. 18, no. 2, pp. 125–145, Nov. 1993.

[7]   M. V. Twigg, *Catalyst handbook*. 1989.

[8]   M. SJARDIN, K. DAMEN, and A. FAAIJ, "Techno-economic prospects of small-scale membrane reactors in a future hydrogen-fuelled transportation sector," *Energy*, vol. 31, no. 14, pp. 2523–2555, Nov. 2006.

[9]   J. J. Bozell and G. R. Petersen, "Technology development for the production of biobased products from biorefinery carbohydrates—the US Department of Energy's 'Top 10' revisited," *Green Chem.*, vol. 12, no. 4, p. 539, Apr. 2010.

[10]   F. Frusteri, S. Freni, L. Spadaro, V. Chiodo, G. Bonura, S. Donato, and S. Cavallaro, "H2 production for MC fuel cell by steam reforming of ethanol over MgO supported Pd, Rh, Ni and Co catalysts," *Catal. Commun.*, vol. 5, no. 10, pp. 611–615, Oct. 2004.

[11]   J. Llorca, P. R. de la Piscina, J. Sales, and N. Homs, "Direct production of hydrogen from ethanolic aqueous solutions over oxide catalysts," *Chem. Commun.*, no. 7, pp. 641–642, Jan. 2001.

[12]   A. N. Fatsikostas, D. I. Kondarides, and X. E. Verykios, "Steam reforming of biomass-derived ethanol for the production of hydrogen for fuel cell applications," *Chem. Commun.*, no. 9, pp. 851–852, Jan. 2001.

[13]   V. A. Zazhigalov, J. Haber, J. Stoch, A. I. Kharlamov, A. Marino, L. Depero, and I. V. Bacherikova, *12th International Congress on Catalysis, Proceedings of the 12th ICC*, vol. 130. Elsevier, 2000, pp. 1805–1810.

[14]   J. Llorca, "Efficient Production of Hydrogen over Supported Cobalt Catalysts from Ethanol Steam Reforming," *J. Catal.*, vol. 209, no. 2, pp. 306–317, Jul. 2002.

[15]   J. . Breen, R. Burch, and H. . Coleman, "Metal-catalysed steam reforming of ethanol in the production of hydrogen for fuel cell applications," *Appl. Catal. B Environ.*, vol. 39, no. 1, pp. 65–74, Nov. 2002.

[16]   D. K. Liguras, D. I. Kondarides, and X. E. Verykios, "Production of hydrogen for fuel cells by steam reforming of ethanol over supported noble metal catalysts," *Appl. Catal. B Environ.*, vol. 43, no. 4, pp. 345–354, Jul. 2003.

[17]   J. SALGE, G. DELUGA, and L. SCHMIDT, "Catalytic partial oxidation of ethanol over noble metal catalysts," *J. Catal.*, vol. 235, no. 1, pp. 69–78, Oct. 2005.

[18]   D. Bürkle and M. Roeb, "DLR scientists achieve solar hydrogen production in a 100-kilowatt pilot plant," *Deutsches Zentrum für Luft- und Raumfahrt*, German Aerospace Center DLR - Deutsches Zentrum fuer Luft- und Raumfahrt, 2008.

[19]   S. Hurst, "Production of hydrogen by the steam-iron method," *Oil Soap*, vol. 16, no. 2, pp. 29–35, Feb. 1939.

[20]   "Reducing and oxidizing apparatus for generating hydrogen from iron ore and steam." 23-Feb-1915.

[21]   "Producing hydrogen by contact of steam with iron oxide promoted with zinc ferrite." 15-Aug-1972.

[22]   "Production of hydrogen via the steam-iron process utilizing dual solids recycle." 06-May-1969.

[23]   T. Nakamura, "Hydrogen production from water utilizing solar heat at high temperatures," *Sol. Energy*, vol. 19, no. 5, pp. 467–475, Jan. 1977.

[24]   M. Friák, A. Schindlmayr, and M. Scheffler, "Ab initio study of the half-metal to metal transition in strained magnetite," *New J. Phys.*, vol. 9, no. 1, pp. 5–5, Jan. 2007.

[25]   E. J. W. Verwey and E. L. Heilmann, "Physical Properties and Cation Arrangement of Oxides with Spinel Structures I. Cation Arrangement in Spinels," *J. Chem. Phys.*, vol. 15, no. 4, p. 174, 1947.

[26]   S. Cocchi, "A chemical loop approach for methanol reforming," Università di Bologna, 2012.

[27]   F. Fresno, R. Fernández-Saavedra, M. Belén Gómez-Mancebo, A. Vidal, M. Sánchez, M. Isabel Rucandio, A. J. Quejido, and M. Romero, "Solar hydrogen production by two-step thermochemical cycles: Evaluation of the activity of commercial ferrites," *Int. J. Hydrogen Energy*, vol. 34, no. 7, pp. 2918–2924, Apr. 2009.

[28]   T. Kodama, Y. Kondoh, R. Yamamoto, H. Andou, and N. Satou, "Thermochemical hydrogen production by a redox system of ZrO2-supported Co(II)-ferrite," *Sol. Energy*, vol. 78, no. 5, pp. 623–631, May 2005.

[29]   T. Kodama, N. Gokon, and R. Yamamoto, "Thermochemical two-step water splitting by ZrO2-supported NixFe3–xO4 for solar hydrogen production," *Sol. Energy*, vol. 82, no. 1, pp. 73–79, Jan. 2008.

[30]   P. Gupta, L. G. Velazquez-Vargas, and L.-S. Fan, "Syngas Redox (SGR) Process to Produce Hydrogen from Coal Derived Syngas," *Energy & Fuels*, vol. 21, no. 5, pp. 2900–2908, Sep. 2007.

[31]   C.-C. Cormos, "Evaluation of iron based chemical looping for hydrogen and electricity co-production by gasification process with carbon capture and storage," *Int. J. Hydrogen Energy*, vol. 35, no. 6, pp. 2278–2289, Mar. 2010.

[32]   F. Li, H. R. Kim, D. Sridhar, F. Wang, L. Zeng, J. Chen, and L.-S. Fan, "Syngas Chemical Looping Gasification Process: Oxygen Carrier Particle Selection and Performance," *Energy & Fuels*, vol. 23, no. 8, pp. 4182–4189, Aug. 2009.

[33]   R. Sime, "The redox process for producing hydrogen from woody biomass," *Int. J. Hydrogen Energy*, vol. 28, no. 5, pp. 491–498, May 2003.

[34]   K. Matsuoka, T. Shimbori, K. Kuramoto, H. Hatano, and Y. Suzuki, "Steam Reforming of Woody Biomass in a Fluidized Bed of Iron Oxide-Impregnated Porous Alumina," *Energy & Fuels*, vol. 20, no. 6, pp. 2727–2731, Nov. 2006.

[35]   K. GO, S. SON, S. KIM, K. KANG, and C. PARK, "Hydrogen production from two-step steam methane reforming in a fluidized bed reactor," *Int. J. Hydrogen Energy*, vol. 34, no. 3, pp. 1301–1309, Feb. 2009.

[36]   V. Hacker, "A novel process for stationary hydrogen production: the reformer sponge iron cycle (RESC)," *J. Power Sources*, vol. 118, no. 1–2, pp. 311–314, May 2003.

[37]   M. F. Bleeker, H. J. Veringa, and S. R. A. Kersten, "Pure Hydrogen Production from Pyrolysis Oil Using the Steam–Iron Process: Effects of Temperature and Iron Oxide Conversion in the Reduction," *Ind. Eng. Chem. Res.*, vol. 49, no. 1, pp. 53–64, Jan. 2010.

[38]   M. F. Bleeker, S. R. A. Kersten, and H. J. Veringa, "Pure hydrogen from pyrolysis oil using the steam-iron process," *Catal. Today*, vol. 127, no. 1–4, pp. 278–290, Sep. 2007.

[39]   M. Bleeker, S. Gorter, S. Kersten, L. Ham, H. den Berg, and H. Veringa, "Hydrogen production from pyrolysis oil using the steam-iron process: a process design study," *Clean Technol. Environ. Policy*, vol. 12, no. 2, pp. 125–135, Jul. 2010.

[40]   U. Cornaro and D. Sanfilippo, "Catalytic system and process for the production of hydrogen," 2004/0152790 A102-Feb-2004.

[41]   H. Imanishi, A. Maeda, T. Maegawa, S. Matsuno, and T. Aida, "Effects of reduction conditions on the cycling performance of hydrogen storage by iron oxides: Storage stage," *Chem. Eng. Sci.*, vol. 63, no. 20, pp. 4974–4980, Oct. 2008.

[42]   K. GO, S. SON, and S. KIM, "Reaction kinetics of reduction and oxidation of metal oxides for hydrogen production," *Int. J. Hydrogen Energy*, vol. 33, no. 21, pp. 5986–5995, Nov. 2008.

[43]   D. Barrett, "Partial Oxidation of Methane Using Iron Oxide as Donor," *Ind. Eng. Chem. Process Des. Dev.*, vol. 11, no. 3, pp. 415–420, Jul. 1972.

[44]   J. de Wiebren, "Sustainable Hydrogen Production by Thermochemical Biomass Processing," in *Hydrogen Fuel*, CRC Press, 2008, pp. 185–225.

[45]   V. Hacker, G. Faleschini, H. Fuchs, R. Fankhauser, G. Simader, M. Ghaemi, B. Spreitz, and K. Friedrich, "Usage of biomass gas for fuel cells by the SIR process," *J. Power Sources*, vol. 71, no. 1–2, pp. 226–230, Mar. 1998.

[46]   M. Ni, D. Y. C. Leung, and M. K. H. Leung, "A review on reforming bio-ethanol for hydrogen production," *Int. J. Hydrogen Energy*, vol. 32, no. 15, pp. 3238–3247, Oct. 2007.

[47]   H. Song and U. S. Ozkan, "Economic analysis of hydrogen production through a bio-ethanol steam reforming process: Sensitivity analyses and cost estimations," *Int. J. Hydrogen Energy*, vol. 35, no. 1, pp. 127–134, Jan. 2010.

2. CHARACTERIZATION TECHNIQUES AND SET-UP OF LABORATORY SCALE PLANT

2.1. INTRODUCTION

In this chapter are described the physical and chemical techniques used to characterize the looping materials before, during and after cycling. For each technique the general principle of the technique is recalled and the apparatus and method used are given. The solids have been tested for the chemical looping with anaerobic oxidation of ethanol and re-oxidation of the reduced material by water. Two laboratory-scale plants have been set-up for the process, the method of analysis of the reaction products and the calculation protocols are also presented in this chapter.

2.2. CHARACTERIZATION TECHNIQUES

2.2.1. Metal content measurements (ICP)

The quantitative chemical analyses of the various catalysts were carried out by atomic absorption spectroscopy or atomic emission spectroscopy (AES) in Argon plasma (ICP - Inductively coupled plasma) on a SPECTROLAME-ICP spectrometer from SPECTRO. The solids (about 10 mg) were first solubilized in an aqueous solution (100 mL) containing HF (5 mL) H_2SO_4 (5 mL) and HNO_3 (5 mL) at 270°C under stirring for 4 h. The solution was then vaporized in the plasma and the emission intensity of a radiation characteristic of the analyzed element was measured. The precision of analysis is better than 1%.

2.2.2. Carbon content measurements (CHNS)

The carbon contents of the materials after the each one of the two steps was determined using a CHNS/Oxygen automatic elemental analyzer Thermo Scientific MASS 200R. The samples were homogenized and loaded in small aluminum capsules and analyzed. For each samples two analyses were carried out in order to check for the homogeneity of the solid. Results were given as weight % of C, and the precision of the measurement was 0.3%.

2.2.3. X-ray diffraction (XRD)

2.2.3.1. Standard powder X-ray diffraction

This technique is the primary tool for the study of solid-state crystallography and to determine the nature of the crystalline phases. Diffractograms are obtained by measuring the diffraction angles at which the sample diffracts an X-ray beam. The information on the sample is given by the position, intensity, sharp and width of the diffraction lines. The

diffraction angle 2θ and the spacing between two planes (h,k,l) *d* are related by the Bragg law [1]:

$$2\ d\ \sin\theta = n\ \lambda \quad (1)$$

where λ is wavelength of incident X-ray and n is the diffraction order.

X-ray diffraction (XRD) patterns of the solids before and after cycling were obtained using a Bruker D8 X-ray diffractometer equipped with a 9-sample holder. The X-ray source was Cu Kα radiation. 2θ diffraction angle was varied from 5 to 80° during the measurement. The International Center for Diffraction Data (ICDD) library was used for phase identification. The phase identification was done by comparison of the experimental diffraction pattern with patterns in database such as the Powder Diffraction File (PDF) of the International Centre for Diffraction Data.

2.2.3.2. High temperature X-ray diffraction

To better understand the behavior of the material during the reduction, a Panalytical X'Pert Pro MPD X-ray diffractometer has been equipped with a feeding system in order to run in-situ tests and record the XRD patterns in function of temperature. The instrument allows to heat the powders during the analysis and to feed gas on it. In the main chamber of the instrument, a feeding system was mounted in order to regulate the flow rate of the stream fed and achieve a flow similar to the one used in the reactivity testing apparatus. As it is possible to see in Figure 2-1 the ethanol (or water) is put into a syringe and pushed through a diffusion pump into a heated line, connected to the inlet of the sample chamber.
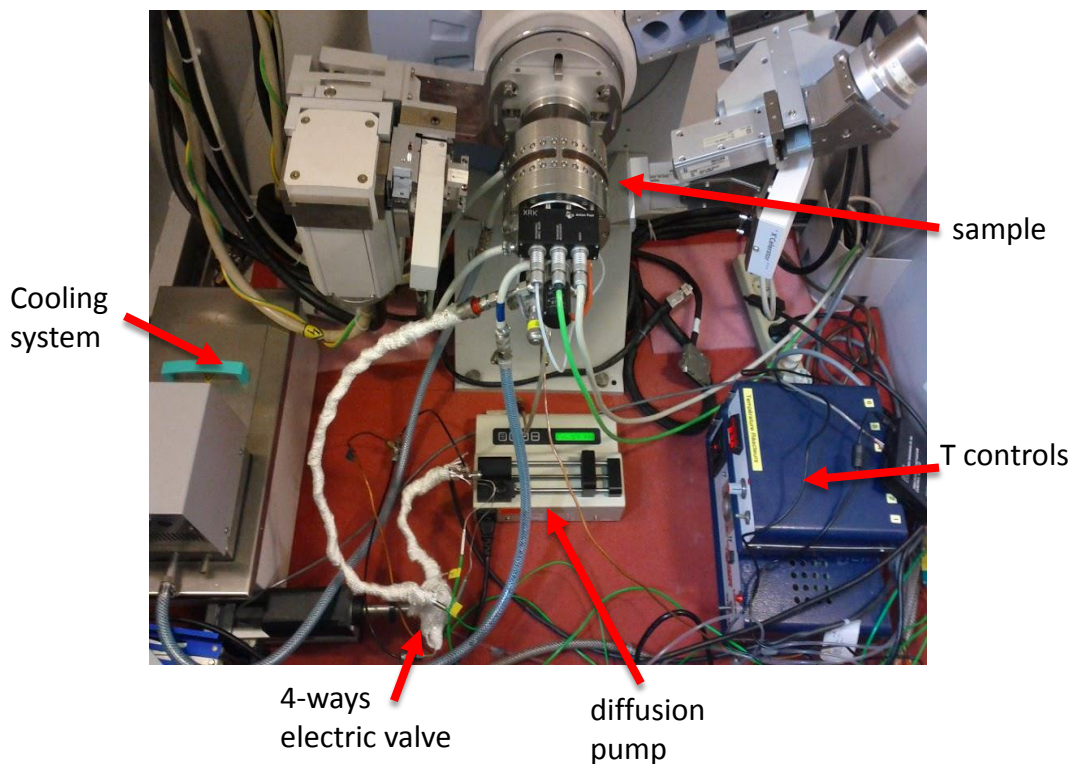
Figure 2-1. Configuration of the apparatus for in-situ XRD analysis

The liquid was vaporized in this line and added to a flow of N_2. The inlet stream can be controlled through a 4-ways electronic valve connected to a remote control. This allowed switching between the feeding of either ethanol/water or only gas (during the analysis). The temperature of the lines was kept at 130°C by means of heating stripes.

A typical procedure used for an in-situ experiment was as follows: the material was loaded into the sample chamber and the lines were mounted. At this point a first analysis was done to record the pattern at room temperature. Then the sample was slowly heated up to 450°C and a second diffractogram was recorded under a N_2 flow. At this point the ethanol was fed, then replaced with N_2, and the patter was recorded while flowing N_2.

2.2.3.3. Analysis of the X-ray diffraction data

TOPAS-4.2 program was used to refine the unit cells of the crystalline phases and to calculate the relative phase content in compounds. This program is based on the Rietveld method [2]. With this method a crystal structure, together with instrumental and microstructural information, is used to generate a theoretical diffraction pattern that can be compared to the measured profile. The profile can be modeled using the calculated counts y_i^{calc} at the ith step of 2θ by summing the contribution from neighboring Bragg reflections plus the background:

$$y_i^{calc} = y_i^b + \sum_\phi S_\phi \sum_h j_{\phi,h} \cdot Lp_{\phi,h} \cdot P_{\phi,h_i} \cdot A_{\phi,h} \cdot \left|F_{\phi,h}\right|^2 \cdot \Omega_{i,\phi,h}$$

where y_i^b is the background intensity,

S_ϕ is the scale factor of the phase ϕ,

$j_{\phi,h}$ is the multiplicity factor of the hth reflection,

$Lp_{\phi,h}$ is the Lorentz-polarization factor,

$P_{\phi,h}$ is the preferred orientation function,

$A_{\phi,h}$ is the absorption correction,

$F_{\phi,h}$ is the structure factor,

$\Omega_{i,\phi,h}$ is the reflection profile function that models both instrumental and sample effects.

This technique uses a least squares approach to minimize a function χ^2 that represents the difference between the calculated y_i^{calc} and observed y_i^{obs} intensities at equal angular intervals, by adjusting model parameters.

$$\chi^2 = \sum_{i=1}^{n} w_i \left\{ y_i^{obs} - y_i^{calc} \right\}^2$$

with $w_i = \dfrac{1}{\sigma_i^2}$, where σ_i^2 is the variance of the observed intensity y_i^{obs}.

The Full Width at Half Maximum (FWHM) of a powder diffraction reflection is influenced by several factors including instrumental factors, the presence of defects and microstructural effects i.e., strain and size effects. Since the FWHM can be described as the convolution of the instrumental resolution and the sample effect, the microstructure effects can be separated from other factors by using the combination of the Rietveld method with the instrumental resolution function, and particles size can be calculated.

2.2.4. Temperature programmed reduction (TPR)

The reducibility properties of the different ferrites was studied by temperature programmed reduction (TPR) using a TPD/RO catalytic surface analyzer by Thermo Quest Company. Samples of about 0.2 mg were first contacted with He flow to remove adsorbed species. Subsequently, the samples were contacted with a flow of 5% H_2/Ar (20 ml/min) and heated at a rate of 10°C/min up to 650°C, and finally maintained at this temperature for 1h. Hydrogen consumption, expressed in mmol of consumed H_2 per gram of ferrite, was determined taking into account a calibration analysis performed with CuO.

2.2.5. Specific surface area measurement

N_2 adsorption/desorption was used to characterize the textural properties of the solids. The specific surface area and total pore volume of the catalysts were measured by physisorption of liquid nitrogen at -196°C using a MICROMERITICS ASAP 2020 instrument. The samples, around 0.5 g, were degassed at 300°C for 3 h under secondary vacuum (10^{-4} Pa) to remove adsorbed species. Specific surface areas were measured by the BET method [3].

2.2.6. X-ray photoelectron spectroscopy (XPS)

XPS provides information on the chemical composition, chemical environment and oxidation state of the elements present in the near surface layers of the solids. In particular, this technique is very important for evaluating the changes of the oxidation state and modification of surface composition that may occur during reactions.

XPS measurements were performed using a Kratos Axis Ultra DLD spectrometer. The base pressure in the analysis chamber was better than 5.10-8 Pa. XPS spectra were measured at 90° (normal angle with respect to the plane of the surface) using a monochromatic Al Kα X-ray source with a pass energy of 20 eV. Binding energies were corrected in relation to the carbon 1s signal at 284.6 eV. The signal intensities of Fe, Ni, and Co $2p_{3/2}$, and O 1s were measured using integrated areas under the detected peaks and used to determine surface cationic ratios. The Fe/Co ratio was calculated using the integrated areas under the Co 2p peak, since a satellite line of Fe ($L_3M_{4,5}M_{4,5}$) superposes to Co $2p_{3/2}$. The experimental precision on the calculated cationic ratio was considered about 10%.

2.2.7. Mössbauer spectroscopy

The Mössbauer effect consists of the "recoilless" emission of γray photons from certain radioactive nuclei, and the selective reabsorption of those photons by other nearby nuclei. The process is sensitive to small differences between the structure of the emitting and the absorbing nuclei. Mössbauer spectroscopy uses this phenomenon to explore the nuclear and atomic structure of materials.

Through Mössbauer spectroscopy it is possible to obtain important information, such as oxidation state and structure of Fe species in a solid. The technique takes advantage of the Mössbauer effect, which consists in recoil-free, resonant adsorption/emission of γ-ray in solid materials. The main nuclear interactions used for the interpretation of the resonance spectra are three: (1) the Isomer Shift (IS), which is the shift in nuclear energy levels induced by the static charge of nearby atomic electrons (2) the Quadrupole Splitting

(QS) which is the shift in nuclear energy levels induced by a strong electric field gradient due to nearly electrons and (3) Magnetic (or Hyperfine) Splitting (HS) corresponding to the energy level splitting in a nucleus due to the magnetic fields induced by the nearby atomic electrons.

The γ-ray source is attached to a vibrating mechanism driven so as to cause a triangular velocity waveform. That is, the velocities of the emitting source are swept through a specified range, increasing and then decreasing linearly with time. The velocity range is selected with a dial control, with maximum velocity (up to 10 mm/s in the study). The γ-rays, which pass through the sample, are detected by a proportional counter. Signals from the counter pass through a pre-amp and a linear amplifier before reaching a single-channel analyzer (SCA), which generates a digital pulse if the analog signal falls within a selected pulse-height range. The digital output from the SCA is fed into the computer, which sorts the event into the associated velocity bin. The computer accumulates data in 5l2 channels, each corresponding to a specific source velocity. Phase is maintained between the computer and driving electronics so as to produce one pass through all bins for each velocity cycle. This produces a spectrum with two zero-velocity positions, with the maximum speed at the end bins, and zero velocity at the center. The data corresponding to the two sub-spectra are summed leading to a 256 points final spectrum.

The Mössbauer spectrometer was a homemade apparatus using a ^{57}Co/Rh γ-ray source and a conventional constant acceleration Mössbauer spectrometer. The solids were pressed into thin discs and the analysis took about one day to be completed (in some cases it can require even longer time).

Isomer shifts were given with respect to α-Fe. All spectra were taken at room temperature and ambient atmosphere; samples were diluted in sucrose at about 50 wt % concentration. Integrated areas under individual deconvoluted peaks were used to obtain the relative populations of different iron species, assuming an equal recoil-free fraction for all the species.

The parameters characterizing a Mössbauer spectrum were determined by least-squares fitting and the goodness of the fit statistics by minimizing the χ^2 quadratic function:

$$\chi^2 = \sum_i \frac{(y_i th - y_i exp)^2}{y_i exp} \cdot \frac{1}{N-K} \qquad (1)$$

where N is the number of measured points, K the number of the parameters to be determined, y_i *exp* and *th* respectively measured and calculated spectral values in velocity for each point *i*. The calculations were made using pure Lorentzian functions.

2.2.8. Diffuse Reflectance Infrared Fourier Transform Spectroscopy coupled with mass spectrometry analysis of the effluents gas

To study the interaction of ethanol on the different ferrites we used a DRIFT spectrometer connected to a quadrupole mass spectrometer; a feeding apparatus was built (Figure 2-2).
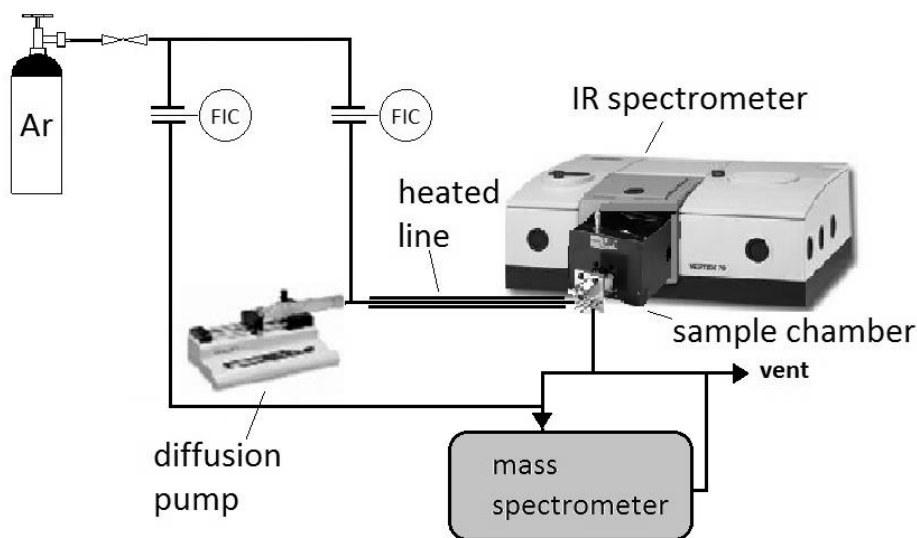

Figure 2-2.Schematic representation of the DRIFTS apparatus with feeding system and mass spectrometer

The sample was put into a ceramic holder with small holes at the bottom allowing the gas to flow through the sample. The feeding apparatus consists in a syringe pump connected to a heated line. Ethanol was injected and vaporized in the line where an inert carrier (He or Ar) also flew. The gas coming out from the DRIFTS apparatus was sent to a mass spectrometer (MS). Since the mass analyzer requires about 22 ml/min of gas, an additional stream of 20 ml/min of pure Ar was added to the effluent gas in order to reach the required flow.

The standard procedure included a pretreatment of the sample, by heating at 450°C under an Ar flow of 4.5 ml/min for about 45 min, in order to remove the weakly adsorbed species (mainly water). The sample was then cooled down to room temperature and a background spectrum was recorded. At this point ethanol was fed for about 15 minutes, while controlling its signal through the MS. Once the signal was stable, which indicated the saturation of the material, the feeding was stopped and Ar was let to flow until the weakly adsorbed ethanol was completely desorbed. The complete desorption was controlling by recording an IR spectrum. At this point, temperature was increased up to 150°C for 1.5 min and then cooled down again at 30°C in order to carry on the IR analysis. This procedure was repeated by increasing temperature at each step (200, 250, 300, 350 and 400 °C).

2.2.8.1. Mass spectrometry analysis of the effluent gas (MS)

The outlet gas stream was analyzed continuously through a quadrupole mass analyzer by its heated capillary probe. The software gave the results reporting the mass-to-charge ratio (m/z) versus time. The contribution of each compound to each m/z signals shown in Table 2-1.

Table 2-1. m/z values considered for the attribution to the different compounds

M/Z	Main Compound	Other compounds
2	Hydrogen	
16	Methane	
25	Ethylene	
28	Carbon monoxide	Ethylene, Ethane
29	Acetaldehyde	Ethanol, Ethyl ether
30	Ethane	
31	Ethanol	Ethyl ether
40	Argon	
41	Crotonaldehyde	Butene
43	Ethyl acetate	Acetaldehyde Acetic acid Acetone
44	Carbon dioxide	Acetaldehyde
45		Ethanol Ethyl ether Acetic acid
56	Butene	
58	Acetone	
59	Ethyl ether	
60	Acetic acid	
61	Ethyl acetate	

2.2.9. High-resolution transmission electron microscopy (HRTEM)

In high-resolution transmission electron microscopy (HRTEM), a beam of electrons is transmitted through a thin specimen, interacting with it as it passes through. An image is formed from the interaction of the electrons transmitted through the specimen; the image is magnified and focused onto an imaging device.

The microscope used was a JEOL 2010 (200 kV); the gun is provided with a filament tip LaB$_6$ single crystal providing a flow of electrons of 40 A/cm. The resolution is 0.196 nm in point to point mode and 0.147 nm in network mode. Before each analysis, the analyzed

catalysts is crushed and dispersed ultrasonically in water or pure ethanol. Then a drop of the homogenized suspension is deposited on 2-3 mm diameter carbon-coated copper grids (100 - 400 mesh). Ultramicrotomed cuts have also been realized for specific analyses and structure analyses.

The study by electron microscopy allows the direct observation of catalyst morphology with a magnification in the range 10^{-4}-10^{-10} m. The shape and size of particles and active phases distribution can be obtained from images. Electron microscopy brings also the structural information such as symmetry, unit cell parameter of crystallite, crystal orientation.

2.3. REACTIVITY EXPERIMENTS

2.3.1. Long-cycles tests

Figure 2-3 shows the schematic representation of the laboratory-scale plant used to carry out the reactivity tests in the laboratory of Bologna. The apparatus consists of a feeding zone, where the flow rate of gases, N_2 used as carrier and, in certain cases, air, were controlled using mass flow meters and sent to a line kept at 140°C by means of a heating stripe. In this line, liquids (ethanol during the 1st step and water in the 2nd step) were fed by means of a syringe pump and vaporized before being sent to the reactor. The reactor is made of a fixed-bed quartz continuous-flow reactor (internal diameter 19 mm, length of 30 cm; catalytic bed height was less than 2 mm) inserted into a furnace; while the temperature of the catalytic was measured by means of an axial thermocouple placed inside. In order to increase the speed of the outlet flow, the zone under the catalytic bed was filled with small glass-balls.

The third part is the analysis zone, where the exit flow is sent to a micro-GC connected to a computer. Two different configurations were adopted for this zone, depending on the compound fed: when ethanol was fed, the stream containing the products was sent directly through an heated line to the micro-GC, while when water was fed, the gases passed first through a water trap, and were then sent to the micro-GC; this was necessary because otherwise a large amount of water could damage the columns. The instrument used was an Agilent 3000A micro-GC installed on-line. The instrument was equipped with 3 columns: (a) a Plot Q column, carrier N_2, for the separation of CH_4, CO_2, H_2O and ethanol; (b) a OV1 column, carrier N_2, for the separation of CO_2, acetaldehyde, H_2O, ethanol; (c) a Molecular Sieve 5A column, carrier Ar, for the separation of H_2, O_2, N_2, CH_4, and CO. A Plot U backflash column was installed in order to avoid CO_2 and H_2O poisoning of the third column.
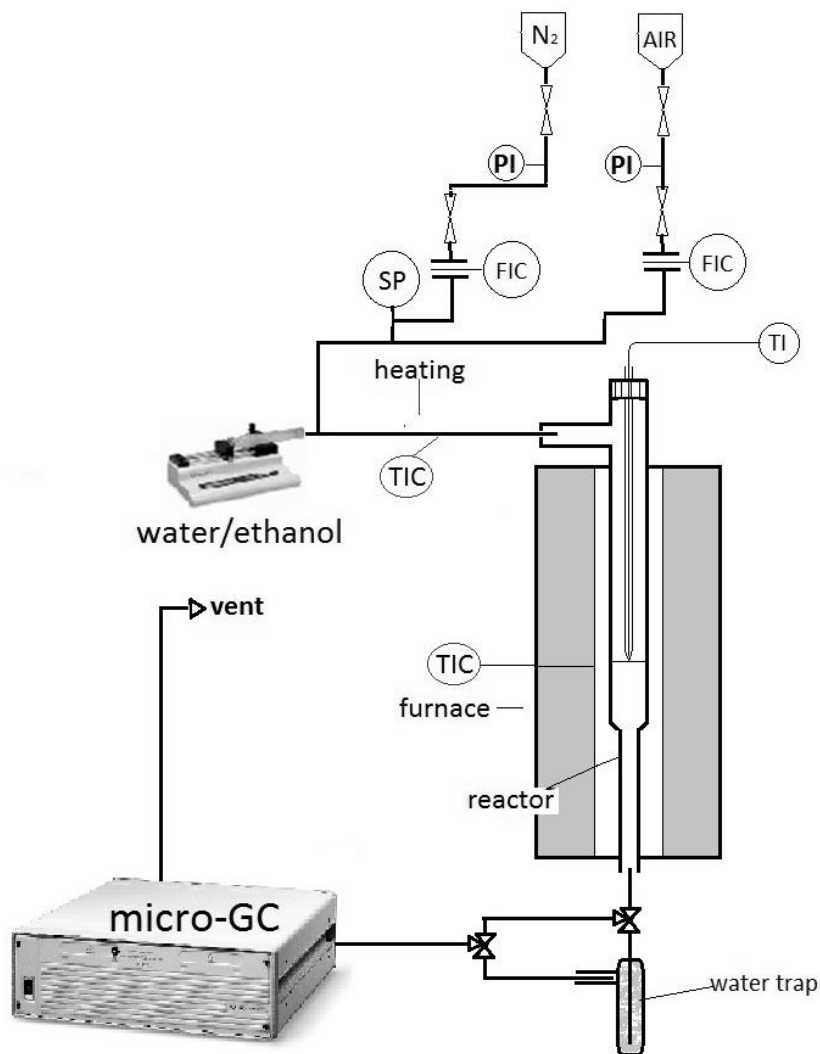
Figure 2-3. Schematic representation of the lab-scale plant used for long and 20-minute cycles

The instrument allowed to carry out an analysis every 5 min during the 1st step, and every 2 min during the 2nd step. This resulted in a large amount of data to be treated; therefore, the use of an Excel "macro" was necessary.

2.3.2. Short-cycles tests

Cycles shorter than 1h were carried out in the aim of finding the best reaction time and conditions for each step. Two types of short cycles were made.

2.3.2.1. Twenty minutes-step cycles

In Bologna, using the same apparatus than for the 1h-step cycles, further tests were performed. Operative conditions used were the same, but feeding was switched from ethanol to water and vice versa every 20 minutes, repeated over 5 cycles. Moreover, in order to characterize materials during cycling, the oxides were collected at different moments: (a) after the first reduction, (b) after the first complete cycle, (c) after the last reduction (4 complete cycles and 1 reduction), and (d) after the 5 complete cycles. These samples were characterized by means of by XRD, Mössbauer spectroscopy and carbon content measurement.

2.3.2.2. Two and five minutes-step cycles

In Lyon, another test apparatus, shown in Figure 2-4, has been set up. In this configuration the feeding zone consisted of two diffusion pumps, one for ethanol and one for water, connected through heated lines to a four-ways electronic valve allowing switching the feeding in a fraction of second. Both water and ethanol were vaporized in the lines heated at 140°C and their respective flow were added to a 30 ml/min N_2 stream and sent to the reactor.
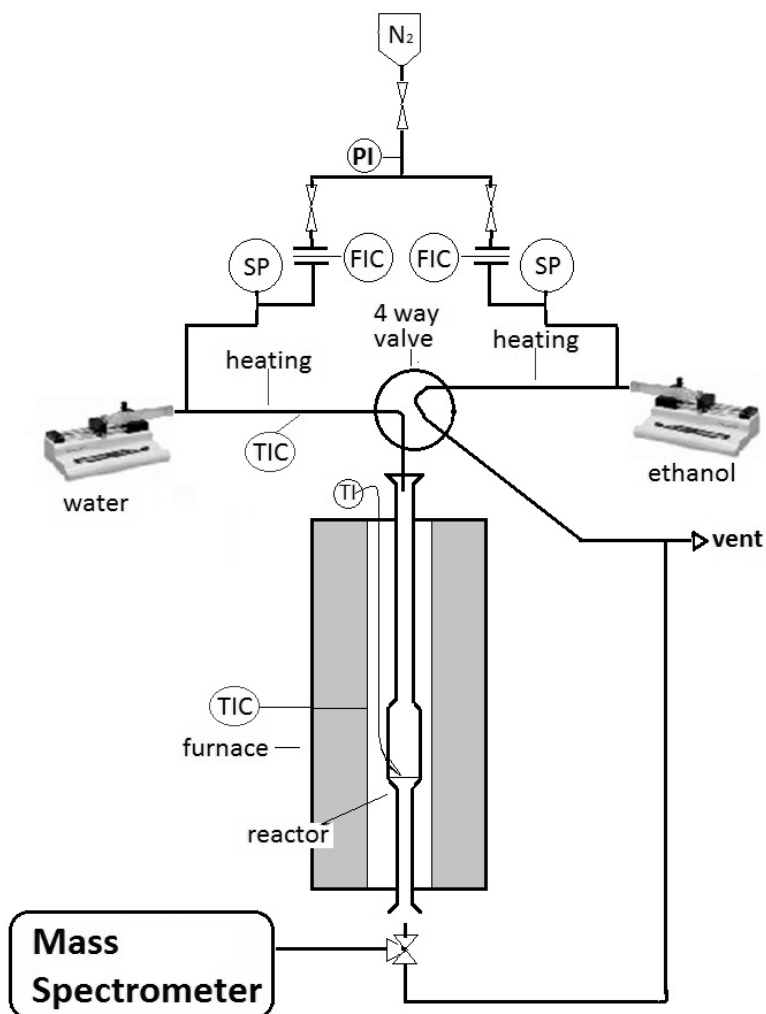
Figure 2-4. Schematic representation of the lab-scale plant used for the 2 and 5 minutes-step cycles

The "reaction zone" is made of a quartz fixed-bed reactor inserted into a furnace. The lower part of the reactor was not filled in this case, because its diameter was already smaller than that of the upper part. Also in this case, the temperature inside the catalytic bed was monitored by means of a thermocouple.

At the exit, the reactor was connected to the capillary of a portable mass spectrometer APSEC QMS (prototype) by SRA Instruments, which allowed analyzing the outgassed stream with a frequency of one analysis every 7-8 s.

2.3.3. Data processing and parameters calculation

For the reduction step, we decided to feed a flowing gas containing 15.6 % of ethanol in 30 ml/min of nitrogen [4], at 450°C. The resulting contact time was calculated as:

$$\tau = \frac{\text{Vcat(ml)}}{\text{V'tot (ml/s)}}$$

and corresponded to 0.27 s.

Results obtained from the micro-GC analysis were expressed as vol % in the outlet stream. In order to calculate yields and conversion the following formulas were used:

$$Y_{P,A} = \frac{n_{P,out}}{n_{A,in}} = \frac{\%_v^{P,out} * \dot{V}_{tot}^{out}}{\%_v^{A,in} * \dot{V}_{tot}^{in}} = \frac{\%_v^{P,out}}{\%_v^{A,in}} * F_{vol}$$

$$X_A = \frac{\dot{n}^{A,in} - \dot{n}^{A,out}}{\dot{n}^{A,in}} = 1 - \frac{\%_v^{A,out}}{\%_v^{A,in} * F_{vol}}$$

* Considering a generic reaction A→P

F_{vol} is volumetric factor, which is obtained experimentally using N_2 as internal standard, and represents the change of the volumetric flow due to the variation of the number of moles.

$$F_{vol} = \frac{\%_v^{N_2,out}}{\%_v^{N_2,in}}$$

After calibration, it was possible to determine the "instantaneous" molar yield (relative to the sampling instant) of the following compounds: CO, CO_2, CH_4, acetaldehyde, ethylene, ethylacetate, diethylether, propylene, propane, acetone, H_2 and H_2O.

As the solid released oxygen to form products, until complete reduction was achieved, and due to the fact that coke or carbonaceous residues might accumulate on the solid during reaction, it was not possible to make an atomic balance neither of O atoms nor of C atoms. Therefore, an instantaneous balance on H atoms (the only species which was not contained in an accumulation term in material balances for the flow reactor) was carried

out, which allowed to calculate: (a) the instantaneous balance on C and hence the amount of C accumulating on catalyst (expressed with the term "coke"), (b) the instantaneous balance of O and hence the amount of O released from the catalyst, and (c) the reduction degree of the solid. The main H-containing products were H_2, CH_4 and H_2O.

For the oxidation step, since water was trapped before the GC and therefore was not analyzed, it was necessary to determine the concentration of the different products, considering also water, by means of these equations:

$$\text{Conc}^{vol,i} = \%_{GC}^{vol,i} * \frac{\%_{in}^{vol,N2}}{\%_{GC}^{vol,N2}} \qquad \text{(where i = } H_2O, CO_2, CO, CH_4)$$

$$\text{Conc}^{vol,H2O} = 100 - \text{Conc}^{vol,H2} - \%_{in}^{vol,N2}$$

$$\%_{real}^{vol,j} = \frac{\text{Conc}^{vol,j}}{\sum \text{Conc}^{vol,j} + \%_{in}^{vol,N2}} \qquad \text{(where j = } H_2O, CO_2, CO, CH_4)$$

From the so calculated concentrations, it was finally possible to calculate yields and conversions for the 2nd steps.

Reactivity experiments were carried out by loading 400 mg of ferrite, shaped in particles with diameter ranging from 0.25 to 0.6 mm; the reduction step was carried out by feeding continuously a stream of ethanol vapor (15.6 mol %) in N_2; contact time was 0.27 s. For the re-oxidation step water vapor (29.3 mol %) was fed in a N_2 stream.

References

[1]   W. L. Bragg, "The Diffraction of Short Electromagnetic Waves by a Crystal," *Proc. Camb. Philol. Soc.*, vol. 17, pp. 43 – 57, 1913.

[2]   H. M. Rietveld, "A profile refinement method for nuclear and magnetic structures," *J. Appl. Crystallogr.*, vol. 2, no. 2, pp. 65–71, Jun. 1969.

[3]   S. Brunauer, P. H. Emmett, and E. Teller, "Adsorption of gases in multimolecular layers.," *J. Am. Chem. Soc.*, vol. 60, no. 309, 1938.

[4]   S. Cocchi, "A chemical loop approach for methanol reforming," Università di Bologna, 2012.

3. SYNTHESIS AND CHARACTERIZATION OF THE LOOPING MATERIALS

3.1. INTRODUCTION

In this chapter it will be shown how the materials were synthesized, and how the choice of the annealing temperature was made. The analysis of the results from the different characterization techniques used on the as-synthesized materials will be presented.

3.2. SYNTHESIS OF THE MATERIALS

The materials synthesized were of the type $A^{2+}Fe_2^{3+}O_4^{2-}$, where A^{2+} was either Fe^{2+}, Co^{2+}, Ni^{2+} or Cu^{2+} (the first one corresponds to the unmodified magnetite). The list of the chemicals used for the preparations is given in Table 3-1. The co-precipitation method chosen is described in details elsewhere [1]. It can be summarized as follows.

For the $CoFe_2O_4$ ferrite, two solutions of $Fe(NO_3)_3 \cdot 9H_2O$ (1M) and $Co(NO_3)_2 \cdot 6H_2O$ (0.5M) were prepared and added drop-wise to a NaOH (2M) solution, at 50°C. The pH of the resulting solution was higher than 11. Afterwards this solution was kept at 50°C under vigorous stirring for 3h. The precipitate formed was separated by filtration under vacuum and washed several times with bi-distillated water. The same method was used for the other ferrites, using $Ni(NO_3)_2 \cdot 6H_2O$ as the Ni^{2+} source in the case of $NiFe_2O_4$, $FeSO_4 \cdot 7H_2O$ and $FeCl_3$ for the Fe^{2+} and Fe^{3+} sources in the case of magnetite and $Cu(NO_3)_2 \cdot 2.5H_2O$ as Cu^{2+} source for $CuFe_2O_4$. The materials were dried at 120°C for 1 night (in the case of magnetite the drying temperature was only 80°C, in order to avoid oxidation of Fe^{2+} into Fe^{3+}). The solids were finally annealed in air at 450°C for 8h, increasing the temperature by 10°C/min. In the case of magnetite the heat treatment was conducted under a N_2 flow.

Table 3-1. Chemicals used for the synthesis of the ferrites samples.

Compound	Reference	Purity
$Fe(NO_3)_3 \cdot 9H_2O$	Sigma-Aldrich	98 %
$Co(NO_3)_2 \cdot 6H_2O$	Sigma-Aldrich	99 %
$Ni(NO_3)_2 \cdot 6H_2O$	Acros organics	99 %
$Cu(NO_3)_2 \cdot 2.5H_2O$	Sigma-Aldrich	98 %
$FeSO_4 \cdot 7H_2O$	Merck	99.5 %
$FeCl_3 \cdot 6H_2O$	Sigma-Aldrich	98 %
NaOH	Sigma-Aldrich	>99 %

3.2.1. Effect of thermal annealing

In previous studies ([2, 3]), it has been shown that the annealing temperature significantly affects the structure of materials, as it is can be seen in Figure 3-1 where the X-ray diffractograms of the cobalt ferrite, both as synthesized and annealed at 450 and 750°C, are shown.
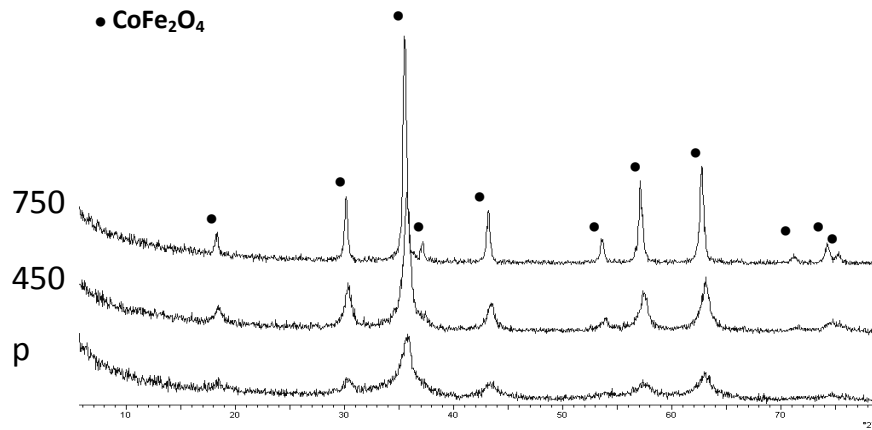
Figure 3-1. X-ray diffractograms on CoFe$_2$O$_4$ calcined at different temperatures ("p" is for "precursor")

The pattern obtained was that typically shown by ferrites with the spinel structure. It is possible to note that with increasing the annealing temperature the peaks became narrower. This indicates the presence of larger particles, which is confirmed by the calculation of the crystallite sizes, which in this case was 12nm for the sample calcined at 450°C and 36nm for that one calcined at 750°C. A further confirmation was obtained from the results of the BET specific surface area measurements, reported in Table 3-2.

Table 3-2. BET surface area and crystallite sizes of synthesized materials

Catalyst	Calcination temperatures (°C)	BET surface area (m²/g)	Crystallite size (nm)
Fe_3O_4	Precursor	164	-
	450	85	10
$CoFe_2O_4$	Precursor	180	-
	320	106	-
	450	72	12
	750	11	36
$NiFe_2O_4$	Precursor	197	-
	320	165	-
	450	94	7
	750	18	-
$CuFe_2O_4$	Precursor	177	-
	450	74	8

In all the ferrites, increasing the calcination temperature led to a decrease of the specific surface area from values between 160-200 m^2/g for the precursors to values between 10-20 m^2/g for samples annealed at 750°C. Moreover, it is possible to note that although surface area values were rather similar for all materials, small differences existed, that

allowed to classify the surface area of the different solids annealed at 450°C (the only common temperature) in the order $NiFe_2O_4 > Fe_3O_4 > CuFe_2O_4 > CoFe_2O_4$.

3.2.2. Conclusions and choice of the annealing temperature

A high surface area is important in order to make easier ferrites reduction, as explained by Cocchi et al [2]. It has been shown that by increasing the calcination temperature, the surface area decreased continuously. Moreover, the annealing temperature cannot be lower than the reaction temperature. As it will be shown, the lower reaction temperature at which it was possible to obtain a fast reduction of the ferrites was 450°C. Because of these reasons it was decided to anneal all ferrites at 450°C.

3.3. CHARACTERIZATION OF THE SYNTHESIZED MATERIALS

In this section all the characterization measurements performed on the ferrites after synthesis will be reported, in order to understand their structure and highlight the transformations taking place during the looping reactions.

3.3.1. XPS measurements

By means of XPS it was possible to determine the surface composition of oxides. Results for Fe_3O_4, $CoFe_2O_4$ and $NiFe_2O_4$ annealed at 450°C are shown in Table 3-3.

Table 3-3. Binding energies and quantitative analysis of ferrites

Solid		Binding Energy (eV)	Fe/M (M=Ni,Co)	$I_{sat}/I_{Fe2p3/2}$
Fe_3O_4	Fe $2p_{3/2}$	710.1	-	0.16
	Fe sat.	719.0		
$CoFe_2O_4$	Fe $2p_{3/2}$	710.3	3.4	0.15
	Fe sat.	719.0		
	Ni $2p_{3/2}$	780.0		
$NiFe_2O_4$	Fe $2p_{3/2}$	710.4	2.1	
		719.2		
	Ni $2p_{3/2}$	854.7		

In the case of nickel ferrite, the Fe/Ni ratio was 2.1, which corresponds to the theoretical bulk value. However, in the case of cobalt ferrite, the Fe/Co ratio was much higher (3.4), which could indicate an iron enrichment at the surface. This is not surprising since it is known that in a large temperature range (100–500°C), nanoscaled ferrites oxidize or reduce as a function of oxygen partial pressure into cation-deficient spinels without formation of ferric oxide phase [4, 5].

The enrichment is balanced by cationic vacancies (□), leading to the surface stoichiometry $Fe^{3+}_{2+2x}Co^{2+}_{1-3x}\square_xO_4$ (with $0 \leq x \leq 0.5$). The surface Fe/Co ratio equal to 3.4 would correspond to $x=0.11$.

Results on magnetite were in agreement with literature reports [6], with binding energies of 710.1 and 724.1 eV attributed to Fe 2p3/2 and Fe 2p1/2 levels, respectively. However, analysis of the spectrum in the Fe 2p region (Figure 3-2) showed the presence of a relatively intense satellite line, which indicates the presence of a high amount of Fe^{3+}.
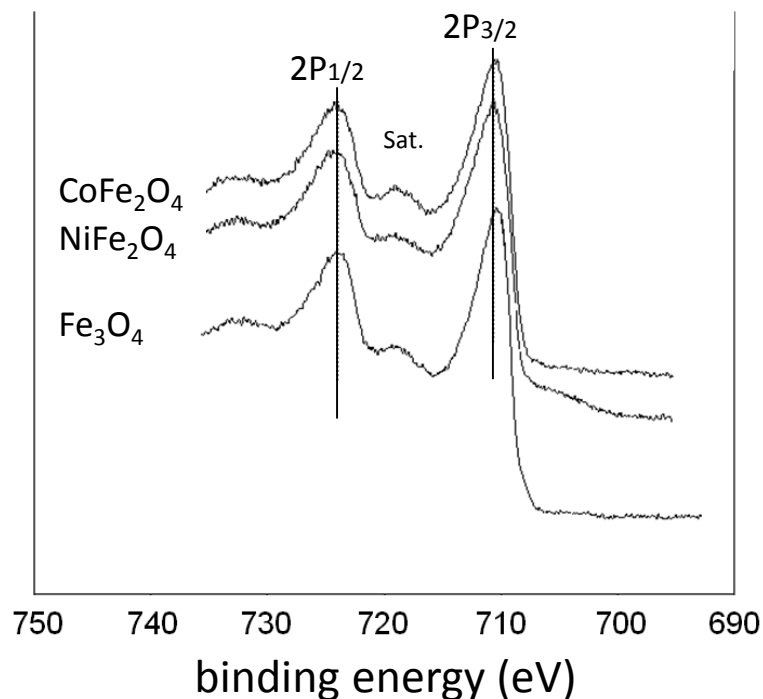
Figure 3-2. XPS spectra of the Fe 2p region on the ferrites analyzed

Comparing the intensity of the satellite line to that of the Fe 2p3/2, peak it is possible to evaluate the excess of Fe^{3+} on the surface of the ferrites (Table 3-3). The satellite line on $NiFe_2O_4$ has not been taken into account because of its low intensity; however its presence indicates that also in this case the surface exhibited a slight excess of Fe^{3+}.

3.3.2. Chemical analysis (ICP) measurement

In order to measure the concentration of the different metals in the bulk of the synthesized ferrites, chemical analyses of the samples after annealing at 450°C were performed. The results are reported in Table 3-4.

Table 3-4. Composition of the synthesized ferrites as obtained from ICP analysis

Wavelength (nm)	221.647-231.604	324.700-327.395	259.940-238.207	228.616-238.892
Sample	Ni (wt %)	Cu (wt %)	Fe (wt %)	Co (wt %)
Theoretical concentration	25.0	26.6	72.4 (magnetite) ~47 (others)	25.1
Fe_3O_4			65.3	
$CoFe_2O_4$			43.4	22.9
$NiFe_2O_4$	23.7		43.3	
$CuFe_2O_4$		23.3	43.3	

The theoretical concentration of Fe in magnetite is 72.4%, which is around 7% higher than what was measured. For the mixed ferrites the concentration of Fe should be around 47%, while the concentration of the other metals around 25% (26% in the case of copper ferrite). In all cases, the concentration measured was lower than the theoretical one. This could be due to the slight hydration of the samples powders.

However, considering the ratio between the two metals and comparing it with their theoretical ratio it is possible to see that they were quite similar (Table 3-5).

Table 3-5. Comparison between the measured through ICP and the theoretical metal ratios

Sample	Fe/Co		Fe/Ni		Fe/Cu	
	measured	theoretical	measured	theoretical	measured	theoretical
CoFe$_2$O$_4$	1.89	1.89				
NiFe$_2$O$_4$			1.83	1.90		
CuFe$_2$O$_4$					1.86	1.76

In the case of cobalt ferrite the measured ratio was exactly the same as the calculated one. In the nickel ferrite, the measured ratio was slightly lower (Δ = 0.07) than the theoretical one, whereas in the case of copper ferrite it was slightly higher (Δ = 0.1). These results clearly showed that the surface iron excess evidenced by XPS was only due to the equilibration of the ferrites samples in the annealing oxidative atmosphere.

3.3.3. X-Ray diffraction (XRD) study of synthesized materials

The materials have been analyzed by X-Ray diffraction after annealing at 450°C in order to confirm the effective presence of the spinel structure and characterize it.
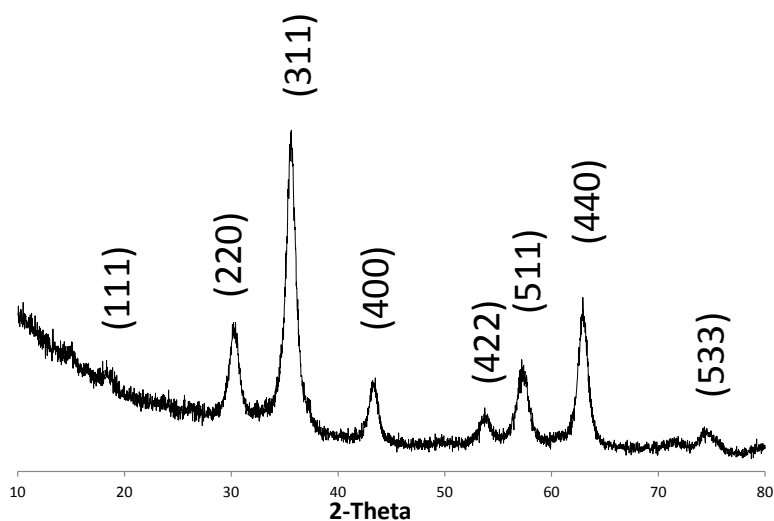
Figure 3-3. XRD pattern of Fe_3O_4 annealed in N_2 at 450°C

The synthesized magnetite diffractogram (Figure 3-3) was found to correspond to the calculated one [7], a clear indication that the ferrite structure had been achieved; however it appeared not to be very crystalline, since its reflections were very broad.
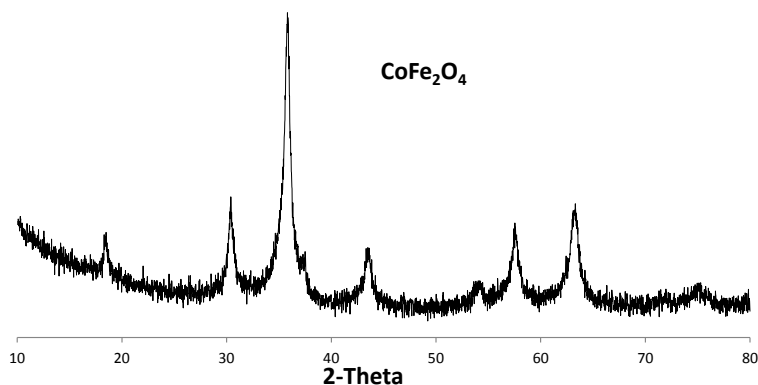
Figure 3-4. XRD pattern of $CoFe_2O_4$ calcined at 450°C
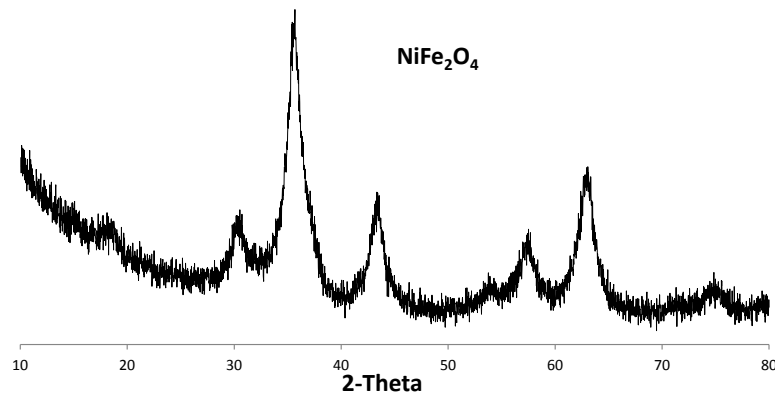
Figure 3-5. XRD pattern of NiFe$_2$O$_4$ calcined at 450°C

Both cobalt ferrite (Figure 3-4) and nickel ferrite (Figure 3-5) showed the same diffractograms of the magnetite, which is common for all the ferrites. However, comparing the two patterns, NiFe$_2$O$_4$ seemed to be less crystalline than CoFe$_2$O$_4$ since its peaks were broader. This is also confirmed by what shown in Table 3-2, where the crystallite size of the cobalt ferrite (12nm) was larger than that one of nickel ferrite (7nm).
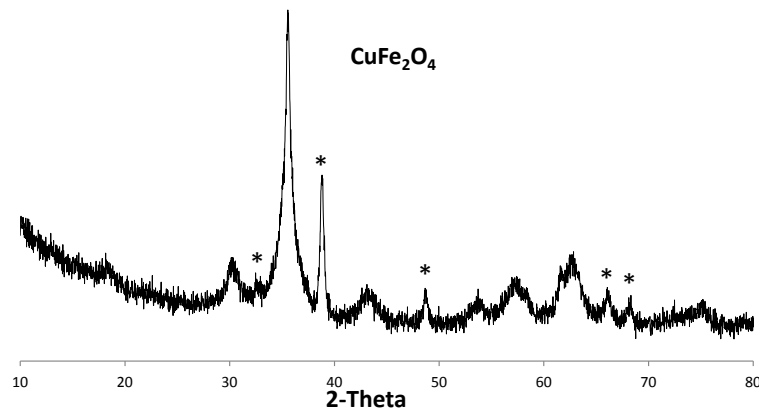
Figure 3-6. XRD pattern of CuFe$_2$O$_4$ calcined at 450°C (∗ = CuO)

In the case of copper ferrite, the main phase was still the cuprospinel; however, the presence of several additional peaks was also shown, that indicates that a part of Cu did

not enter the pattern of the ferrite, but remained segregated as copper oxide (CuO) (Figure 3-6). This segregation, which did not occurs with the other materials, can be due to the higher ionic radii of Cu^{2+} compared to Fe^{2+}. In fact, as it possible to see in Table 3-6, the copper has a significantly higher size and mass compared to the other metals.

Table 3-6. Ionic radii and masses of the different divalent ions

Compound	O_h ionic radii[1]	Atomic mass
Fe_3O_4	0.61	55.8
$CoFe_2O_4$	0.65	58.9
$NiFe_2O_4$	0.69	58.7
$CuFe_2O_4$	0.73	63.5

[1] For the divalent ion in $A_{Oh}^{2+}B_{2\,(Oh,Th)}^{3+}O_4^{2-}$

3.3.4. Mössbauer analysis of synthesized materials

Mössbauer characterization has been performed at room temperature on all the annealed materials in order to confirm the structure and investigate on the oxidation state of iron in the various ferrites.

a) Fe_3O_4

Magnetite, Fe_3O_4, is a ferromagnetic iron oxide with some iron atoms occupying sites with tetrahedral coordination (A-sites) and others sites with octahedral symmetry (B-sites). These sites are characterized by well-distinguishable Mössbauer signals. At room

temperature, Fe^{2+} and Fe^{3+} ions in the octahedral sites exchange electrons at a hopping rate that the corresponding Mössbauer lines show as for a single state ($Fe^{2.5+}$). The resulting ^{57}Fe Mössbauer spectrum shows two sextets, one of them corresponding to the contribution of the magnetic hyperfine interaction of Fe^{3+} in A-sites and the other to $Fe^{2.5+}$ in B-sites of the spinel structure (AB_2O_4).

Figure 3-7 shows the room temperature transmission Mössbauer spectrum of the Fe_3O_4 nanoparticles, from which we can find that the spectrum is well fitted by the two magnetic sextets respectively characterized by 48.6T and 45.5T internal magnetic fields, and 0.15mm/s and 0.53mm/s isomer shifts, corresponding to iron cations at A and B sites. The relative spectral area of the two sites has an intensity ratio B:A equal to 1.8 close to the theoretical one (2.0). The slight discrepancy may be caused by magnetite non-stoichiometry and the electron transfer process between Fe^{2+} and Fe^{3+} ions on the B sites. The hyperfine fields at site A and site B are smaller than the corresponding values characteristic of bulk Fe_3O_4 [8].
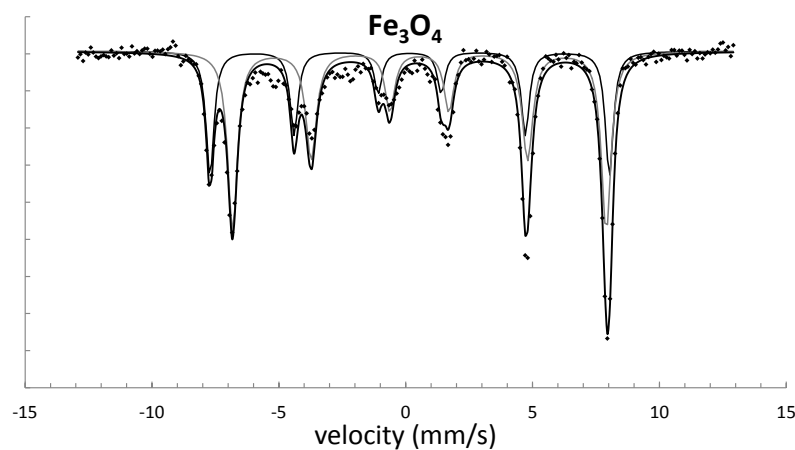
Figure 3-7. Mössbauer spectrum of Fe_3O_4 sample, recorded at 25°C;

the solid line is derived from least-square fit.
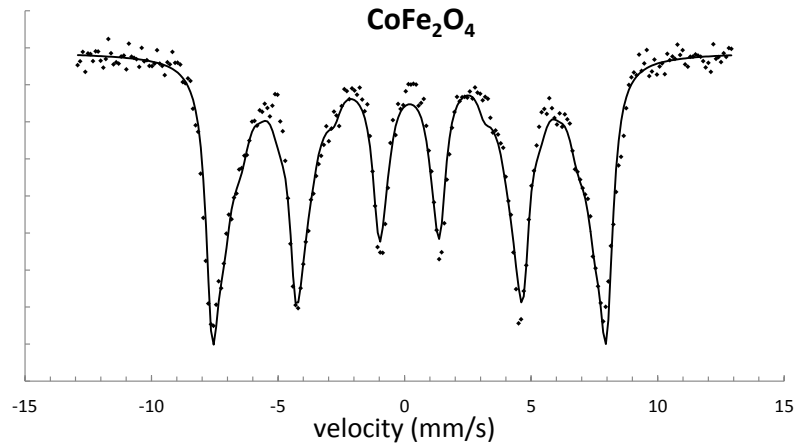
b) $CoFe_2O_4$

$CoFe_2O_4$, like the other ferrites and magnetite, is a ferromagnetic oxide with iron atoms occupying sites with tetrahedral coordination (A-sites) and others with octahedral symmetry (B-sites). However the distribution of Co and Fe cations over the two types of sites leads to various environments for the Fe cations, which are characterized by several internal magnetic fields.

Sawatzky et al. have studied the possible environments for Fe cations [9], [10] and found five major ones explained by the inverse spinel configuration of $CoFe_2O_4$, where half of octahedral sites are occupied by Co^{2+} cations and the other half by Fe^{3+} ones. On the other hand, tetrahedral sites are completely filled by Fe^{3+} in the so-called high-spin field distribution. The corresponding general formula is:

$$(Co^{II}_{1-\delta}Fe^{III}_{\delta})_{Th}(Fe^{III}_{2-\delta}Co^{II}_{\delta})_{Oh} O_4 \quad \text{with } 0<\delta<1 \qquad (1)$$
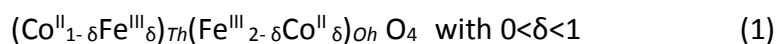
where δ is the inversion degree of the oxide. Such configuration leads to five different sextets for typical crystalline mixed ferrite spectra.

The room temperature spectrum of the cobalt ferrite sample is shown in Figure 3-8. It is different from what could be expected for a typical crystalline ferrite, and it has been fitted with a distribution of internal magnetic fields comprised between 34 and 51T, and an isomer shift equal to 2.44 mm/s. The differences between the spectrum experimentally obtained and a typical spectrum for a bulk ferrite can be due both to the small particle size distribution, that may lead to an inhomogeneous hyperfine coupling and asymmetric line broadening, and to a poor crystallinity of the ferrite sample. With that respect, it has been shown in the previous paragraph that after calcination at 450 °C the crystallization to ferrite was not complete.

Figure 3-8. Mössbauer spectrum of the CoFe$_2$O$_4$ sample, recorded at 25°C;

the solid line is derived from least-square fit.

c) NiFe$_2$O$_4$

In the case of nickel ferrite, its Mössbauer spectrum was very different and consisted in only a quadrupolar doublet (Figure 3-8). This is due to the fact that the NiFe$_2$O$_4$ particles were smaller, which led to a superparamagnetic effect.

Magnetic particles are nanosized with rapidly fluctuating magnetization, that is, with a time scale shorter than the hyperfine Larmor time $\tau_L \sim= 10^{-8}$s associated with ^{57}Fe [11]. The magnetization (or Néel vector) of a particle with volume V fluctuates according to an Arrhenius law, $1/\tau = 1/\tau_0 \exp(-U/k_BT)$, where $\tau 0 \sim= 10^{-10}$-10^{-11}s is a microscopic trial time and U = KV is the anisotropy barrier, K being the density of anisotropy energy (K $\sim=104 -105$ ergs/cm^3) characteristic of the material. The "blocking volume" V_b(T) at temperature T for ^{57}Fe Mössbauer spectroscopy is such that $1/\tau = 1/\tau_L$; it is given by the expression V_b(T) = k_BT/K . $\ln(\tau_L/\tau_0)$, and it is an increasing function of T. Particles have V < V_b , implying $1/\tau > 1/\tau_L$, and show at room temperature a spectrum corresponding to a quadrupolar doublet. The doublet used to fit the experimental data has an Isomer Shift (IS) of 0.25mm/s and a quadrupole Splitting (QS) of 0.70mm/s.
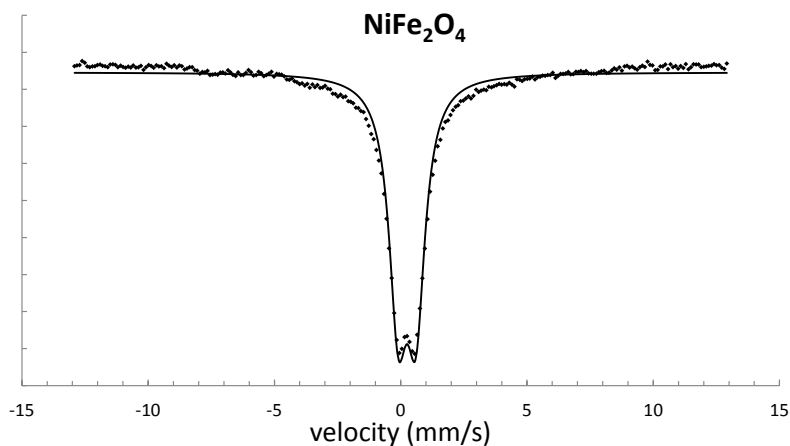
Figure 3-9. Mössbauer spectrum of the NiFe₂O₄ sample calcined at 450°C, recorded at 25°C; the solid line is derived from least-square fit.
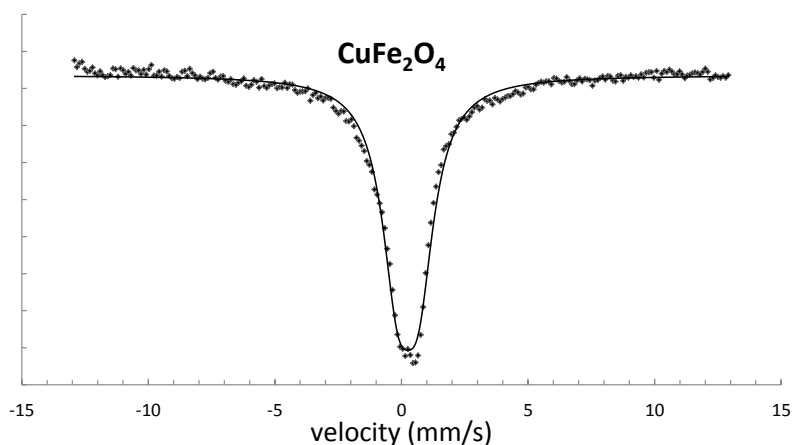

Figure 3-10. Mössbauer spectrum of the NiFe₂O₄ sample calcined at 450°C, recorded at 25°C; the solid line is derived from least-square fit.

d) CuFe$_2$O$_4$

For copper ferrite, a quadrupolar doublet was also obtained (Figure 3-10). It indicates the presence of small particles and superparamagnetic effect. In this case the IS was 0.25mm/s and the QS 0.80mm/s, values close to what reported in literature in a study of Goya and Rechenberg [12], for particle size around 7nm.

3.3.1. Temperature programmed reduction (TPR)

In order to understand the effects of the different cations in the mixed ferrites on their redox properties, temperature programmed reduction experiments using hydrogen were carried out.
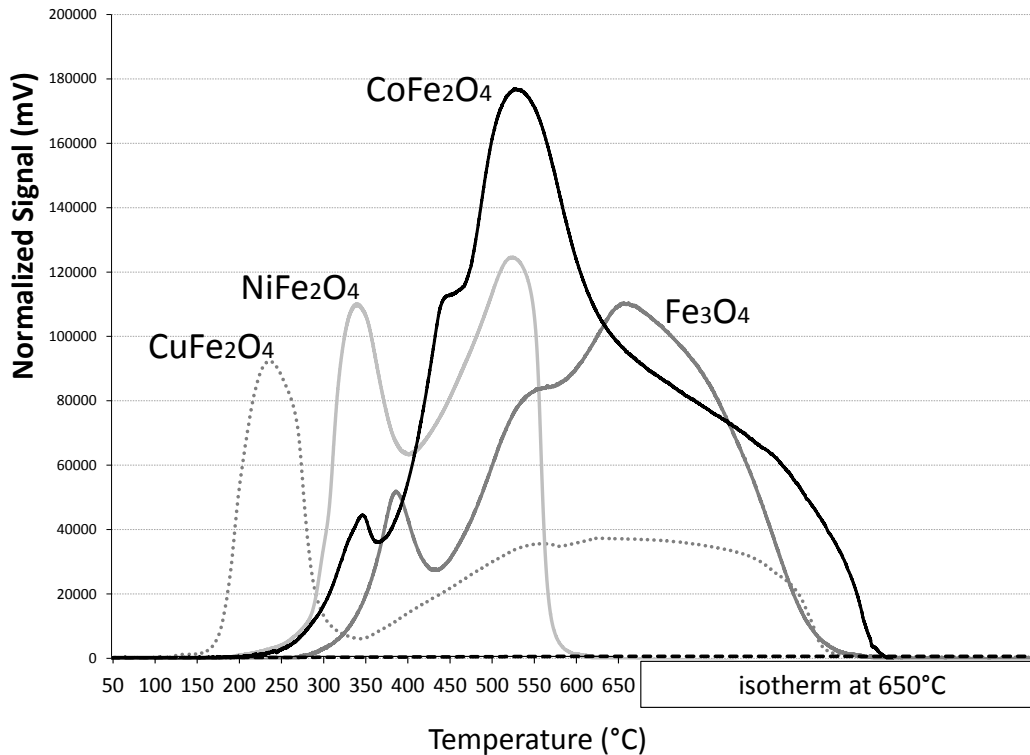
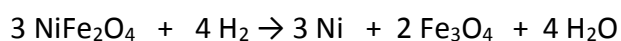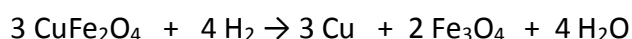**Figure 3-11. H$_2$-TPR profile for the different ferrites annealed at 450°C.**

Figure 3-11 shows the consumption of hydrogen recorded during temperature increase.

The magnetite TPR profile showed the occurrence of three main reduction events (denoted I (400°C), II (550°C) and III (650°C)) [13]. Event-I is attributed to a low-temperature single reduction pathway whereby FeO(OH) impurity species are reduced:

$$6\ FeOOH\ +\ 4\ H_2 \rightarrow 2Fe_3O_4\ +\ 4\ H_2O$$
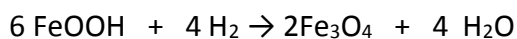
Event -II and –III, which were strongly overlapping, corresponded to the reduction of Fe_3O_4 occurring stepwise into FeO and Fe.

For $CuFe_2O_4$ and the $NiFe_2O_4$ reduction peaks at 250°C and 350°C were attributable to the reduction to Cu or Ni and Fe_3O_4 [14, 15]:

$$3\ CuFe_2O_4\ +\ 4\ H_2 \rightarrow 3\ Cu\ +\ 2\ Fe_3O_4\ +\ 4\ H_2O$$

$$3\ NiFe_2O_4\ +\ 4\ H_2 \rightarrow 3\ Ni\ +\ 2\ Fe_3O_4\ +\ 4\ H_2O$$

As mentioned above, the large peaks between 350 and 650°C were attributed to the reduction of Fe_3O_4 to Fe, which should occur in two steps with the intermediate formation of FeO. It can be observed that the relative intensity of the first peak for copper ferrite is much more intense than for nickel ferrite or even the other materials. It has been shown before from the XRD analysis that the copper ferrite sample taken in consideration was not a pure spinel, but contained CuO which should be concomitantly reduced at 250°C.

The TPR profile of $CoFe_2O_4$ appeared as the most complex one. The first peak at 340°C could correspond to the reduction of the solid surface, which is richer in iron and possibly hydroxylated into magnetite like material. The three following peaks at 460, 560 and 650°C, which are strongly overlapped, could be attributed similarly to those observed in the patterns of $CuFe_2O_4$ and $NiFe_2O_4$.

Considering the temperature at which the first peak is obtained, it can be deduced that the presence of Ni^{2+}, Co^{2+} or Cu^{2+} in the ferrites has a positive effect in increasing the reducibility compared to pure magnetite. Indeed, the temperatures corresponding to the first steps of reduction of the ferrites, 250°C, 350°C and 340°C, corresponded to those of the pure oxides (CuO, NiO and CoO respectively). It can also be noted that nickel and cobalt ferrite were both more easily reduced than magnetite, but that the area behind

the cobalt ferrite curve was much higher than the one of nickel, which could indicate a higher availability of reducing sites, i.e., a synergic effect of Co on the reduction of Fe. The most easily reducible ferrite was the copper ferrite, which could be reduced at lower temperature, around 250°C.

3.3.2. Conclusions on material characterization

It has been shown that all the materials, synthesized with the same co-precipitation protocol chosen for its easy implementation, had the desired spinel ferrite structure. However they showed different crystallinity and texture. All the samples were monophasic, except the copper containing catalyst, which exhibited some copper oxide CuO.

Magnetite was shown to have the highest crystallinity but also the larger particle size. As a consequence, it appeared from TPR analysis to be less easily reducible. However, its properties are not that different from the other compounds.

Nickel and cobalt ferrites have similarly a poor crystallinity and small particle size. These features, evidenced by X-ray diffraction, were also confirmed by Mössbauer spectroscopy, which showed the presence of only superparamagnetic ferrite particles at room temperature. These properties led to good reducing properties at relatively low temperature, which make these ferrites well adapted to be used as looping materials. With that respect, $CoFe_2O_4$ has a higher number of reducing sites, while $NiFe_2O_4$, as seen before, has a higher surface area. The higher number of reducing sites of $CoFe_2O_4$ should be linked to the slight excess of iron, evidenced by XPS at the surface of the solid.

Copper ferrite is the only one which is not monophasic. All attempts to prepare the pure copper ferrite with the selected protocol failed. The presence of CuO in the material seems to confer better reducing properties, as seen from the TPR analysis. However the reactivity pattern, when used for the looping process, might be different from that of the

other materials, and we will have to take this into account when comparing its properties with that of the other ferrites.

References

[1]   N. Ballarini, F. Cavani, S. Passeri, L. Pesaresi, A. F. Lee, and K. Wilson, "Phenol methylation over nanoparticulate CoFe2O4 inverse spinel catalysts: The effect of morphology on catalytic performance," *Appl. Catal. A Gen.*, vol. 366, no. 1, pp. 184–192, Sep. 2009.

[2]   S. Cocchi, M. Mari, F. Cavani, and J.-M. M. Millet, "Chemical and physical behavior of CoFe2O4 in steam–iron process with methanol," *Appl. Catal. B Environ.*, vol. 152–153, pp. 250–261, Jun. 2014.

[3]   S. Cocchi, "A chemical loop approach for methanol reforming," Università di Bologna, 2012.

[4]   E. Kester, B. Gillot, P. Perriat, P. Dufour, C. Villette, P. Tailhades, and A. Rousset, "Thermal Behavior and Cation Distribution of Submicron Copper Ferrite Spinels CuxFe3–xO4(0 ≤x≤ 0.5) Studied by DTG, FTIR, and XPS," *J. Solid State Chem.*, vol. 126, no. 1, pp. 7–14, Oct. 1996.

[5]   E. Kester, B. Gillot, C. Villette, P. Tailhades, and A. Rousset, "Valence states of copper in copper ferrite spinels CuxFe3–xO4 (0 < x ≤ 1) fine powders: Evidence of copper insertion," *Thermochim. Acta*, vol. 297, no. 1–2, pp. 71–78, Aug. 1997.

[6]   T. Yamashita and P. Hayes, "Analysis of XPS spectra of Fe2+ and Fe3+ ions in oxide materials," *Appl. Surf. Sci.*, vol. 254, no. 8, pp. 2441–2449, Feb. 2008.

[7]   "RRUFF™," *University of Arizona*. [Online]. Available: http://rruff.info/magnetite/display=default/R061111.

[8]   R. E. Vandenberghe, C. A. Barrero, G. M. da Costa, E. Van San, and E. De Grave, "Mössbauer characterization of iron oxides and (oxy)hydroxides: the present state of the art," *Hyperfine Interact.*, vol. 126, no. 1–4, pp. 247–259, Jul. 2000.

[9]   G. A. Sawatsky, F. van der Woude, and A. H. Morrish, "Mössbauer Study of Several Ferrimagnetic Spinels," *Phys. Rev.*, vol. 187, no. 01, pp. 747–757, 1969.

[10]   G. A. Sawatzky, "Cation Distributions in Octahedral and Tetrahedral Sites of the Ferrimagnetic Spinel CoFe2O4," *J. Appl. Phys.*, vol. 39, no. 2, p. 1204, 1968.

[11]   S. Mørup, J. A. Dumesic, and H. Topsøe, "Applications of Mossbauer Spectroscopy, vol II," Academic Press, New York, 1980.

[12]   G. F. Goya and H. R. Rechenberg, "Superparamagnetic transition and local disorder in CuFe2O4 nanoparticles," *Nanostructured Mater.*, vol. 10, no. 6, pp. 1001–1011, 1998.

[13]   W. Ramadan, M. I. Zaki, N. E. Fouad, and G. A. H. Mekhemer, "Particle characteristics and reduction behavior of synthetic magnetite," *J. Magn. Magn. Mater.*, vol. 355, pp. 246–253, 2014.

[14]   S. Kameoka, T. Tanabe, and A. P. Tsai, "Self-assembled porous nano-composite with high catalytic performance by reduction of tetragonal spinel CuFe2O4," *Appl. Catal. A Gen.*, vol. 375, no. 1, pp. 163–171, Feb. 2010.

[15]   X. Tan, G. Li, Y. Zhao, and C. Hu, "Effect of preparation method on the surface properties and activity of Ni0.7Cu0.3Fe2O4 nanoparticles," *J. Alloys Compd.*, vol. 493, no. 1–2, pp. 55–63, Mar. 2010.

4. KINETIC AND MECHANISTIC STUDY

In this chapter we report about a study carried out in order to understand the nature of reactions involved in function of the material type and of its degree of reduction during the two steps of the looping process. A first part of the study deals with the study of ethanol adsorption and reaction, performed by means of an "operando" Diffuse Reflectance IR spectroscopy apparatus, equipped with an heated chamber where the catalyst can be placed; a gaseous stream containing ethanol was fed, and the composition of the outlet stream was analyzed by means of an on-line quadrupole mass spectrometer.

The second part deals with tests carried out in the laboratory-scale plant, with a detailed analysis of the reaction products during each step of the cycle process.
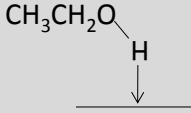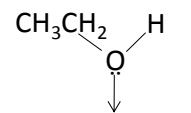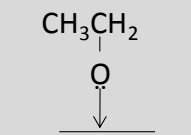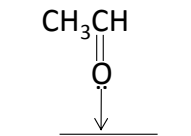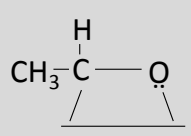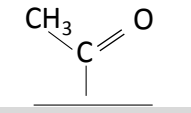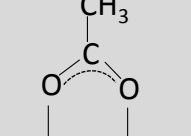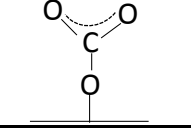
4.1. IN-SITU ("OPERANDO") DIFFUSE REFLECTANCE INFRARED FOURIER TRANSFORM SPECTROSCOPY (DRIFTS) EXPERIMENTS

The aim of this study was to investigate on both how ethanol interacts with the oxidized ferrites, and the nature of products formed by anaerobic oxidation of the alcohol in function of temperature. It can also be expected that during reaction the oxide is progressively reduced, an event which may provide information on the reactivity of each ferrite during the first step of ethanol cycle reforming.

The procedure used for the experiments is described in detail in Chapter 2.2.8. In brief, a stream containing vapors of ethanol and N_2 as the carrier gas was fed to the IR cell; the latter holds the catalyst, maintained at the desired temperature (either isothermal or under a programmed temperature ramp). The apparatus used allow recording the IR spectra of adsorbed species, at the same time recording the mass number of compounds desorbed from the catalyst and contained in the gaseous stream outflowing from the cell.

It is worth first making a brief overview of the typical IR bands reported in the literature, for ethanol adsorbed on various types of metal oxides catalysts. Specifically, Table 4-1 summarizes the most representative intermediates which were found on ferrites with their characteristic bands, according to literature [1]–[3].

Table 4-1. Common species upon ethanol adsorption on ferrites' surface [4]

Species		Characteristic frequency (cm^{-1})
Hydrogen bonded ethanol	CH_3CH_2O ... H	3000-3700 OH ν 1380 CH_3 δ 1500-1200 OH δ (broad)
Chemisorbed undissociated Ethanol	CH_3CH_2 ... H, O	3500-3700 OH ν 1380 CH_3 δ 1270 OH δ (sharp)
Adsorbed ethoxide	CH_3CH_2, O	2970 CH_3 $\nu_{(as)}$ 2930 CH_2 $\nu_{(as)}$ / CH_3 $\nu_{(s)}$ 2875 CH_3 $\nu_{(as)}$ 1107 CO$\nu_{(as)\ monodent}$ 1065 CO$\nu_{(as)\ bident}$ / CC $\nu_{(as)}$
η^1-Acetaldehyde	CH_3CH, O	1650-1700 COν
η^2-Acetaldehyde	CH_3-C-O, H	2755 CHν 1348 CH_3 δ 1275 COν 1148 CC ν 972 CH_3 ρ
Acyl	CH_3, C=O	2978 CH_3 $\nu_{(as)}$ 2901 CH_2 $\nu_{(as)}$ / CH_3 $\nu_{(s)}$ 1636 COν
Acetate	CH_3, C, O ... O	1547 OCO$\nu_{(as)}$ 1445 OCO$\nu_{(s)}$ 1338 CH_3 $\delta_{(s)}$
Carbonate	O ... O, C, O	1547 OCO$\nu_{(as)}$ 1318 OCO$\nu_{(s)}$

According to literature, it is evident that at low temperatures ethanol was mainly adsorbed as ethoxide species; however, increasing temperatures, the species formed

depend on the materials type used, and indeed no common reaction pathway can be identified; therefore, each ferrite will be treated individually.

4.1.1. Temperature-Programmed-Desorption experiments: IR spectra Magnetite - Fe_3O_4
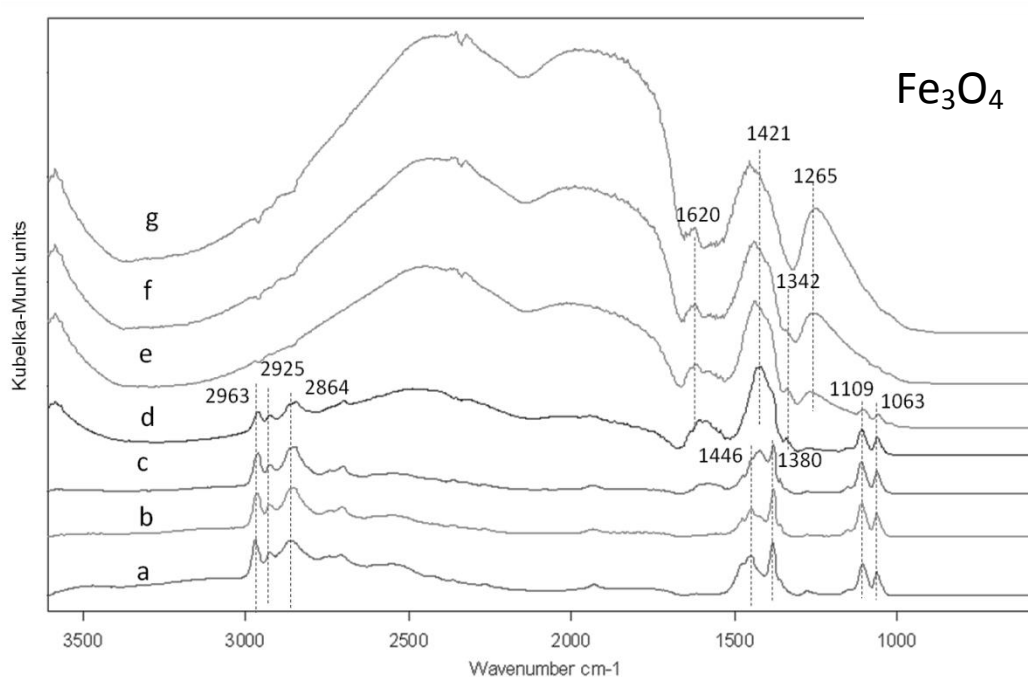

Figure 4-1. DRIFT spectra for Fe_3O_4 annealed in N_2 at 450°C after ethanol adsorption at 30°C (a) and desorption at 150 (b), 200 (c) 250 (d) 300 (e) and 350 (f) and 400°C (g).

Figure 4-1 shows the DRIFT spectra recorded for the magnetite sample after ethanol adsorption at room temperature, and desorption at different temperatures up to 400°C.

In this case, at 30°C it is possible to find bands related to both chemisorbed ethanol (δCH_3 at 1380 cm^{-1}) and ethoxy bands (C-O/C-C stretching at 1063 and 1109 cm^{-1} respectively bi- and mono-dentate). Other bands characteristic to adsorbed ethoxide were found at 2864, 2925 and 2963 cm^{-1}, respectively $CH_3 \nu_{(s)}$, $CH_2 \nu_{(s)}$ and $CH_3 \nu_{(s)}$ [5]. All these bands decreased

their intensity while heating, and disappeared completely between 250 and 300°C. Bands which increase with temperature are those attributable to acetates: the small one at 1342 cm^{-1} for δCH_3 and the broad one at 1421 cm^{-1} for $OCO\nu_{(s)}$, along with the broad band at 1265 cm^{-1} which could belong to η^2-acetaldehyde.

The broad curves formed between 3000 and 1800 cm^{-1} can be due to a partial reduction of the catalyst; in fact, as explained by Busca [6] some semiconducting metal oxides tend to transmit more IR radiation when they are under-stoichiometric, and become opaque when are highly non-stoichiometric.
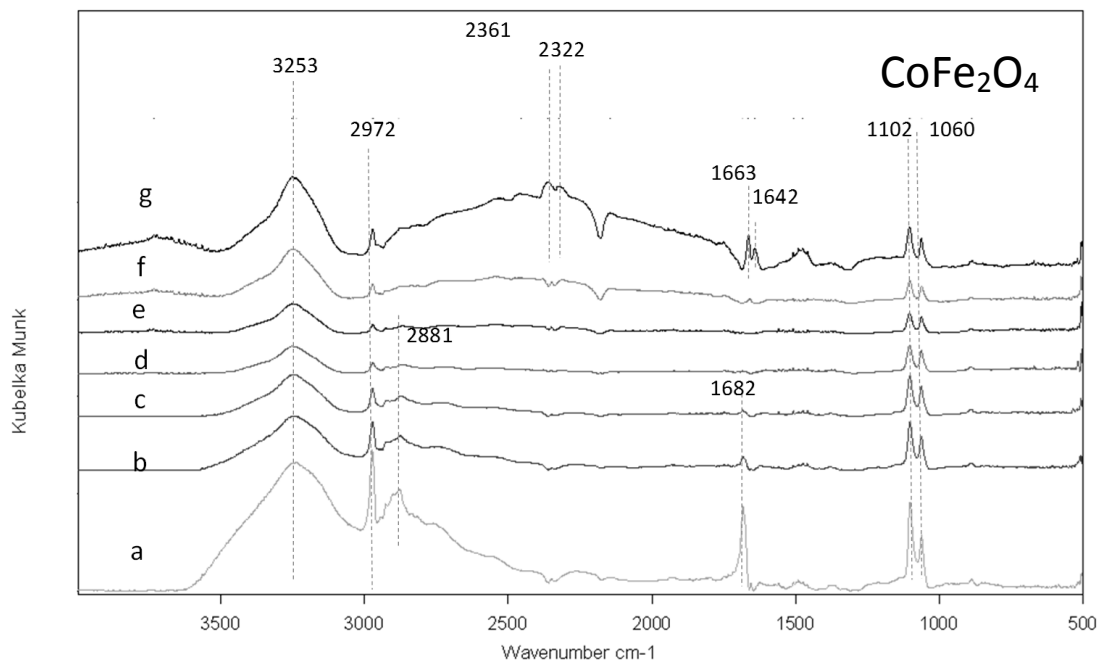
4.1.1.1. CoFe$_2$O$_4$

Figure 4-2. DRIFT spectra for CoFe$_2$O$_4$ calcined at 450°C after ethanol adsorption at 30°C (a) and desorption at 150 (b), 200 (c) 250 (d) 300 (e) and 350 (f) and 400°C (g).

In the case of CoFe$_2$O$_4$ (Figure 4-2), at room temperature the bands of ethanol H-bonded to the surface (OH vibrations at 3253 cm^{-1}) and ethoxide ($CO\nu_{(s)}$ mono- and bi-dentate at

1102 and 1060 cm^{-1} and CH$_{3v(a)}$, and CH$_{3v(s)}$ at 2972 and 2881 cm^{-1}) [5] were clearly visible. Moreover, it is possible to see a band at 1682 cm^{-1} due to adsorbed acetaldehyde, which can be formed from ethanol oxidative dehydrogenation or from disproportionation of ethanol into acetaldehyde and ethane, this reaction being caused by the spinel basicity. Increasing temperature, the H-bonded ethanol band and those attributable to the ethoxide were decreasing, while the band of acetaldehyde disappeared completely at above 200°C.
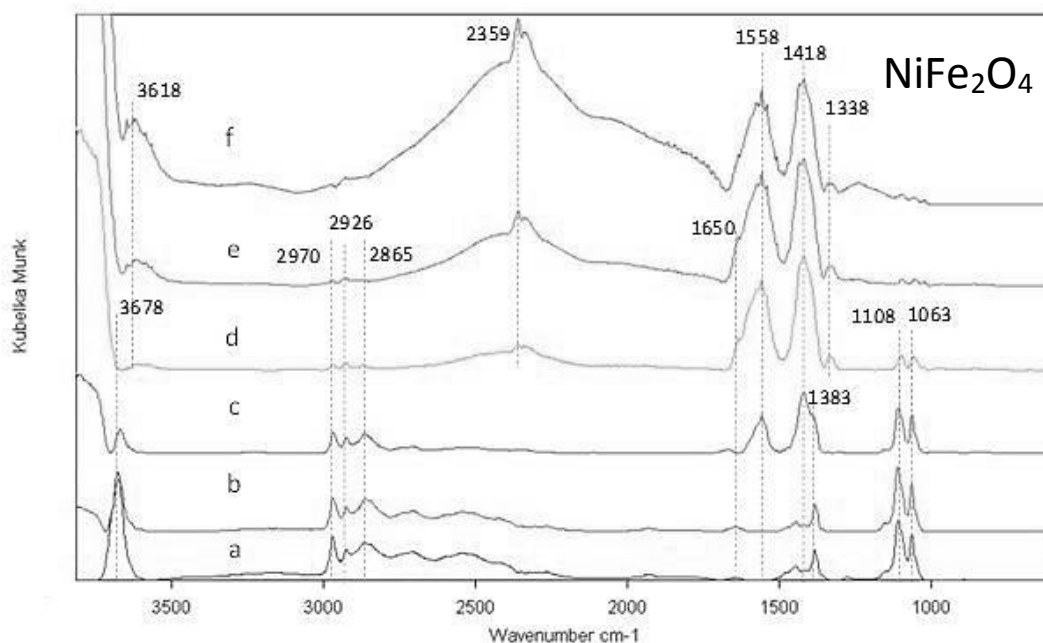
4.1.1.1. NiFe$_2$O$_4$

Figure 4-3. DRIFT spectra for NiFe$_2$O$_4$ calcined at 450°C after ethanol adsorption at 30°C (a) and desorption at 150 (b), 250 (c) 300 (d) 350 (e) and 400°C (f).

Figure 4-3 shows the spectra recorded while feeding ethanol over the nickel ferrite. At room temperature, bands of ethoxide were shown (C-C and C-O stretching at 1063 and 1108 cm^{-1} and CH$_{3v(a)}$, CH$_{2v(a)}$, CH$_{3v(s)}$ at 2970, 2926 and 2865 cm^{-1}), besides those of H-

bonded ethanol at 1383 cm^{-1} (δCH_3 deformation) and some weaker and broader bands between 3000-3500 cm^{-1} due to OH stretching, which soon disappeared when the temperature was raised. Ethoxide bands started to decrease at 250°C and disappeared almost completely after 300 °C. At 250°C, characteristic bands of acetate species appeared at 1338, 1418 and 1558 cm^{-1} (corresponding respectively to δCH_3, $OCOv_s$ and $OCOv_{as}$ vibrations) [7].

The broadening of the band at 1558 cm^{-1} suggests carbonates formation, that also would have OCO stretching frequency at this wavenumber. These species could further produce CO_2, as shown by the band at around 2359 cm^{-1}, the intensity of which started to increase at 300°C. The shoulder at about 1700-1650 cm^{-1} can be assigned to the C=O stretching of acetaldehyde, which can be rapidly oxidized to acetate species, as suggested earlier by Yee et al [8]. As in the case of magnetite, the broad growing feature at 3000-1800 cm^{-1} at temperature higher 350 °C can be due to the material reduction [6].
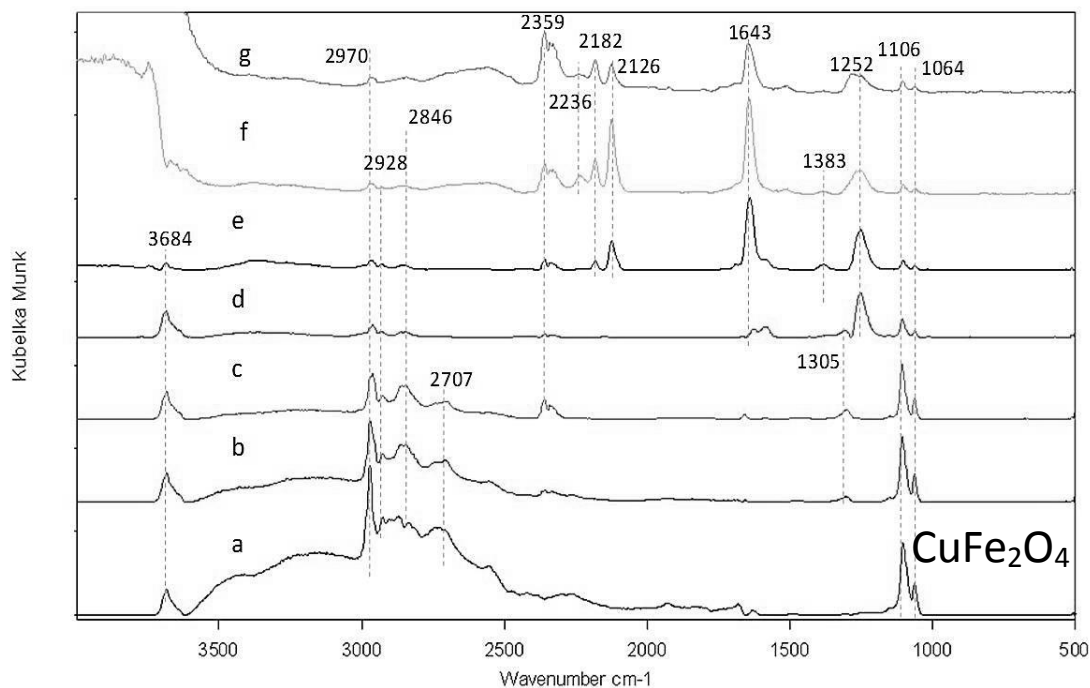
4.1.1.1.CuFe₂O₄

Figure 4-4. DRIFT spectra for CuFe₂O₄ calcined at 450°C after ethanol adsorption at 30°C (a) and desorption at 150 (b), 200 (c) 250 (d) 300 (e) and 350 (f) and 400°C (g).

Regarding the adsorption at low temperature, the behavior was not different from that shown by other ferrites; ethanol was adsorbed on the surface either in a molecular form or in the dissociated form as an ethoxide (bands at 1064 and 1106 cm^{-1}) (Figure 4-4). Already at 250 °C, new bands appeared; the most prominent at 1252 cm^{-1} can be attributed to adsorbed acetaldehyde in the η^2 configuration, which is favored over the partially reduced sample. Afterwards (at 300°C) an intense band at 1643 cm^{-1} appeared, and some other smaller at 2126 and 2182 cm^{-1}, corresponding to the formation of acyl species and of decomposition products (CO and methyl species). The latter species can recombine to release ethane, which formation was also observed by Padilla et al [9]. This

assignment is in agreement with the results of the TPD analysis performed on this sample, which will be shown in the next paragraph.

4.1.2. Temperature Programmed Desorption (TPD) experiments: analysis of the gas-phase

Gaseous species desorbed from the ferrites while increasing temperature during the DRIFT experiments have been analyzed on-line by means of the quadrupole mass spectrometer.

Figure 4-5 plots the m/z signals attributable to the various chemical species desorbed from the catalyst, in function of the temperature of desorption, for the magnetite sample. Ethanol was pre-adsorbed on the sample at 30°C.
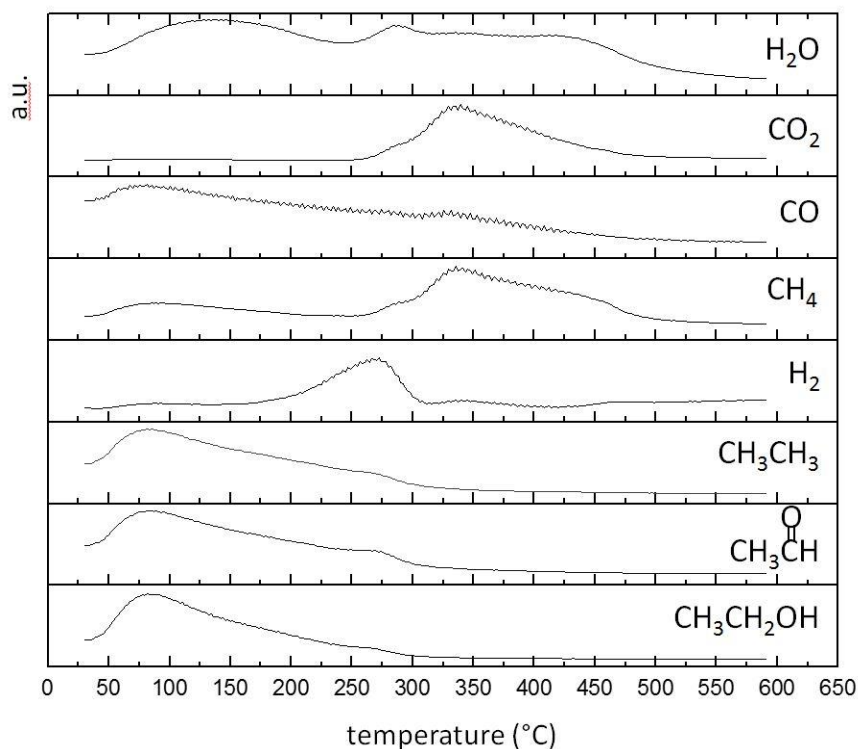

Figure 4-5. TPD profiles (m/z signals) of species desorbed from Fe$_3$O$_4$ after ethanol adsorption at 30°C. Mass profiles are not shown in the same intensity scale, but have been modified in order to better show the trends.

Results obtained confirm DRIFTS experiments. In fact, at low temperatures desorption of both ethanol and acetaldehyde occurred (the latter formed by ethanol oxidative dehydrogenation); the formation of ethane is attributable to the disproportion of ethanol, leading to the co-formation of the alkane and of acetaldehyde. At around 270 °C, the signal of hydrogen desorption, formed by ethanol dehydrogenation, was also shown. At higher temperature, a larger desorption signal of CO_2, with a maximum at around 340°C, was observed, which agrees with the observed reduction in the DRIFT spectra. Methane, CO and water were observed in this temperature range; this can be explained by the decomposition of acetaldehyde and direct oxidation to CO_2 and water.
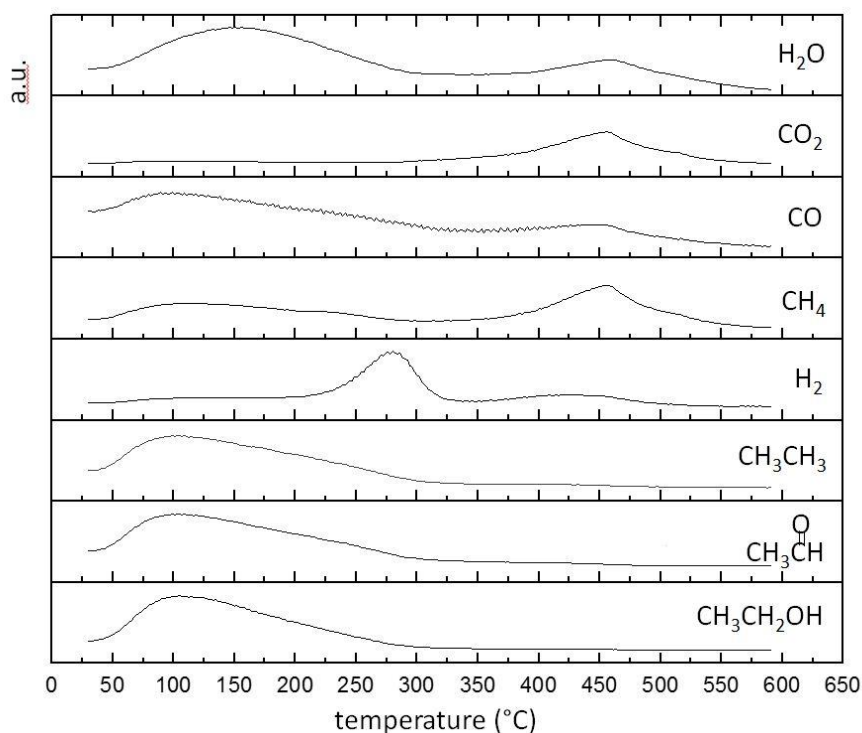

Figure 4-6. TPD profiles (m/z signals) of species desorbed from CoFe$_2$O$_4$ after ethanol adsorption at 30°C. Mass profiles are not shown in the same intensity scale, but have been modified in order to better show the trends.

During ethanol TPD analysis with the cobalt ferrite catalyst (Figure 4-6), methane and CO were observed at low temperature; this can be due to the decomposition of acetaldehyde. Hydrogen desorption was shown at between 250 and 300 °C; this might be due to the fact that the hydrogen formed by ethanol dehydrogenation into acetaldehyde (which occurred over the entire temperature range) remained adsorbed on catalyst, and was then desorbed in this temperature range as observed also by Noronha et al. [10]. An alternative interpretation is that at low temperature acetaldehyde formed by disproportion of ethanol, and not by ethanol dehydrogenation. Conversely, the latter reaction might occur in the T range where hydrogen also formed. In the high temperature range (T > 300 °C), formation of carbon monoxide, methane, carbon dioxide and water were observed (with maxima at around 450 °C). This indicates that the adsorbed species (ethanol, ethoxy and acetaldehyde) were decomposed and oxidized, but at higher temperature than for the nickel ferrite (see below). It is worth noting that DRIFTS experiments highlighted no formation of acetates; this agrees with the results of TPD experiments. In fact, the amount of methane and CO_2 formed with the cobalt ferrite (both products being formed by acetate decomposition) was lower than with the nickel ferrite. On the other hand, there was no H_2 desorption in the high temperature range. On cobalt ferrite, the acetaldehyde formed by ethanol dehydrogenation was more weakly bound than on nickel ferrite. Therefore, with the cobalt ferrite most of acetaldehyde desorbed into the gas phase leading to a more intense m/z signal than with the other catalysts. On the contrary, with nickel ferrite (Figure 4-7) the aldehyde was more strongly bound to the surface, and easily oxidized into acetates, which were finally decomposed in the high temperature range.
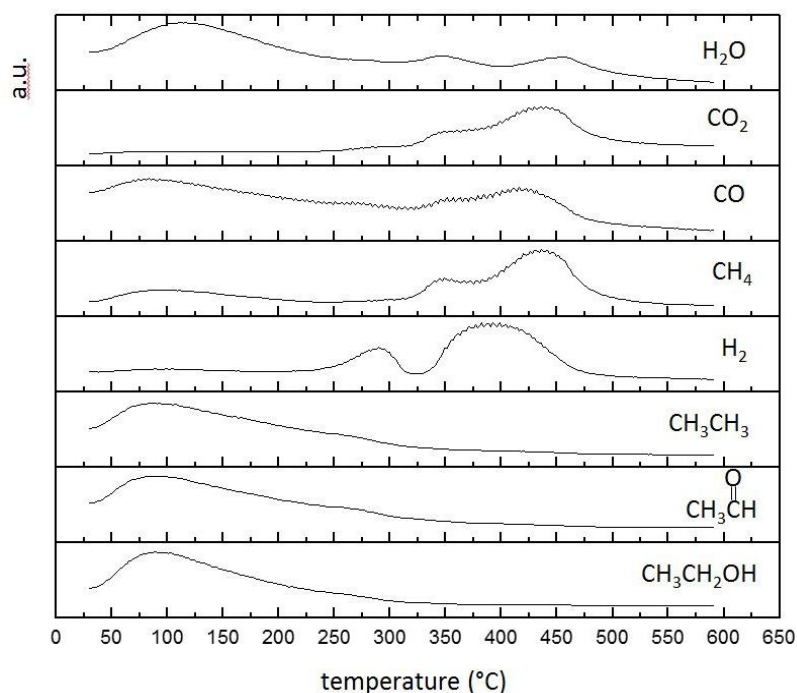
Figure 4-7. TPD profiles (m/z signals) of species desorbed from NiFe$_2$O$_4$ after ethanol adsorption at 30°C. Mass profiles are not shown in the same intensity scale, but have been modified in order to better show the trends.

In the case of Nickel ferrite (Figure 4-7), once again at low temperatures it is possible to see the desorption of ethanol adsorbed on the surface, and its disproportionation into acetaldehyde and ethane. Hydrogen desorbed at 230 °C, which is the same temperature at which the acetates also formed. After 315°C, desorption of methane was shown, that could be related to the formation of the carbonate species from the observed acetates. The very similar trends of CO$_2$ and CH$_4$ support this hypothesis. The same behavior was shown by CO, indicating that acetaldehyde is also being decomposed into methane and CO, which could come from carbonate species.
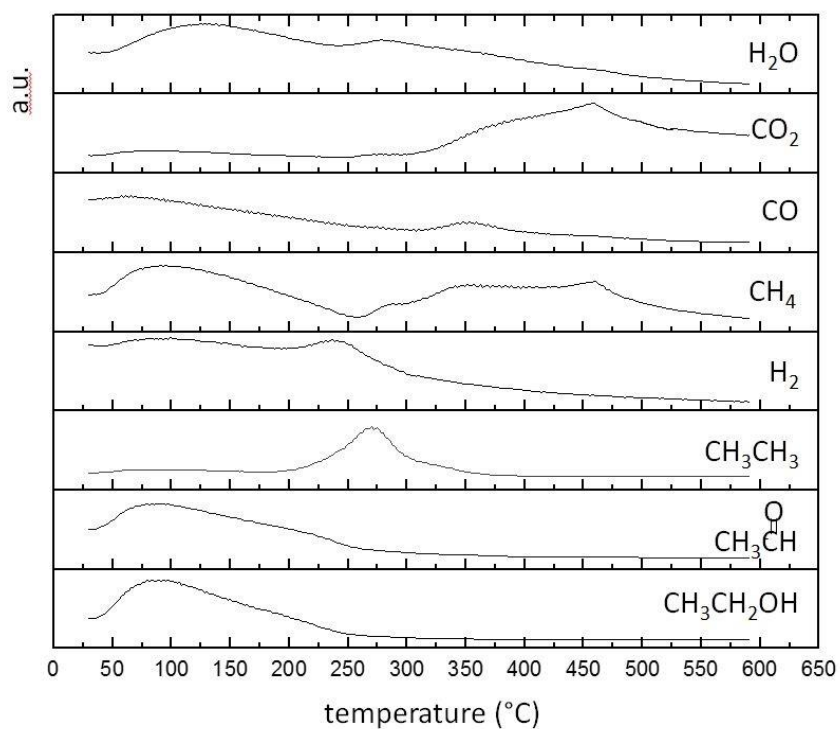
Figure 4-8. TPD profiles (m/e signals) of species desorbed from CuFe$_2$O$_4$ after ethanol adsorption at 30°C. Mass profiles are not shown in the same intensity scale, but have been modified in order to better show the trends.

The low-temperature behavior of the copper ferrite (Figure 4-8) was similar to that shown by the other catalysts, with ethane release in the middle range temperature (200-350°C). However, in contrast to what observed with the other catalysts, a certain amount of hydrogen was released in this temperature range. At high temperature (> 350°C), mainly carbon dioxide and methane formed.

4.1.3. Conclusions on the DRIFTS-MS study

From the results of the experiments shown in this paragraph, it is possible to hypothesize the reaction pathways shown in Figure 4-9.
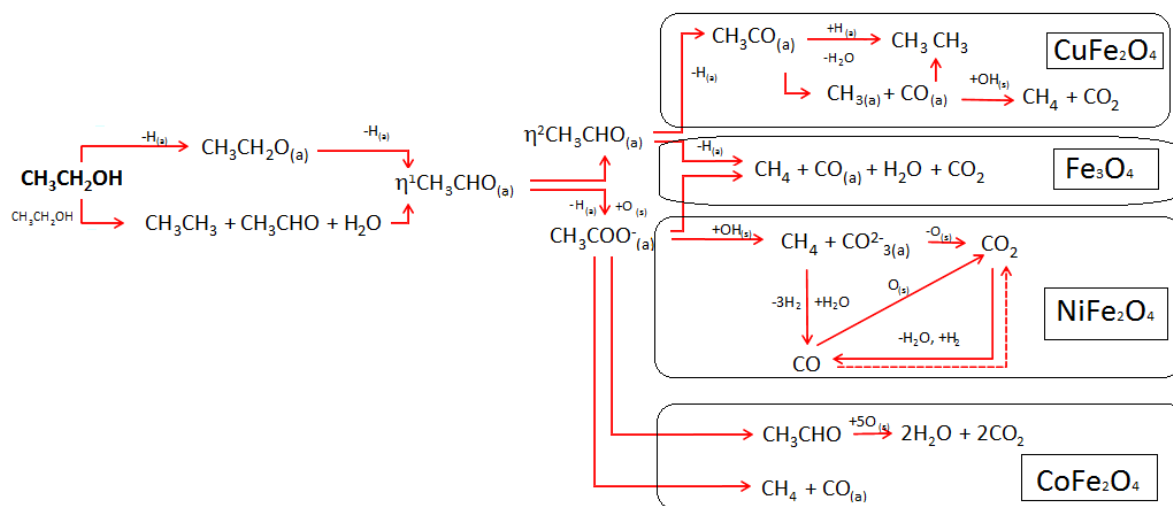

Figure 4-9. Proposed reaction pathways for ethanol anaerobic oxidation on the different ferrites

The first part on the left side of the scheme is common to all materials, and shows the reactions involved at low temperatures such as, for example, the adsorption of ethanol as ethoxide and its disproportionation to give ethane and acetaldehyde. Both of these reactions led to the formation of adsorbed η^1-acetaldehyde, which was weakly bound and very reactive; due to these reasons, sometimes it was not even detected by means of DRIFT spectroscopy. This species can evolve either to the η^2-acetaldehyde (observed at higher temperatures) in the case of magnetite and copper ferrite, or to the acetate species, in case of cobalt and nickel ferrites. Starting from this point, the reactions follow different pathways depending on the material used:

- In the case of **CuFe₂O₄**, the η^2-acetaldehyde is transformed into acyl species, which can saturate to ethane or be further decomposed to CO and methyl species. These can further recombine to give ethane or CO_2 and CH_4, both observed by means of TPD at high temperature.

- Both η^2-acetaldehyde and acetates can form the same products in the case of **Fe$_3$O$_4$**. Since at high temperatures no carbonates bands were detected and no H$_2$ was produced, as seen from the TPD, it is possible to suggest that the main reactions involved were the direct oxidation and decomposition to methane, water and carbon oxides.

- With **NiFe$_2$O$_4$**, the acetates formed by acetaldehyde oxidation, were further decomposed into methane and carbonates (both observed by means of DRIFTS), released as CO$_2$ (observed by means of TPD). CO$_2$ could form, together with H$_2$ (observed only with this ferrite), from water-gas-shift or methane reforming and CO oxidation.

- With **CoFe$_2$O$_4$**, acetaldehyde was observed at low temperatures, which indicates that on this material this molecule is less reactive than on the other ferrites, and only at higher temperatures the acetates gave oxidation and decomposition products.

4.2.   THE ETHANOL STEAM-IRON PROCESS

In order to understand the behavior of the different materials in the chemical loop process of ethanol reforming, the four synthesized ferrites (Fe_3O_4, $CoFe_2O_4$, $NiFe_2O_4$ and $CuFe_2O_4$) were tested using the operative conditions and the laboratory-scale plant described in chapter 2.3.1.

4.2.1. Choice of the operating conditions

Operative conditions were chosen based on the study previously made by Cocchi during his PhD work [11]. The parameters, formerly found to be the optimal ones from methanol, were then used in experiments with ethanol as the reactant. However, we decided to first check whether the temperature range used for ferrites reduction with methanol were usable with ethanol also. In this aim, we carried out an experiment with the cobalt ferrite spinel, at 400°C, for 1 h reaction time, and characterized the material after the reaction. It is worth noting that under these conditions and with methanol as the reducing agent, complete reduction of the spinel was achieved [11]. It should be noted also that the aim of our initial set of reactivity experiments was that of achieving complete reduction of the ferrite also with ethanol, in order to establish relationships between the degree of ferrite reduction and the catalytic behavior.

The reduction with ethanol was carried out for 1h at 400°C, and then the material was characterized by means of XRD and Mössbauer spectroscopy (Figure 4-10 and Figure 4-11).
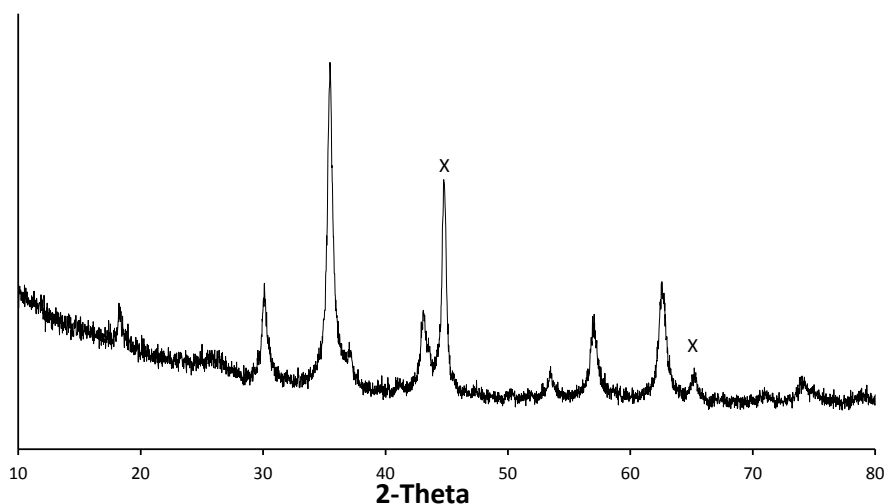
Figure 4-10. XRD pattern of CoFe$_2$O$_4$ after 1h reaction with ethanol at 400°C (x=Co$_3$Fe$_7$) (testing conditions: 0.4g catalyst, ethanol feed rate 0.52 ml/h, N$_2$ flow 30 ml/min).

From the X-ray diffraction pattern it is possible to note that the peaks were slightly sharper than in the case of the fresh material, that indicates an increase of the crystal size due to sintering. Moreover, it is possible to say that the reduction was far to be complete; in fact, the main phase still remained the ferrite, and only part of it had been reduced to a Co$_3$Fe$_7$ alloy (peaks marked with x at 46° and 66° 2θ in Figure 4-10, (ICSD 00-048-1816)). A small broad peak at 26° shows the presence of coke (ICSD 00-026-1077).
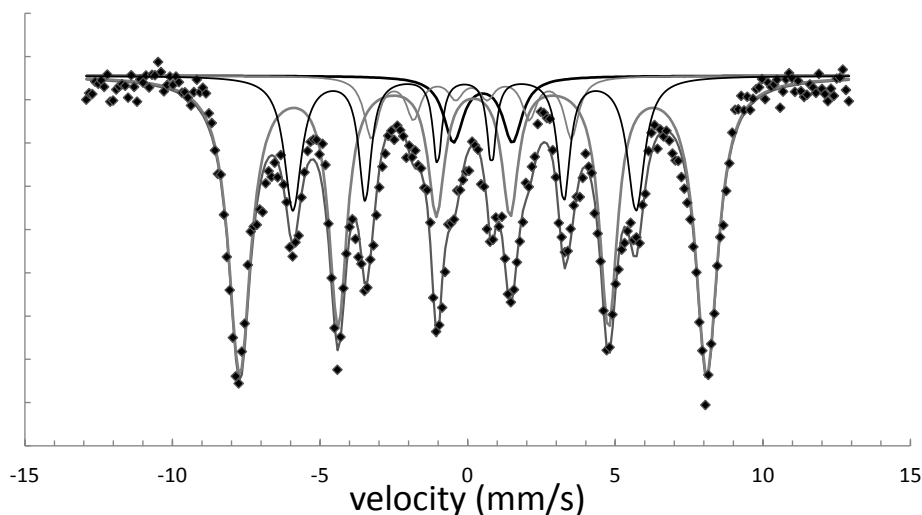
Figure 4-11. Mössbauer spectrum of the CoFe$_2$O$_4$ sample after 1h reaction with ethanol at 400°C, recorded at 25°C; the solid line is derived from least-square fit.

The Mössbauer spectra on the cobalt ferrite reduced at 400°C is shown in **Figure 4-11**. The spectrum was fitted considering one doublet and 3 sextets. The doublet characterized by an IS equal to 0.63mm/s and a QS equal to 2.00mm/s, contributed for 6% of the total spectral area and could be related to the presence of Fe^{2+}, while the smaller sextet (9%) can be attributed to Fe$_3$C (IS 0.24mm/s; H$_{eff}$ 20.9T). A second sextet (IS -0.00mm/s; H$_{eff}$ 35.9T) represents reduced Fe^0 which was the 22% and should correspond to the Co$_3$Fe$_7$ alloy; while the broader sextet (IS 0.30 and H$_{eff}$ 48.9) was attributed to the remaining ferrite (63 % of spectral area). Actually, normally the ferrites are characterized by two sextets that belong respectively to the Fe^{3+} species in the tetrahedral sites, and the mixed valence species Fe$^{2.5+}$ in octahedral sites very close one to each other. Here, since it is certainly not well crystallized, it has been fitted with only one large sextet.

From the results obtained it appears that the ferrite used for the chemical reduction with ethanol at 400°C was only partially reduced, and that therefore it could be more efficiently used if it were totally reduced. Because of these reasons it was decided to carry out the spinel reduction with ethanol at 450°C.
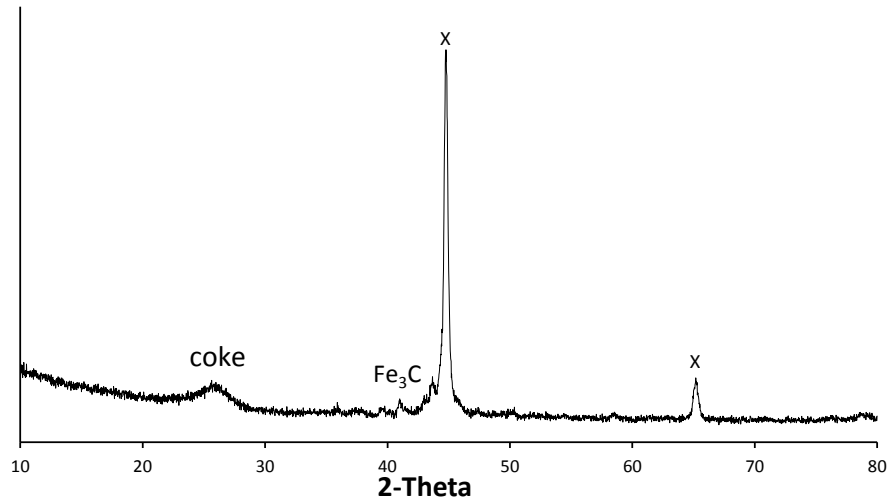
Figure 4-12. XRD pattern of CoFe$_2$O$_4$ after 1h reaction with ethanol at 450°C (X=Co$_3$Fe$_7$). Other experimental conditions as in Figure 4.10.

The comparison of the diffractograms recorded for the cobalt ferrite after reaction at 450°C (Figure 4-12) and at 400°C (Figure 4-10) shows that at the higher temperature the material had been completely reduced. In fact, the pattern showed the reflections of the Co$_3$Fe$_7$ alloy only, characterized by reflections at 46° and 66° 2θ. The drawback is that in this case the reflections were even sharper than after reduction at 400°C, a clear indication of the occurrence of strong sintering phenomena; moreover, the coke signal also was more intense. It is also possible to see the presence of metal carbide that was not shown after reaction at 400°C.
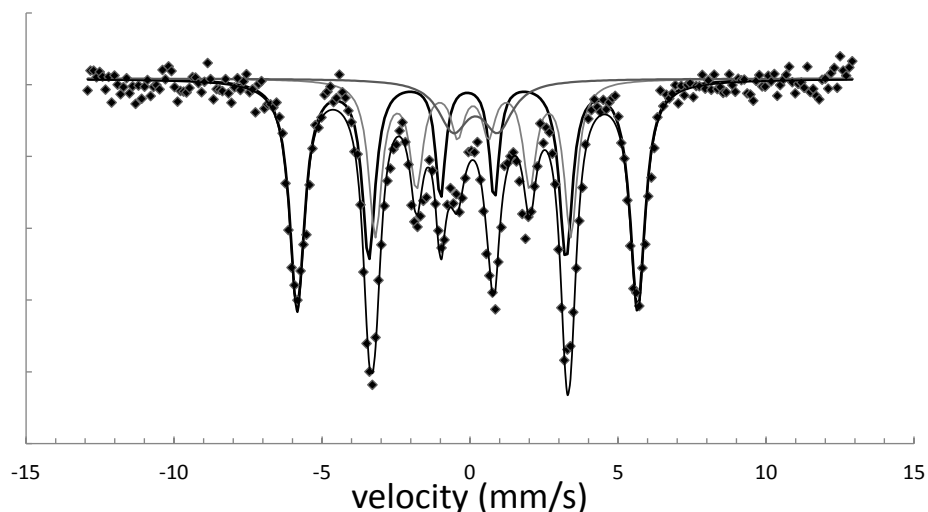
Figure 4-13. Mössbauer spectrum of the CoFe$_2$O$_4$ sample after 1h reaction with ethanol at 450°C, recorded at 25°C; the solid line is derived from least-square fit.

The Mössbauer spectrum of the sample has been fitted with two sextets and one doublet (Figure 4-13). The doublet (IS 0.29 mm/s; QS 1.50mm/s) representing 11% of the total spectrum, could correspond to nanoparticles of an Fe^{3+} phase, maybe a carburized amorphous Co and Fe oxide resulting from the incomplete transformation of the ferrite. The sextet (IS 0.21mm/s; H$_{eff}$ 20.4T; I=33%) corresponds to the carbide Fe$_3$C and the sextet (IS 0.02mm/s; H$_{eff}$ 35.5T; I=56%) to Fe^0 in to the Co$_3$Fe$_7$ alloy.

After these preliminary experiments, we decided to carry out the first set of reduction tests on the other ferrites at the temperature of 450°C.

4.2.2. The 1st step of chemical loop reforming: anaerobic oxidation of ethanol

Preliminary experiments were carried out in the aim of identifying the reaction products during the anaerobic ethanol oxidation, in function of temperature. Heavier compounds were identified by means of accumulation in ethanol for 1 h, and GC-MS analysis. The light products (CO, CO$_2$, CH$_4$, H$_2$) were instead on-line sampled and analyzed by means of a

micro-GC. Main $C_{>1}$ products were: ethylene, ethane, acetaldehyde, propene, acetone, acetic acid, diethyl ether, and ethyl acetate. One general consideration is that the aim of the cycle (chemical loop) process would be to oxidize completely ethanol in the absence of oxygen over the spinel during the first step, and then re-oxidize the reduced spinel with steam to produce hydrogen during the second step. However, a considerable amount of H_2 was also produced during the first step.

In general, the nature and amount of by-products was affected by reaction time; in fact, it has to be reminded that the reaction was carried out in the absence of oxygen, which implies that the spinel underwent reduction during time-on-stream. Other products were butenes, benzene, 2-pentanone, 4-penten-2-one, 3-penten-2-one, xylenes, 2-heptanone and even some C_8/C_9 compounds. Amongst the latter, the product formed in the greater quantity was 2-pentanone. It is worth noting that all $C_{>1}$ compounds take account for an overall selectivity which is 20-25%. A possible pathway for the synthesis of heavier ketones is reported in the literature [5]; the mechanisms leading to the formation of ketones are summarised in Figure 4-14.
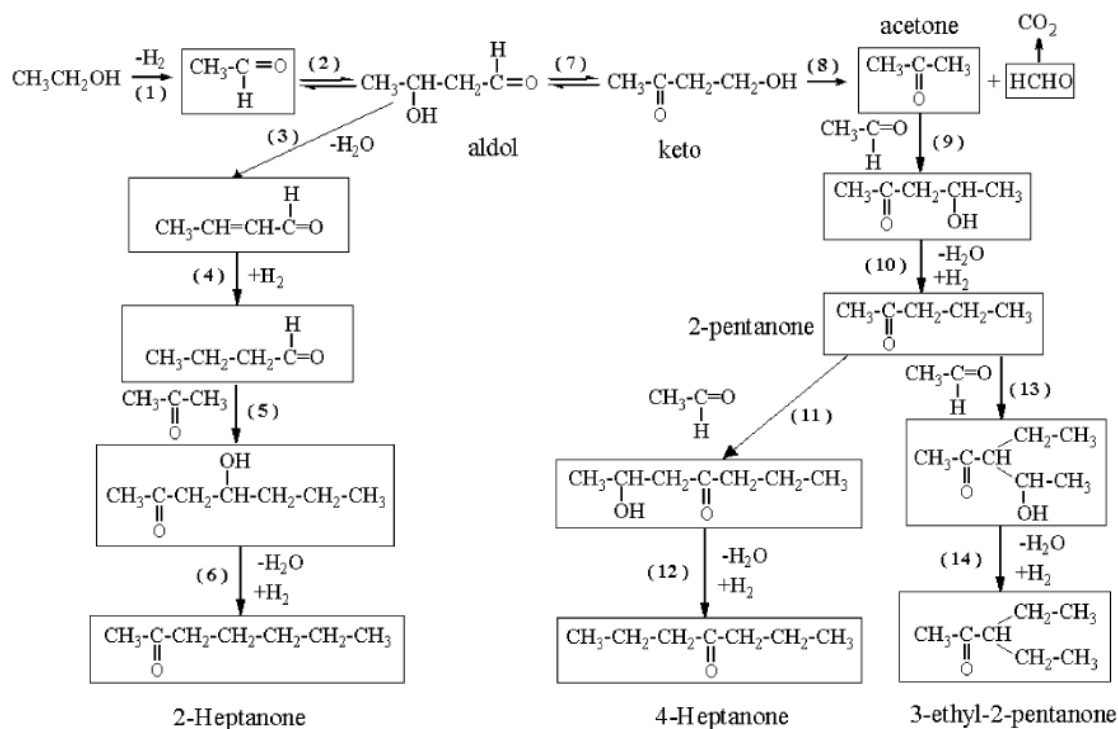
Figure 4-14. Possible reaction pathways for the formation of pentanones and heptanones from ethanol (taken from ref [5]**).**

It is also shown that all of these products form starting from acetaldehyde. In fact, with methanol much fewer products were formed, because formaldehyde lacks the acid α-hydrogen required for aldol condensation. It is clear that all these products will increase the deposition of organics on the solid surface, precursors for the formation of carbonaceous residua. Another factor contributing to ethanol decomposition and coke formation and "hardening", is the degree of spinel reduction. It will be shown later that using shorter reduction time and milder conditions, the amount of residues can be decreased. Another option for the reduction of coke content might be co-feeding steam in less-than-stoichiometric amount during the reduction step (which would correspond to carry out a partial ethanol reforming). Indeed, since the removal of water contained in bio-ethanol implies expensive procedures, the azeotropic mixture is a cheaper and more available reactant than dry ethanol.

Hereafter are reported the trends of yields and conversion obtained during the anaerobic oxidation of ethanol with the various ferrites, in function of time-on-stream. Reaction conditions used are reported in chapter 2.3.1.
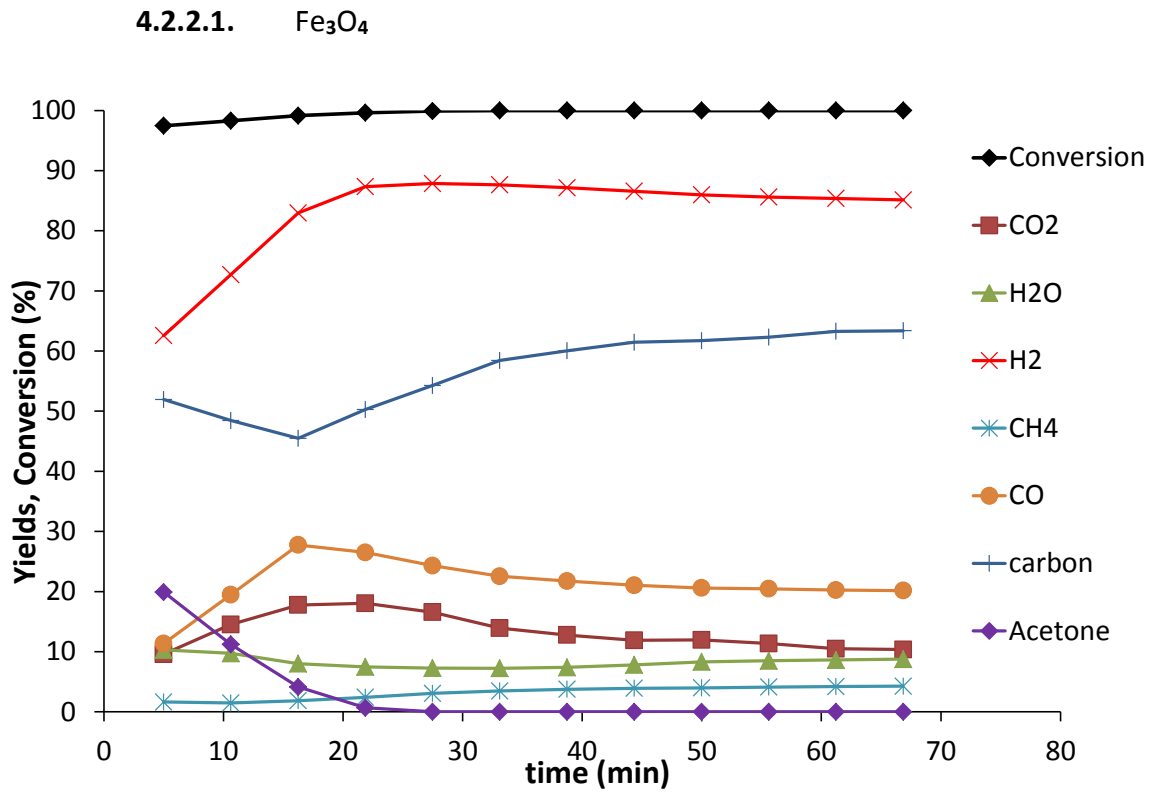
4.2.2.1. Fe_3O_4

Figure 4-15. Conversion and yields o main products during 1h reduction with ethanol at 450 °C on Fe_3O_4

Figure 4-15 reports conversion and yields into main products (those having yield > 2%), obtained during the reaction of ethanol at 450°C with magnetite. Ethanol conversion was close to 100 % from the first minutes of the reaction, and became complete in a few minutes. The main product was hydrogen with an initial yield of 60%, and in 15 min it increased until 85 %. The first 15-20 min is the period of time during which most of the products yield trend changed. This indicates that during this time the material, which at the beginning acted as a reagent, being fully oxidized, rapidly approached the highest reduction degree at the conditions used. Thereafter, it did not change its composition

anymore, because it could not be reduced further, and started acting as a true catalyst; the behavior thus became more stable during time.

Since CO, CO_2 and H_2 yield all showed similar increasing trends, this suggests that main reactions occurring during the initial period was the partial oxidation of ethanol:

- $C_2H_5OH + MeO \rightarrow 2\ CO + 3\ H_2 +\ Me$
- $C_2H_5OH + 3\ MeO \rightarrow 2\ CO_2 + 3\ H_2 + 3\ Me$

At the beginning there was also a relatively high yield to acetone, that however decreased during time. Its formation can be explained by taking into account aldol condensation of the intermediately formed acetaldehyde, followed by isomerization of aldol into the hydroxyketone, and by reverse aldol reaction to yield acetone and formaldehyde. The latter was converted into CO_2 and H_2 as explained in Figure 4-14.

Water yield was around 10% and quite constant during reaction. Water can be produced from several reactions:

- $C_2H_5OH + 6\ MeO \rightarrow 2\ CO_2 + 3\ H_2O + 6\ Me$
- $H_2 + MeO \rightarrow H_2O + Me$
- $C_2H_5OH \rightarrow 2\ C + 2\ H_2 + H_2O$

Finally is possible to note that the yield to "carbon residues" (that is calculated taking into account the C balance, the latter being evaluated from the H balance) first decreased, and then started to decrease at around 15 min. Some tests, described later in this thesis, will allow us to conclude that the initial trend was due to the very quick formation of iron carbides, which was the very first reduced iron species to form. Yield to this species was decreasing because the oxidized solid was progressively being consumed; however, at the same time, accumulation of carbonaceous deposits occurred on the surface. So, when the material was completely reduced and no more carbides were being formed, the carbon balance loss, and consequentially the "carbon" yield, increased. This carbon could be produced from dehydrogenation and total deoxygenation of ethanol:

$CH_3CH_2OH \rightarrow C + CO + 3\ H_2$

$$CH_3CH_2OH \rightarrow 2\ C + H_2O + 2\ H_2$$
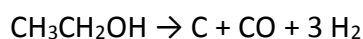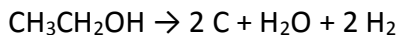
as well as from CO disproportionation (Boudouard reaction):

$$2\ CO \leftrightarrows CO_2 + C$$
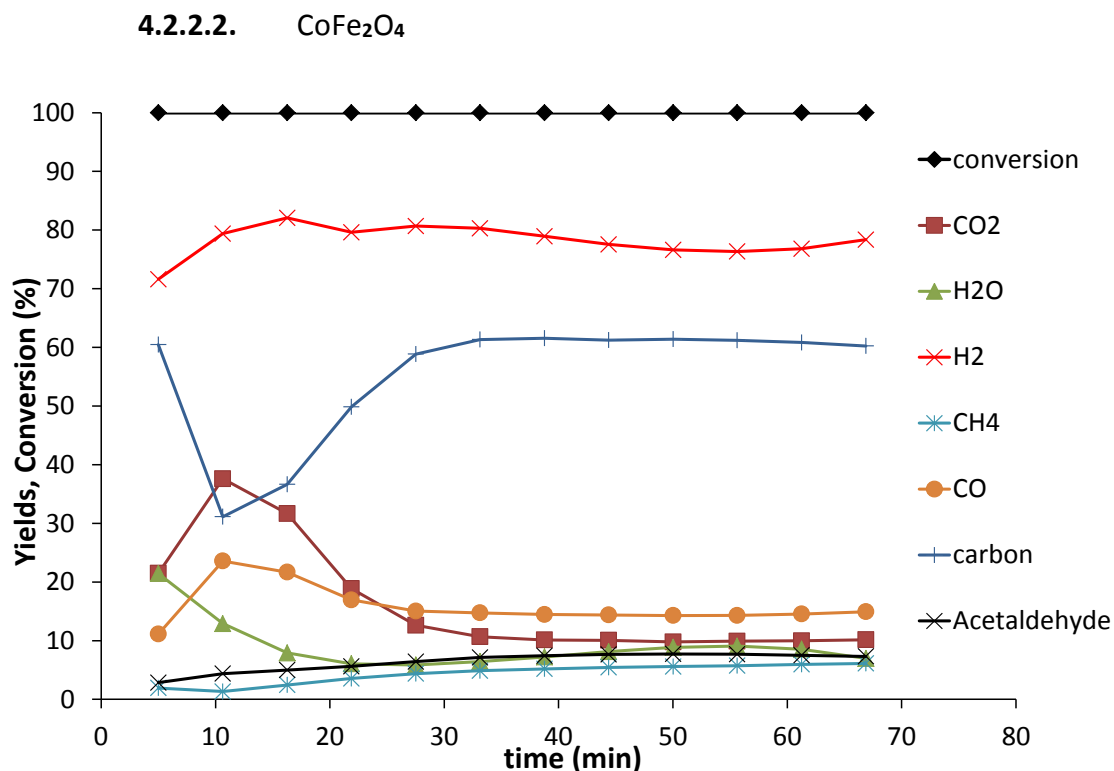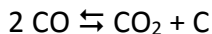
4.2.2.2.   CoFe$_2$O$_4$

Figure 4-16. Conversion and yields in main products during 1h reduction with ethanol at 450 °C on CoFe$_2$O$_4$

In the case of Co ferrite (Figure 4-16), ethanol was converted completely already from the very beginning of the experiment. Hydrogen yield was 70-80 %, slightly less than in the case of magnetite; however the Co ferrite led to a higher yield to CO$_2$ and H$_2$O, with less CO, which indicates the stronger oxidative properties of this catalyst. Moreover, acetone yield was very low, and correspondingly it seems that the acetaldehyde produced was not further converted. These two facts are related, since acetone formation starts from acetaldehyde. This result also agrees with DRIFTS-MS experiments, which highlighted that

on cobalt ferrite acetaldehyde was less reactive. Yield to methane was similar to that obtained with magnetite.
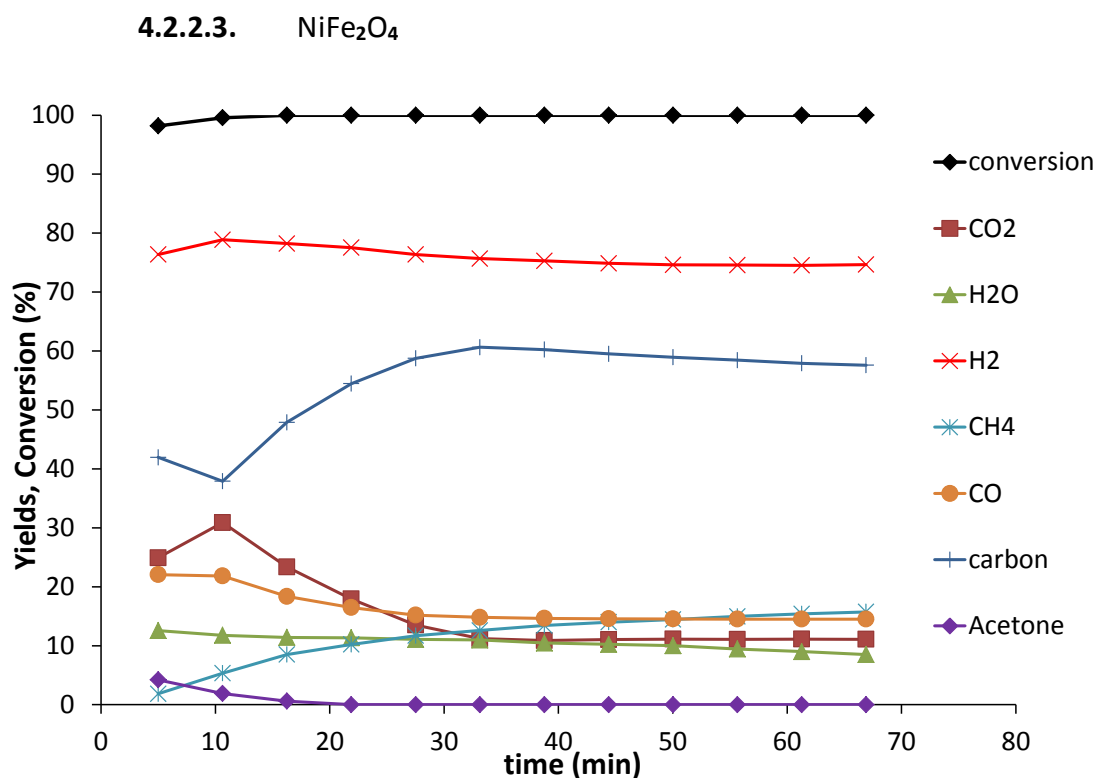
4.2.2.3.   NiFe$_2$O$_4$

Figure 4-17. Conversion and yields in main products during 1h reduction with ethanol at 450 °C on NiFe$_2$O$_4$

Results obtained with nickel ferrite (Figure 4-17) demonstrate the high activity of this material; in fact, ethanol conversion was almost complete since the very first reaction time. At the beginning of the reaction, a high yield to oxygenated products (CO, CO$_2$ and H$_2$O) was shown, whereas when the metallic behavior of the solid started to predominate, methane became one of the prevailing products. Acetone was produced only during the first minutes of reaction; later on, the reactions of reforming and dehydrogenation became the predominant ones.
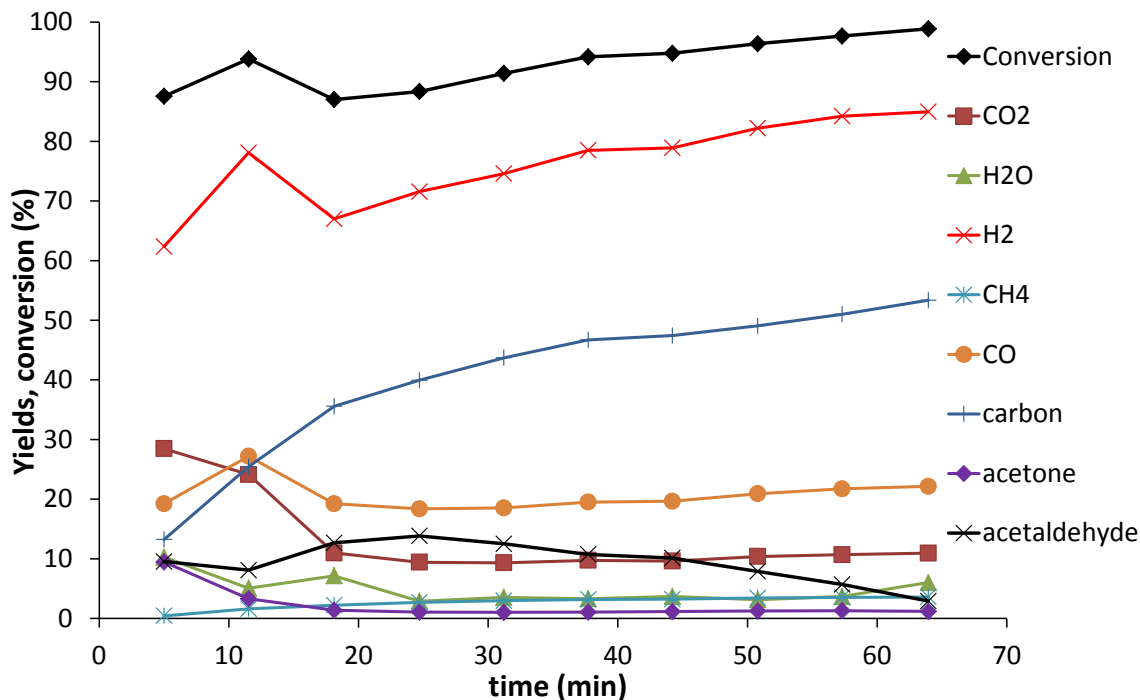
4.2.2.4. $CuFe_2O_4$

Figure 4-18. Conversion and yields in main products during 1h reduction with ethanol at 450 °C on $CuFe_2O_4$

In the case of copper ferrite (Figure 4-18) ethanol conversion during the first minutes of reaction was 85%, and then increased during time; however even after 1h of reaction it was not complete. Hydrogen yield started from 60% and increased up to 80%. Carbon production was very low at the beginning, but then suddenly increased; after 1h of reduction it reached values around 50%. The other predominant products were carbon oxides and acetaldehyde. CO_2 showed an initial yield of 30%, and it stabilized after 20 minutes at values around 20%, while CO yield was stable at about 20% from the beginning of the reaction. Acetaldehyde yield was high compared to the other ferrites, with values ranging between 10-15% at the beginning, then decreasing after the first 25 min reaction time, probably because of the increase of concentration of metallic sites, which favored acetaldehyde decomposition.

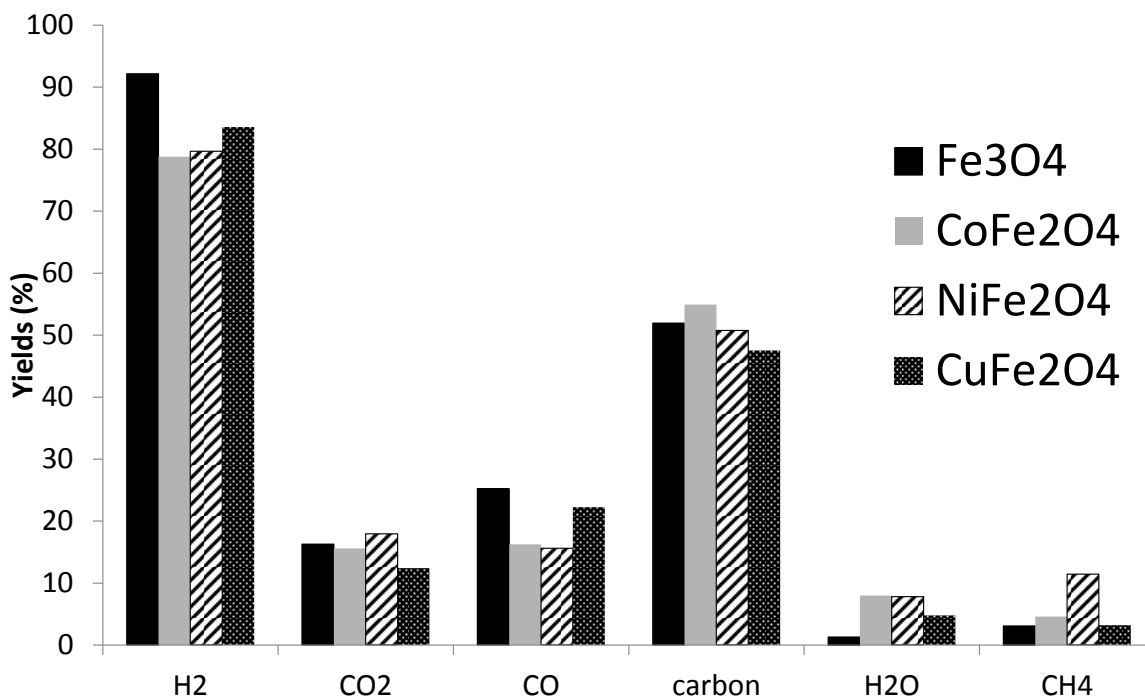### 4.2.3. Conclusions on the 1st step tests

Figure 4-19. Integrated yields to the main products obtained feeding ethanol for 1h at 450°C on the different ferrites.

Figure 4-19 reports the yields to the main products obtained during the first step with the different ferrites; the values were obtained by integrating the curve reporting instantaneous yields in function of time-on-stream. It is possible to distinguish two main different behaviors:

1. **Fe_3O_4** and, less pronouncedly, **$CuFe_2O_4$** produced more hydrogen and more CO than the other two ferrites, which indicates that these two materials favor reactions like:

   - $C_2H_5OH + MeO \rightarrow 2\ CO + 3H_2 +\ Me$
   - $CH_3CH_2OH \rightarrow C + CO + 3H_2$

2. **$CoFe_2O_4$** and **$NiFe_2O_4$** both produced more water and, in case of nickel ferrite, also more methane. Moreover, with the former system greater yield to acetaldehyde was also achieved.

All materials produced similar amounts of CO_2 and carbon; the latter is the main issue of this process. In overall the ferrites used showed the greater differences at the beginning of the reaction time, when they were still oxidized.

The (unexpected) high yield to H_2, which is not the target product during the first step, is a positive aspect of the process, because the gas produced during the first step could be used to give the energy for heating up the system, or could be eventually sent to an H_2-enriching system like a WGS reactor.

Since the chemical behavior of the different ferrites over a prolonged reaction time was similar, it will be important to check their structural modifications and the possibility to restore the original structure by steam oxidation, in order to decide which one of the four systems investigated is the most promising one.

4.3. THE 2ND STEP OF THE CHEMICAL LOOP: WATER REDUCTION ON REDUCED

FERRITES

Tests were carried out on the same apparatus used for the reduction step, feeding water by means of a syringe pump at 450°C, for 1 hour, after the reduction step. The gas mixture outflowing from the reactor was first passed through a water trap, in order to avoid a higher water concentration which could be harmful for the micro-GC columns. The analytical method used allowed us to carry out an analysis every few minutes. Reaction conditions are detailed in Chapter 2.3.1.
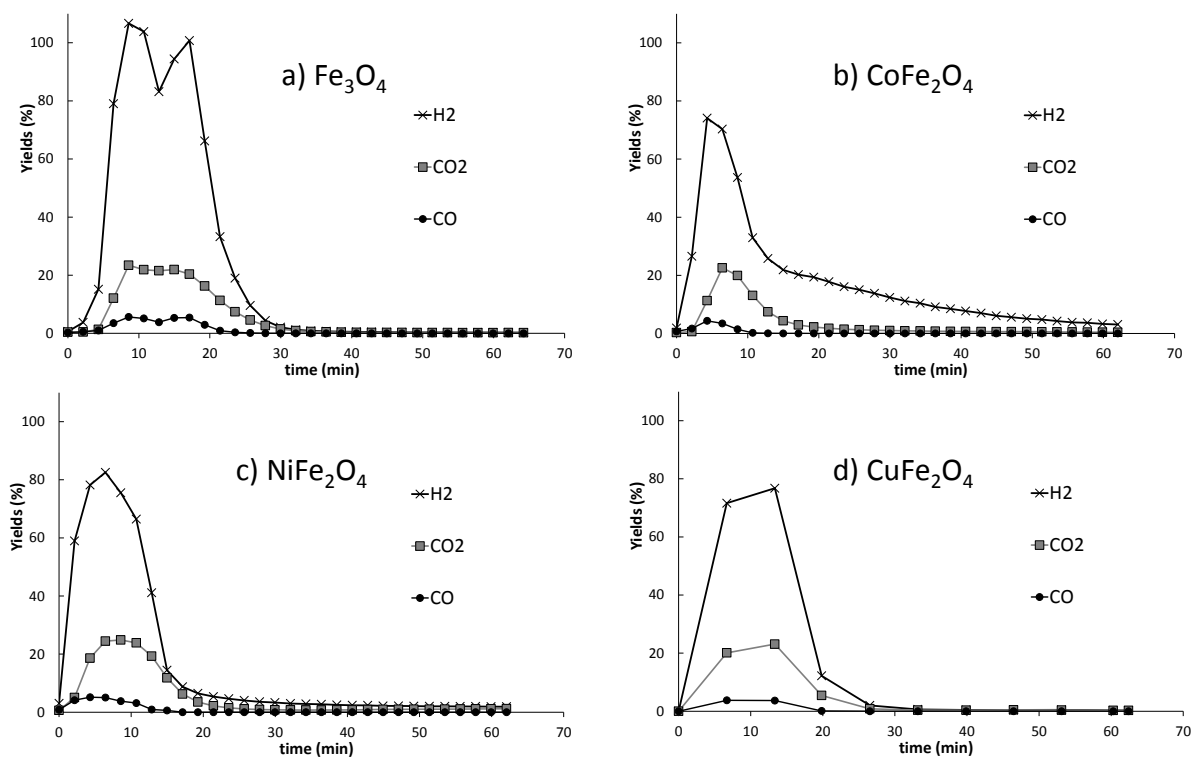

Figure 4-20. Yields obtained from the re-oxidation step with water at 450 °C on a) Fe₃O₄, b) CoFe₂O₄, c) NiFe₂O₄ and d) CuFe₂O₄

Figure 4-20 reports yields to H_2, CO_2 and CO versus time, obtained from GC analysis (all yields have been calculated based on the H content of the molecule, with respect to the

molar percentage of water fed). It is important to notice that the trends shown, with an increase during the first 6-10 minutes, indeed was an artifact due to the fact that the stream containing unconverted steam and products took a few minutes to reach the catalyst and then the on-line GC apparatus after the start-up of the reaction.

Magnetite is the ferrite that produced the greater amount of hydrogen among the four materials tested. The common drawback was the production of CO and CO_2, due to the reforming of the coke accumulated during the reduction step. It is evident that improvements are needed in this latter step, which should be carried out under conditions limiting the deposition of carbonaceous compounds. Another common behavior is that all the materials were apparently completely re-oxidized in less than 30 min, with the exception of the cobalt ferrite that went on producing hydrogen over the entire duration of the test. Comparing the overall number of hydrogen moles obtained from the integration of the curves (Figure 4-21), it is possible to conclude that the hydrogen produced was the greater for magnetite, and comparable for the mixed ferrites; however the cobalt ferrite took longer time than the other materials to conclude the re-oxidation step.
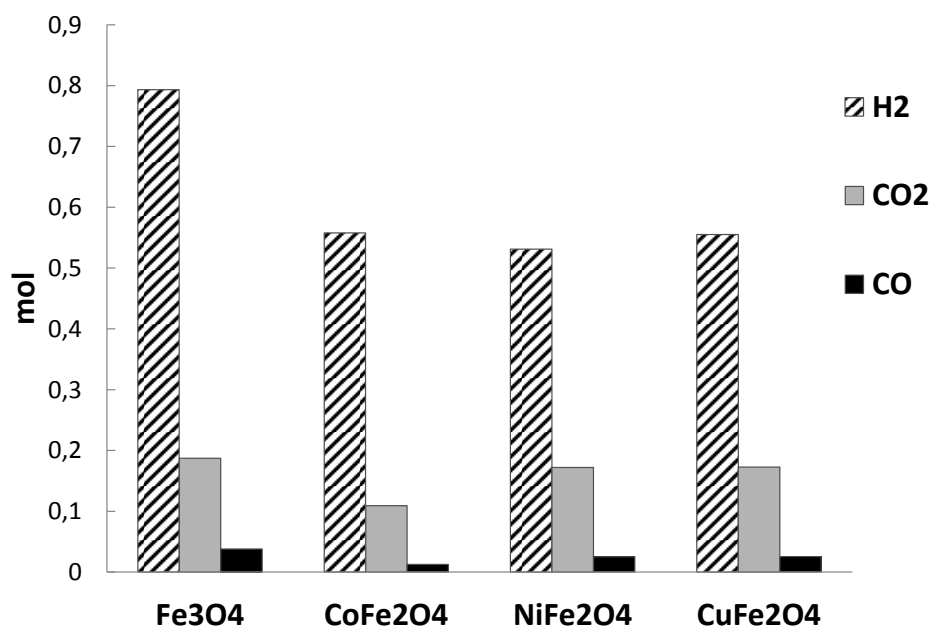

Figure 4-21. Moles of H_2, CO_2 and CO obtained during re-oxidation

Figure 4-21 shows that the production of CO_x was also similar, with the exception of cobalt ferrite, which produced an overall amount of both CO and CO_2 compared to the other ferrites. The behavior shown by the cobalt ferrite might be attributable to the occurrence of a more important sintering phenomenon and to the formation of a more stable type of coke, which hindered the diffusion of water inside the bulk of the material.

4.3.1. Conclusions and possible improvements

In this paragraph we have shown that besides H_2 the products obtained during the 2nd step of the chemical loop were CO and CO_2, obtained from the following reactions:

- $Me + H_2O \rightarrow MeO + H_2$
- $3MeO + H_2O \rightarrow Me_3O_4 + H_2$
- $C + H_2O \rightarrow CO + H_2$
- $C + 2 H_2O \rightarrow CO_2 + 2 H_2$

We were wondering whether the metal species in reduced ferrites might catalyze the oxidation of C into CO and CO_2. In order to elucidate on this aspect, we carried out an experiment by loading 0.2 g of carbon (Commercial C Norit grains; Surface area = 1200 m^2/g; particles diameter > 175nm) ground to powder into the reactor and feeding water for 30 minutes. The experiment was then repeated by loading 0.1 g of metallic Fe and 0.2 g of carbon. In order to better mix the two compounds, they were ground and pressed together into a disc. The disc was then ground again and the powder was loaded in the reactor. In both cases, the reactor was weighted before and after the reaction. In the case of the test carried out with only carbon, the mass loss was about 8.4%, while in the presence of Fe also, the mass loss was about 11.1%, which indicates that very likely the reactions which give the formation of carbon oxides are catalyzed by iron:

- $Me + H_2O \rightarrow MeO + H_2$
- $3MeO + H_2O \rightarrow Me_3O_4 + H_2$
- $MeO + C \rightarrow CO + Me$
- $2MeO + C \rightarrow CO_2 + 2Me$
- $2Me_3O_4 + C \rightarrow CO_2 + 6MeO$

4.4. MODIFICATIONS OF FERRITES DURING CYCLING

All samples were characterized after reaction with ethanol by means of XRD, Mössbauer spectroscopy and measurement of the carbon content, in order to characterize the structural modifications, the oxidation state of the iron and the amount of carbon deposited or removed during reaction.

4.4.1. Characterizations of materials after reduction with ethanol
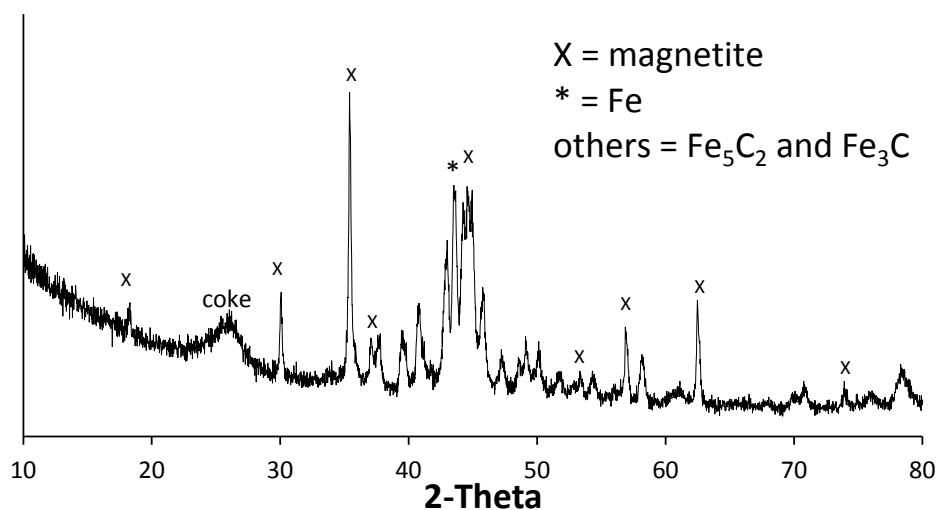
4.4.1.1. Fe_3O_4

Figure 4-22. XRD of Fe_3O_4 after 1h reaction with ethanol at 450°C (X=magnetite, * = Fe^0, other peaks = carbides)

The X-ray diffraction pattern of reduced magnetite shows that not all of the material had been reduced. The main phases formed after reduction were iron αFe and Iron carbides (Fe_5C_2 and Fe_3C). There was also a broad reflection at 26° 2θ, that indicates the presence of an amorphous type of coke (ICSD 00-026-1076)
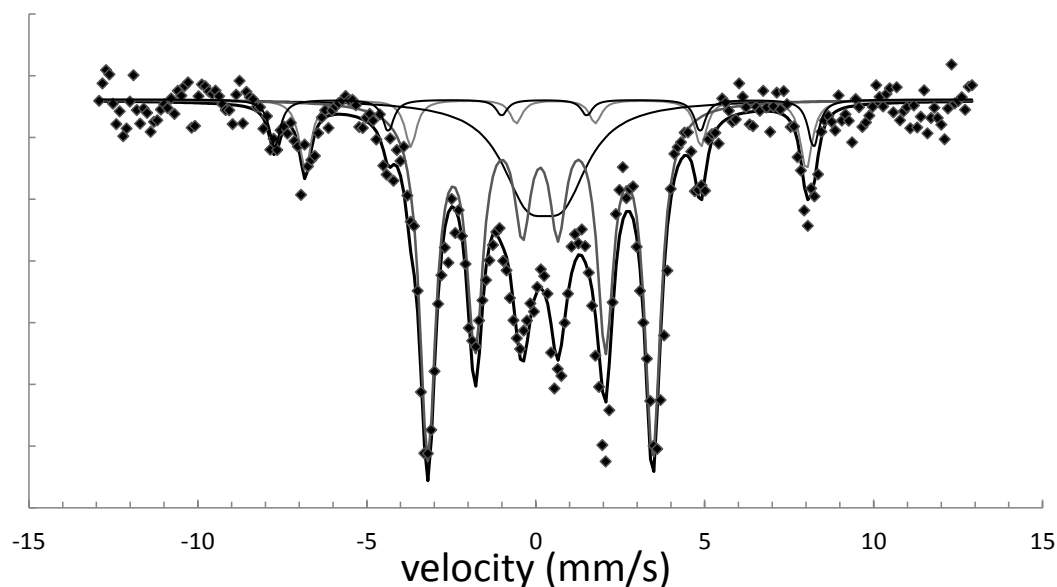
Figure 4-23. Mössbauer spectrum of the Fe₃O₄ sample after 1h reaction with ethanol at 450°C, recorded at 25°C; the solid line is derived from least-square fit.

The Mössbauer spectroscopic analysis allowed to confirm the presence of the species previously found by means of XRD, and to quantify their content in the material. The main reduced phase identified (62%) was Fe_3C, as also inferred from the XRD pattern; this phase was characterized by an internal magnetic field of 20.5T and an isomer shift of 0.15mm/s. The un-reduced ferrite was characterized as usually by the two sextets that represent the species Fe^{3+} and the mixed valence species $Fe^{2.5+}$; the former is referred to the trivalent iron cation in tetrahedral position, while the latter is a species that derives from the electron hopping between Fe^{2+} and Fe^{3+} in octahedral positions, in accordance with Sawatzki et al. [12]. The sextet representing the Fe^{3+} (6%) is characterized by an isomer shift of 0.28mm/s and an internal magnetic field of 45.9T, while the sextet representing the $Fe^{2.5+}$ (9%) has an IS of 0.61mm/d and an Heff of 49.3.

4.4.1.2. CoFe₂O₄

The diffractogram of the cobalt ferrite after reduction with ethanol was already shown before in Figure 4-12; it showed, that this oxide was completely reduced to cobalt-iron alloy and carbides, differently from what observed with magnetite. By means of Mössbauer analysis it was possible to find that in the reduced material 63% Fe was in the alloy and 37 % in the carbide. The relative proportion of cobalt and iron did not fit the starting composition of the ferrite. This means that some Co^0 or CoO was present in the sample and also maybe that the stoichiometry of the alloy was richer in cobalt.
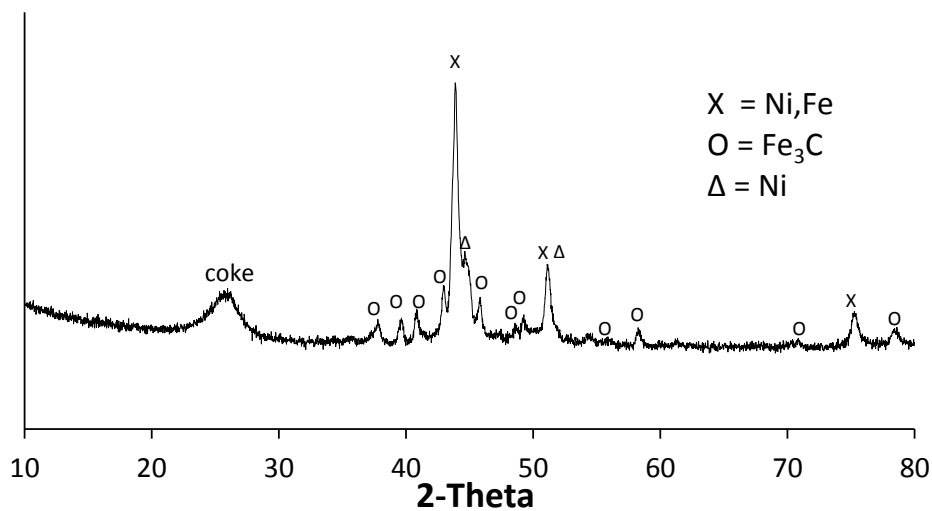
4.4.1.3. $NiFe_2O_4$

Figure 4-24. XRD pattern of $NiFe_2O_4$ after 1h reaction with ethanol at 450°C (X=Ni Fe alloy, O = carbides, Δ=Ni^0)

In the case of nickel ferrite (Figure 4-24), it is possible to see that this ferrite was completely reduced to a nickel-iron alloy and iron carbides, but a part of the nickel had been reduced and segregated as Ni^0. The peak of coke was relatively more intense than in the other materials.
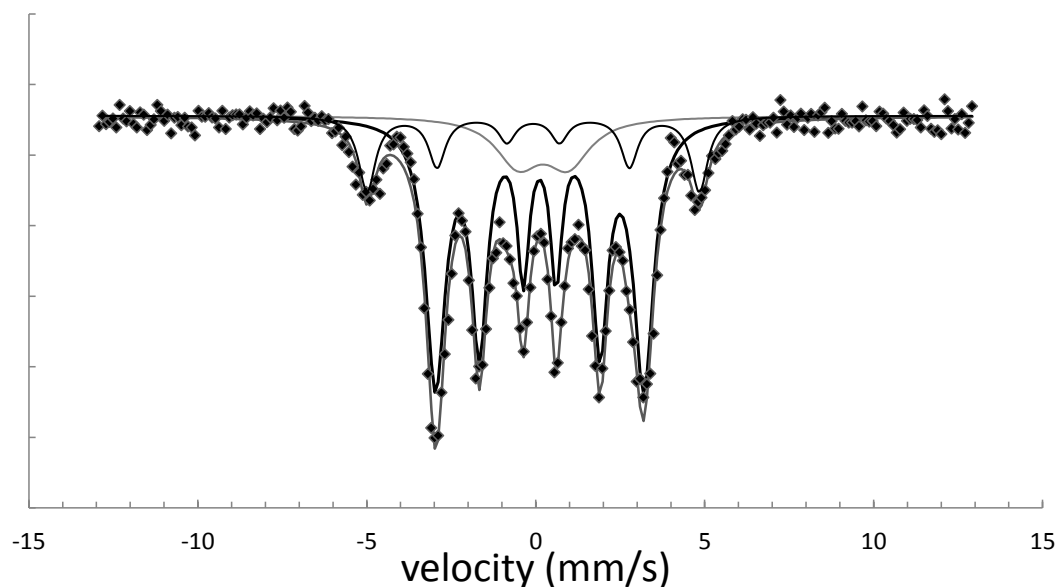
Figure 4-25. Mössbauer spectrum of the NiFe$_2$O$_4$ sample after 1h reaction with ethanol at 450°C, recorded at 25°C; the solid line is derived from least-square fit.

The Mössbauer spectra of the reduced nickel ferrite confirms the complete reduction of the material as observed in the X-ray diffraction pattern (Figure 4-25). The main contribute (80%) is represented by a sextet with an isomer shift of 0.13mm/s and an internal magnetic field of 19.0T, which is characteristic of Fe$_3$C. Another sextets used to fit the spectrum was attributed to the reduced specie Fe^0 in the alloy (20%) having an IS of 0.04mm/s and a H$_{eff}$ of 30.3T.

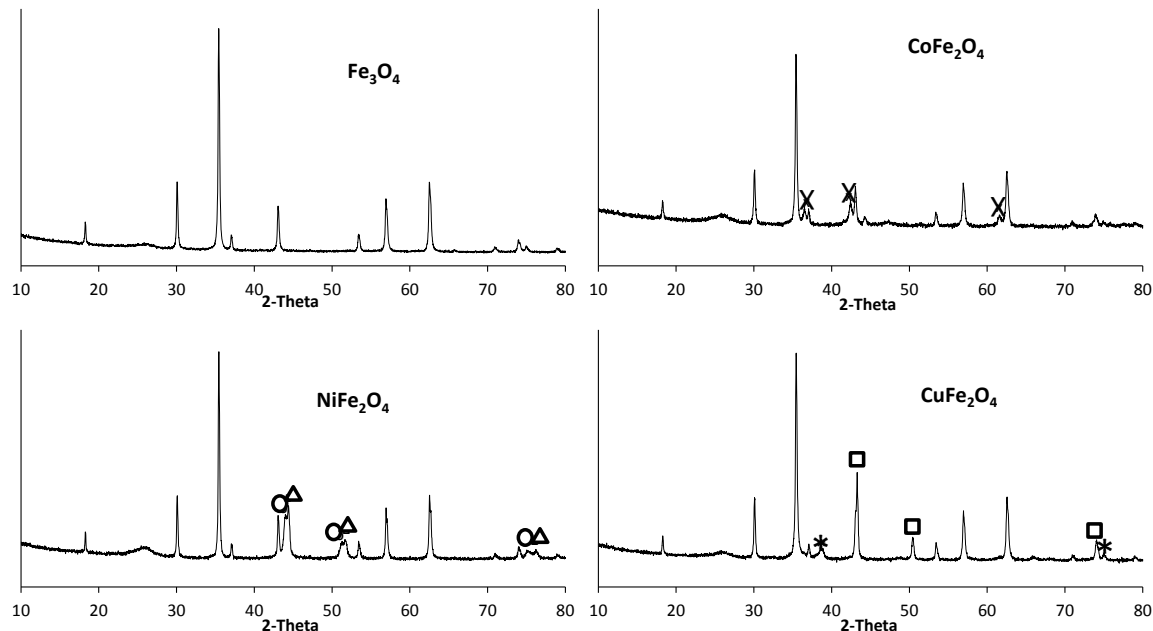### 4.4.2. Characterizations of materials after re-oxidation with water

4.4.2.1.XRD

Figure 4-26. XRD patterns after re-oxidation with water on pre-reduced ferrites at 450 °C. (X = CuO; Δ = Ni[0]; O = Ni-Fe; □ = CuO; * = Cu[0])

X-ray diffraction patterns obtained on the different ferrites after re-oxidation were quite similar (Figure 4-26). In fact, in all cases the structure was now that of a well-crystalized ferrite, with narrow peaks. This can be due to a sintering phenomenon that occurs on the materials during cycling. Another aspect is the presence of a low broad reflection due to C shown in all patterns, which indicates that carbon had not been completely re-oxidized with water. Moreover, in mixed ferrites it is possible to see the segregation of the metal: in cobalt ferrite a part of the cobalt segregated as CoO (reflections with X), in nickel ferrite, nickel segregated both in the form of both Ni[0] (reflections with Δ) and Ni,Fe alloy (reflections with O). In this case the incomplete re-oxidation could be due to the fact that carbon was covering part of the material and hindered the contact with water. This is also confirmed by the peak of coke shown at around 25° 2θ, which was more intense than for the other ferrites. Finally with copper ferrite it is possible to see copper segregated both

in its reduced form (Cu^0, reflections with *), and in its oxidized form CuO (reflections with □).
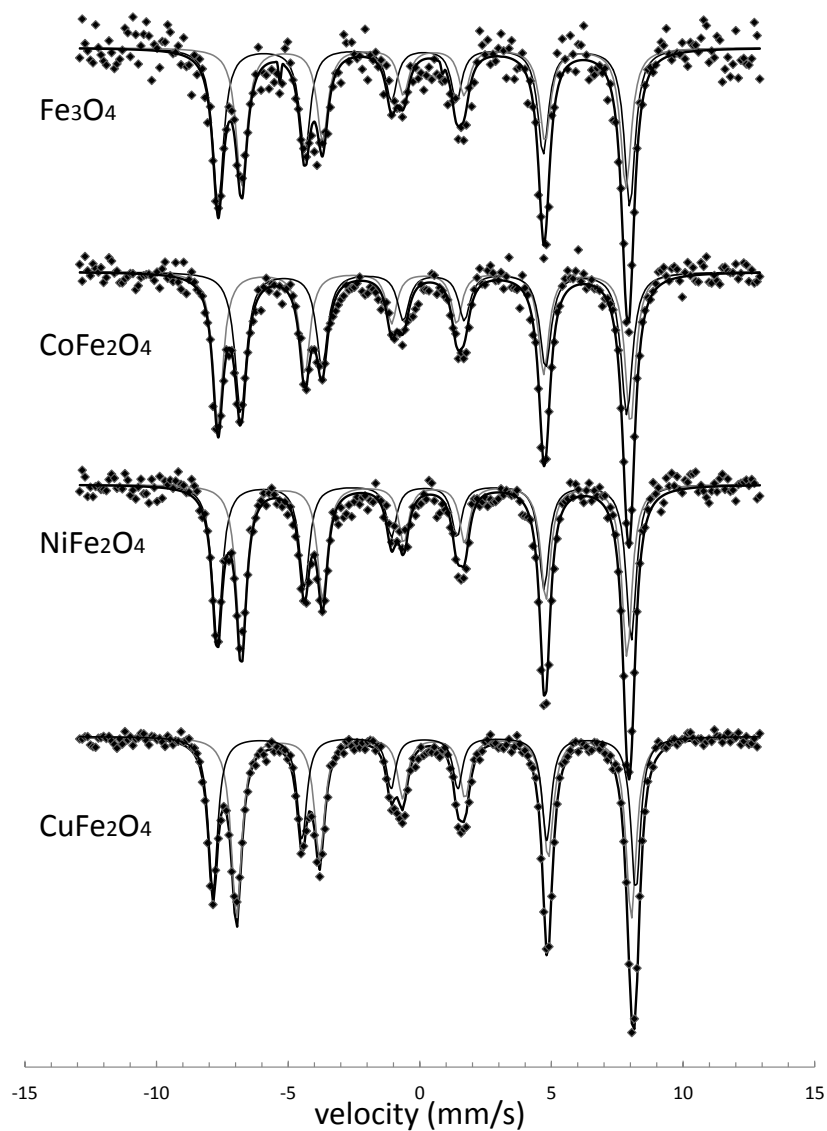
4.4.2.2. Mössbauer

Figure 4-27. Mössbauer spectrum of the various ferrites after 1h re-oxidation with water at 450°C, recorded at 25°C; the solid line is derived from least-square fit.

From the Mössbauer analysis of the different oxides after re-oxidation it is possible to observe that all of them show the typical pattern of the ferrite with small differences on the ratio between the Fe^{3+} species (the sextet with the bigger hyperfine magnetic field) and $Fe^{2,5+}$ (the sextet with smaller hyperfine magnetic field). This means that sintering and segregation rendered the mixed ferrite more similar to the magnetite.

4.4.2.3. Determination of carbon content in the materials

In order to evaluate the amount of coke present on the materials after each step of the reaction, an elemental analysis (CHNS) on the different materials was carried out.

Table 4-2. Amount of C expressed in weight % in the materials after each step of the cycle.

	% of C $^w/_w$ after reduction	% of C $^w/_w$ after re-oxidation	% loss	Moles of C (from GC)
Fe_3O_4	41.0 %	28.6 %	12.4 %	0.22
$CoFe_2O_4$	43.8 %	36.9 %	6.9 %	0.12
$NiFe_2O_4$	49.1 %	39.3 %	9.8 %	0.19
$CuFe_2O_4$	43.4 %	32.6 %	10.8 %	0.19

Table 4-2 compiles the results of CHNS analysis on the different ferrites. The oxide on which less C formed during the reduction step was magnetite, while the ferrite that accumulated more C was the nickel ferrite. Moreover, it is important to note that the amount of C "burned" during the re-oxidation step was around 10 % in all cases, and it was higher with magnetite and lower with cobalt ferrite. This confirms also the results, obtained from the GC analysis, of the number of moles of CO_x (CO_2 + CO) produced from coke combustion.

4.4.2.4.Study by transmission electron microscopy (TEM)

The cobalt ferrite has been analyzed after 1 cycle of reaction through Transmission Electron Microscopy coupled with EDX analysis, in order to confirm both the segregation of cobalt and understand how the coke had formed in the material.
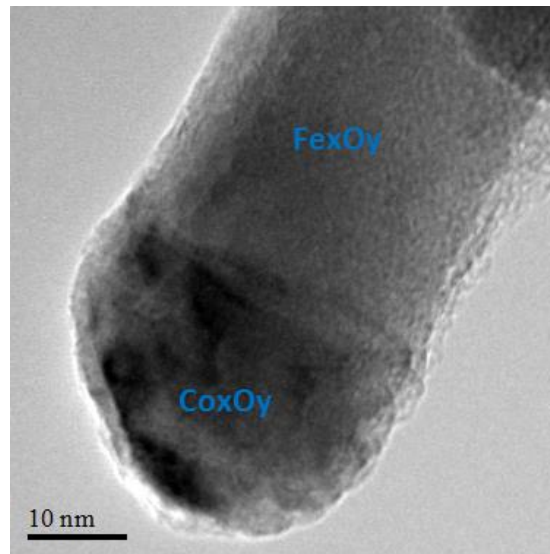

Figure 4-28. TEM picture of CoFe$_2$O$_4$ after a complete cycle

The ferrite turned out to be covered by a layer of coke which had grown with filament-like shape. Moreover, several spots were found where there Fe content was largely prevailing over Co (Figure 4-28).

4.5.   THE 1ST STEP OF THE CHEMICAL LOOP: ANAEROBIC OXIDATION OF THE

AZEOTROPIC MIXTURE

Results obtained in ethanol anaerobic oxidation have demonstrated that one of the main issues of this kind of process is the deposition of carbonaceous deposits and coke during the reduction step. In the attempt to decrease this deleterious phenomenon, we carried out the reduction step by feeding the ethanol-water azeotropic mixture, instead of absolute ethanol. The presence of small amount of water could help to prevent the deposition of C by "reforming" it as soon as it started to grow. On the other hand, it is evident that co-feeding water might hinder the reduction of the spinel, giving rise to a steady-state redox cycle corresponding to ethanol reforming. The co-feeding of a less-than-stoichiometric water amount might lead to the combination of ethanol reforming and ethanol anaerobic oxidation (the latter leading to spinel reduction) and decomposition. Moreover, bio-ethanol already contains a certain amount of water, which is expensive to remove, so an azeotropic mixture could have several advantages even from an economic point of view allowing to avoid expensive dehydration processes.

Tests were carried out using the same operating conditions previously used with pure ethanol: 450 °C, 1h, 15.6 % of azeotrope in 30 ml/min of N_2.
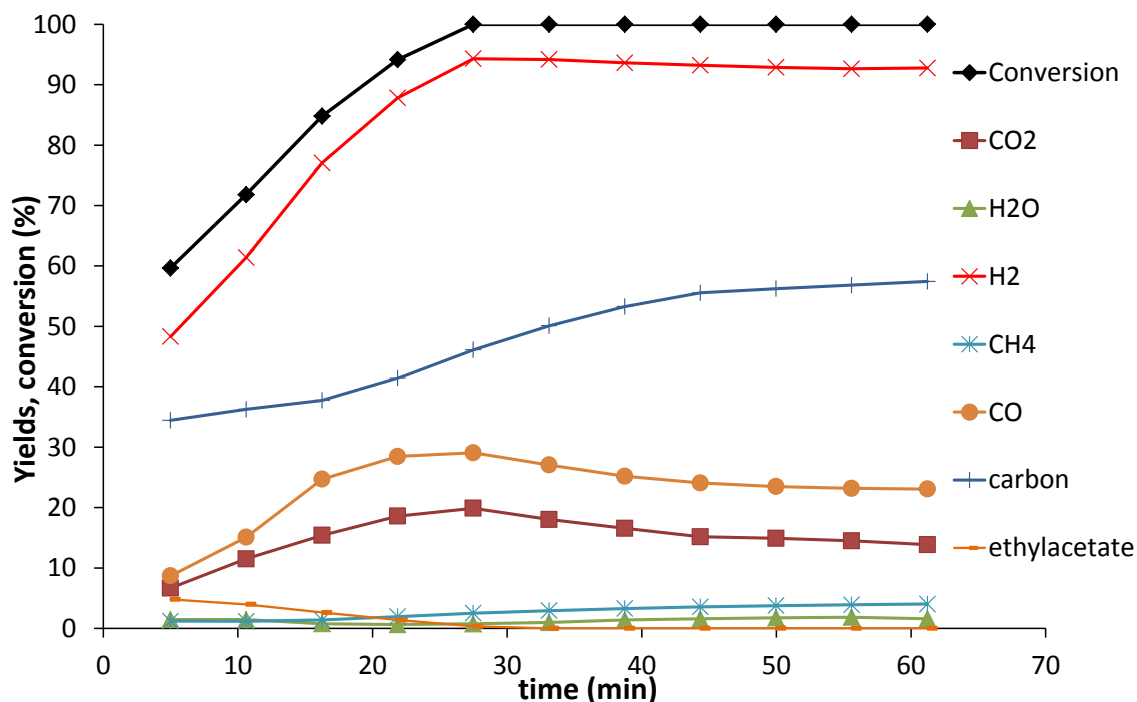
4.5.1.1. Fe_3O_4

Figure 4-29. Conversion and yields in main products obtained on the reduction of Fe_3O_4 at 450 °C using an azeotropic mixture feed

Figure 4-29 reports conversion and yields to main products obtained during the 1-hour reduction step. In this case it took longer time to reach complete ethanol conversion compared to the case with pure ethanol, when conversion was almost complete from the very first minutes of reaction. This confirms the hypothesized weaker reducing properties of the azeotrope compared to pure ethanol. Even hydrogen yield was lower at the beginning; however, it reached slightly higher values (>90%) after 20 minutes. Carbon yield was slightly lower during the entire reaction time compared to pure ethanol feed, which confirms the hypothesized role of steam, but still coke yield remained high.

The yields to CO_x were quite similar in the two cases; however, one major difference concerned acetone yield, which was negligible in this case, but was as high 20% with pure ethanol. We also noticed the formation of ethylacetate on the oxidized ferrite, perhaps obtained by Tishchenko dimerisation of acetaldehyde:

2 $CH_3CHO \rightarrow CH_3COOCH_2CH_3$ (Tishchenko reaction)
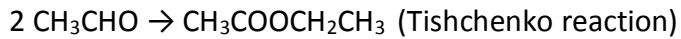
Acetaldehyde (not reported) showed an initial yield around 2% and the same trend as ethylacetate.
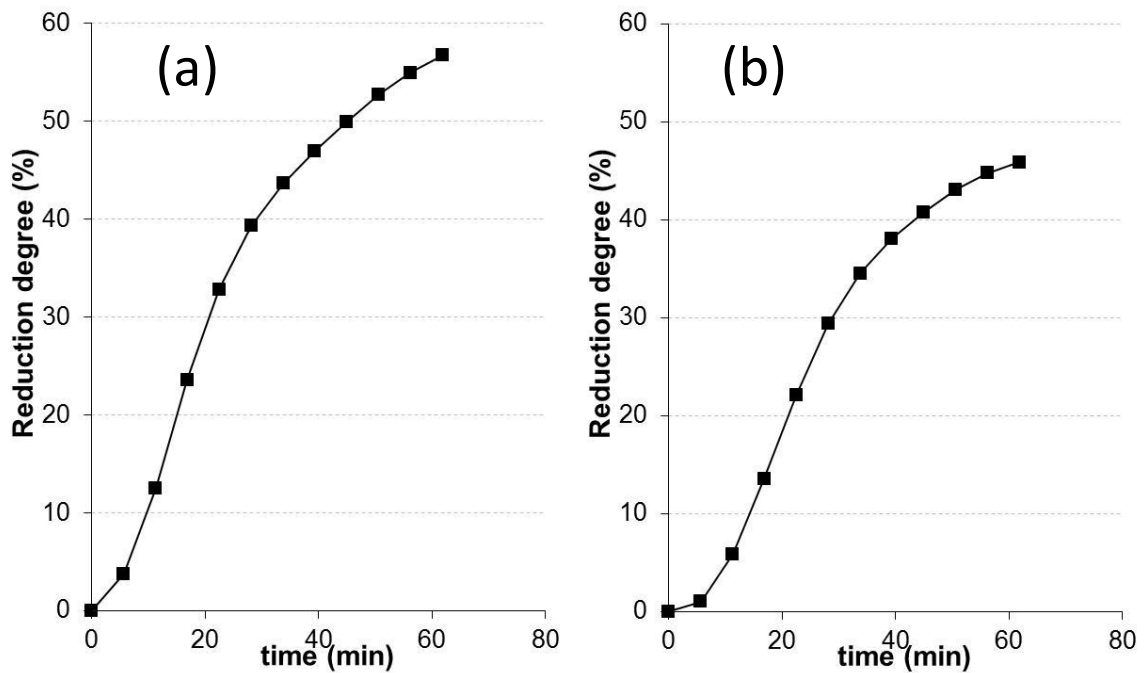
Figure 4-30. Reduction degree of Fe₃O₄ reduced 1h at 450°C feeding a) pure ethanol; b) azeotrope

Comparing the reduction degree calculated through O balance (Figure 4-30), allows to see that using pure ethanol for magnetite reduction led to a 10% higher reduction degree. As mentioned above, this difference is attributable to the partial re-oxidation of Fe by the water present in in the feedstock.

The spent sample was characterized by means of XRD and Mössbauer spectroscopy.
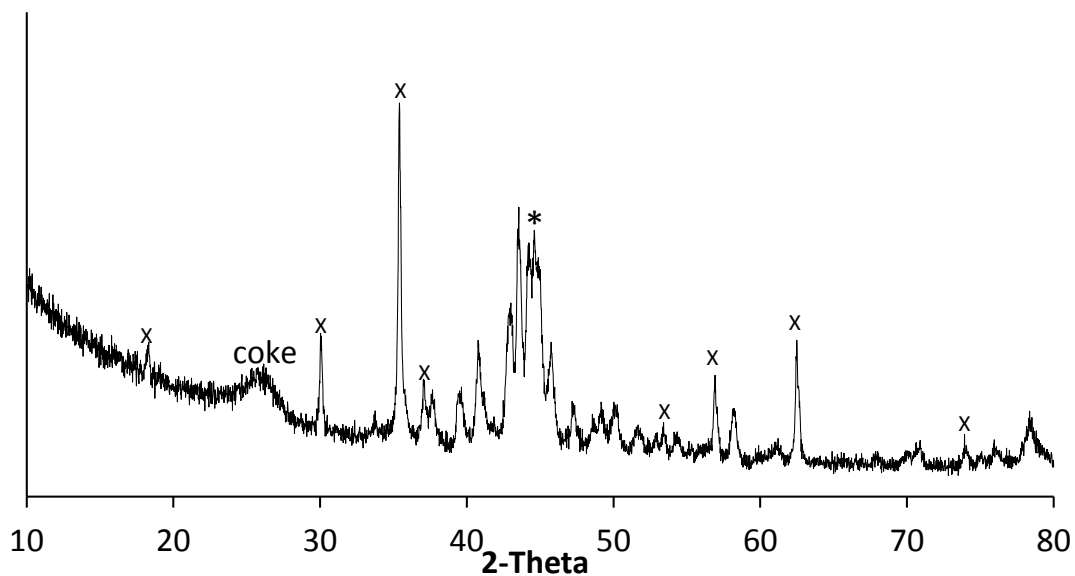
Figure 4-31. X-Ray diffractogram of Fe$_3$O$_4$ reduced 1h at 450°C feeding azeotrope (*= Fe^0, X= magnetite, other peaks= carbides Fe$_5$C$_2$)

The XRD pattern shown in Figure 4-31 for the magnetite reduced with the azeotrope confirms the presence of non-reduced magnetite. Moreover, it is possible to see the presence of Fe^0, but here the magnetite was mainly reduced to carbides. To better quantify the amount of the different species a Mössbauer analysis was also carried out (Figure 4-32):
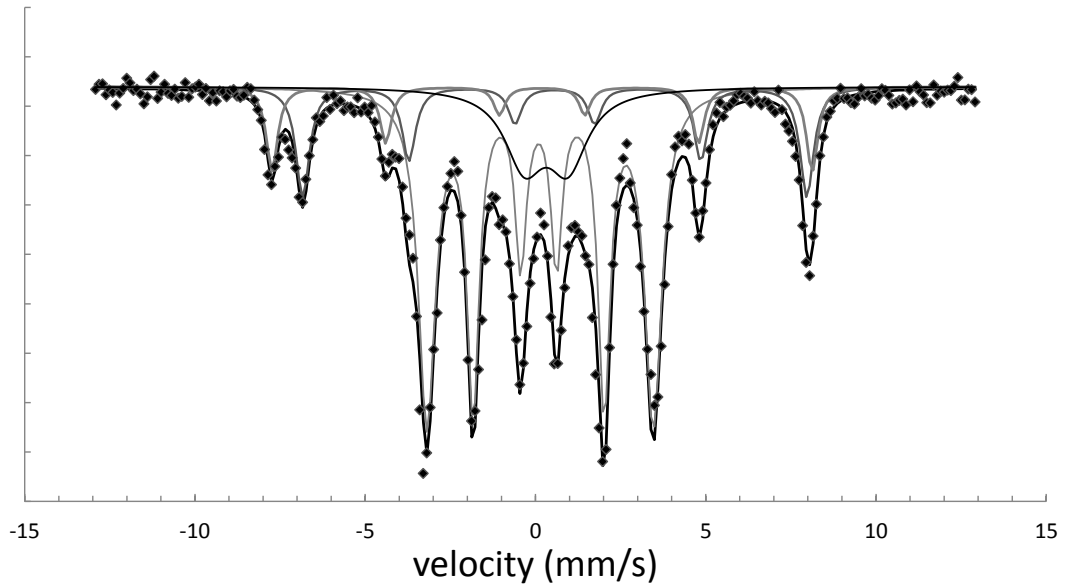
Figure 4-32. Mössbauer spectrum of the Fe_3O_4 sample after 1h reaction with azeotrope at 450°C, recorded at 25°C; the solid line is derived from least-square fit.

From the fitting of the spectra it was possible to determine the content of the different iron species after the reduction, as shown in Table 4-3.

Table 4-3. Results of Mössbauer analysis on Fe_3O_4 reduced with azeotrope.

Specie	%	H (kOe)	IS	QS
Fe^{3+}	15	45.7	0.68	/
$Fe^{2.5+}$	10	49.0	0.30	/
Fe_3C	60	20.5	0.22	0.04
Fe^{3+} n.p.	15	0.0	0.42	1.27

It is shown that all the magnetite which had been reduced transformed into carbides (Fe_3C), the amount of which correspond to the 60% of the material.

This means that the non-reduced amount is the 40% that includes 15 % of Fe^{3+} in nanoparticles (doublet), 15% of Fe^{3+} in the tetrahedral sites, plus a 10% of the mixed specie $Fe^{2.5+}$ in octahedral sites.

4.5.1.2. $CoFe_2O_4$
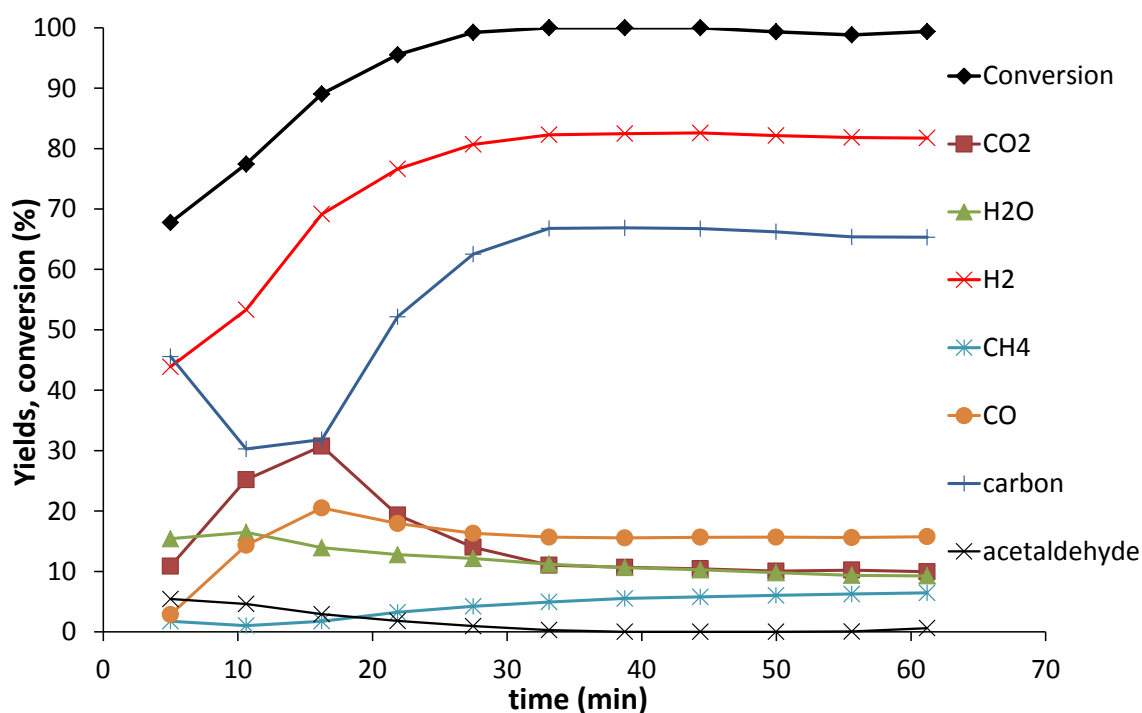
Figure 4-33. Conversion and yields in main products during 1h reaction of azeotrope on $CoFe_2O_4$ at 450°C

The reduction of the cobalt ferrite with the azeotropic mixture (Figure 4-33) gave results similar to those obtained with magnetite. The conversion was low at the beginning (70%) of the experiment, and it was complete only after 30 min reaction time. Hydrogen yield started from values around 40% and reached its highest value of 80% after ca 30 min.

114

Carbon yield was similar to that obtained feeding pure ethanol on cobalt ferrite. Also CO_2 and CO showed the same trends as in the case of pure ethanol; however their values were slightly lower, 30 and 20% respectively, compared to 40 and 25% with pure ethanol.

4.5.1.3. $NiFe_2O_4$

Figure 4-34. Conversion and yields in main products during 1h reaction of azeotrope on NiFe$_2$O$_4$ at 450°C

Figure 4-34 shows the results obtained with Ni ferrite. Ethanol conversion was not complete at the beginning, although, in this case, it started from 80% and reached 100% after about 10 min reaction, which indicates that the presence of cobalt in the structure enhances the activity of the solid in ethanol transformation. Hydrogen yield also started from a low value (40%) and reached 70% after 30 min. In this case, differently from magnetite, the highest hydrogen yield was obtained with pure ethanol (80%). The lower amount of H_2 produced can be explained by taking into account the higher formation of

other H-containing species such as methane, acetaldehyde and water, which formed in higher amounts with this material. Methane yield increased during time, which confirms that along with the increase of the reduction degree a higher activity in methanation was shown. Methane could be produced starting either from coke by reaction with hydrogen:

$$C + 2H_2 \rightarrow CH_4$$
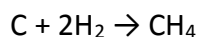
or from CO_X, but in this case there should be a higher production of water that, on the contrary, showed a decreasing trend during time.

There was a relatively high production of acetaldehyde (up to 15% yield), due to the strong dehydrogenation properties of nickel; however there no trace of products such as ethylacetate or acetone was found.

When acetaldehyde yield decreased, an enhancement of hydrogen and methane yields was shown. Methane might be produced from the hydrogenolysis of acetaldehyde:

$$CH_3CHO + 3H_2 \rightarrow 2CH_4 + H_2O$$

However hydrogen yield was increasing and water was decreasing, which do not support this hypothesis. Acetaldehyde likely decomposed to coke and hydrogen, because of the enhancement of the dehydrogenation power of the material shown for an increase of the reduction degree.
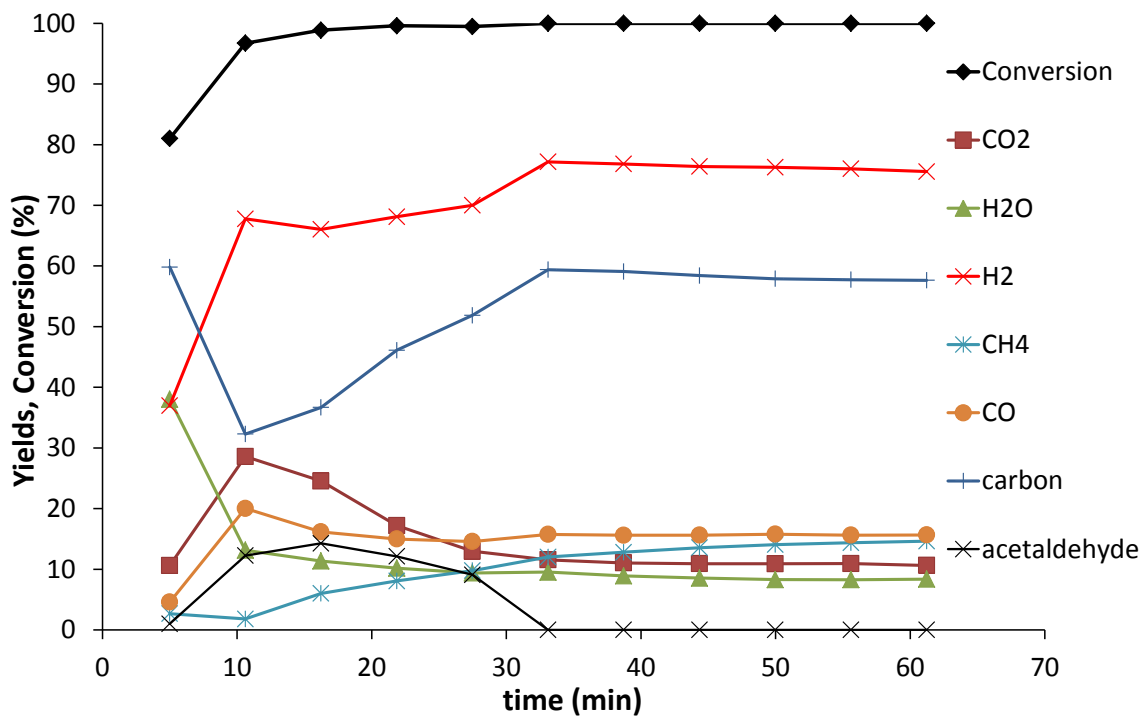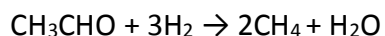
4.5.1.4.CuFe$_2$O$_4$
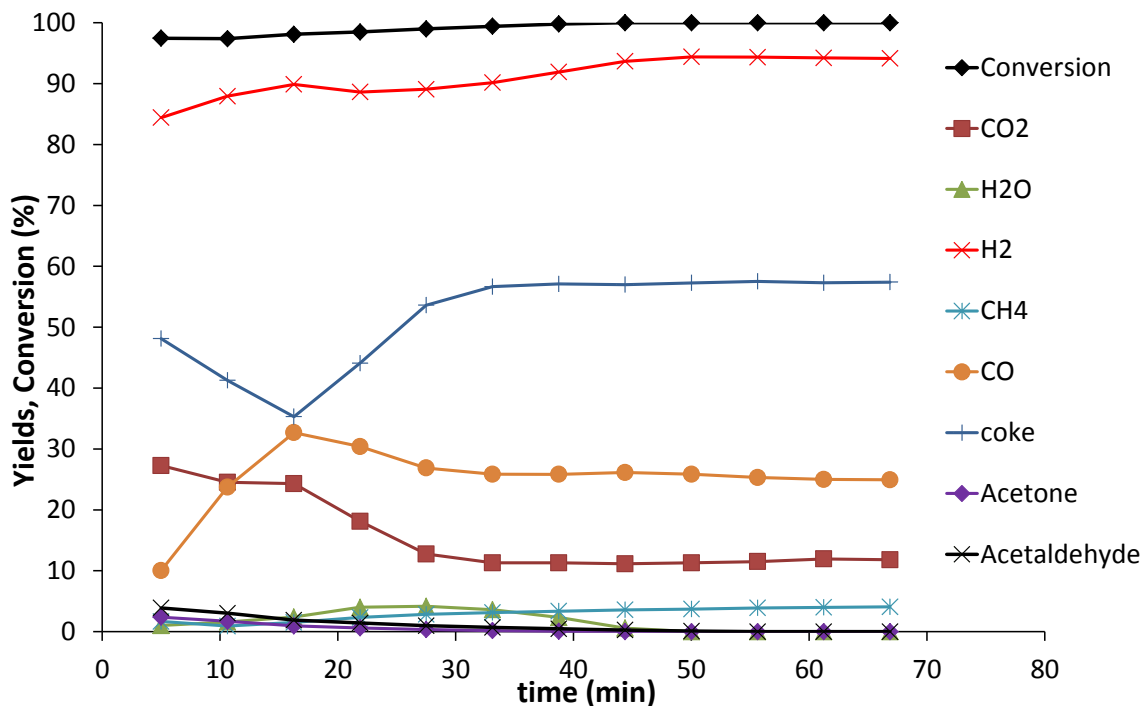
Figure 4-35. Conversion and yields in main products during 1h reaction of azeotrope on CuFe$_2$O$_4$ at 450°C

Figure 4-35shows the results obtained with the azeotropic mixture on copper ferrite catalysts. Results were unexpected; in fact, differently from the other ferrites, where the presence of water led to a decrease of the activity, here the conversion was almost complete from the very first minutes of reaction, and also hydrogen yield was relatively high, over 90% after 40 min time. Small amounts of acetaldehyde and acetone, but not of ethylacetate, also formed, however acetaldehyde yield never reached the high values shown with pure ethanol. With this material the reforming catalytic activity was relevant; in fact main products were H$_2$, CO and CO$_2$. Even in this case, however, the presence of water did not help in the reduction of the amount of carbon produced.

4.5.2. The re-oxidation step

Our results demonstrated that the presence of water in the feed had an effect on the reduction of the material. Moreover, conversion took longer time to be complete, and the maximum reduction degree obtained in 1 hour was lower compared to the case of pure ethanol feeding. Finally, the purpose of adding water in order to reduce the amount of carbon formed had not been reached.

Since results were not very positive, the re-oxidation step with water has been carried out only with the cobalt ferrite sample. Results are shown in Figure 4-36, compared with those obtained with pure ethanol feed for the reduction step.
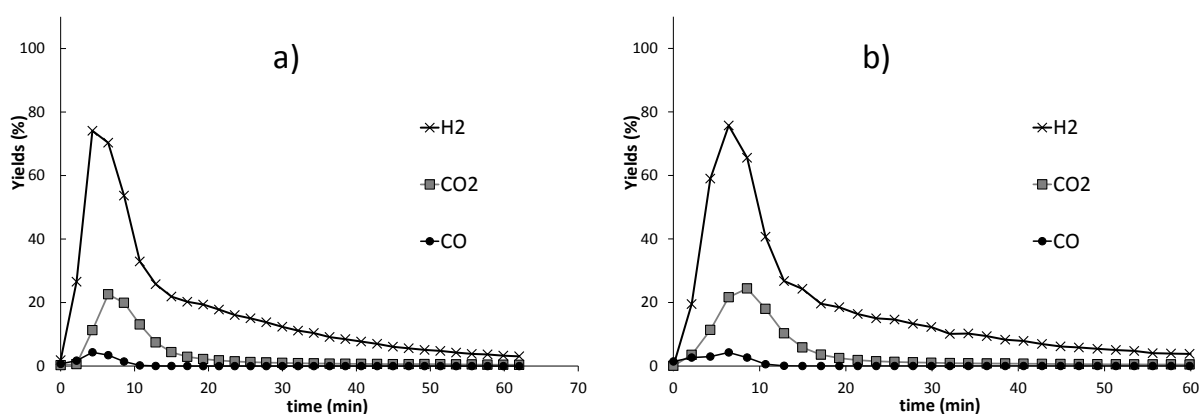
Figure 4-36. Comparison between yields in main products obtained during re-oxidation with water of CoFe$_2$O$_4$ reduced with a) absolute ethanol; b) azeotrope

The behavior shown during the re-oxidation step was similar in the two cases; the yields to H$_2$, CO and CO$_2$ obtained in the two tests were comparable: the maximum hydrogen yield was close to 80% in both cases, maximum CO$_2$ yield was 20%, CO yield 5%. The integral values of H$_2$ produced during 1 hour of reaction were also quite similar: in both cases 0.56 moles hydrogen and 0.01 moles CO were produced, while the amount of CO$_2$ was slightly different, 0.11 for the ferrite reduced with pure ethanol, 0.13 for the sample reduced with the azeotrope.

4.6.   THE 1ST STEP OF THE CHEMICAL LOOP: ANAEROBIC OXIDATION OF THE ETHANOL DURING 20 MINUTES REDUCTION CYCLES

Experiments carried out with ethanol for 1 hour reduction time clearly highlighted some drawbacks of this approach, amongst which the most important was the accumulation of carbonaceous residues and coke on the catalyst. The instantaneous yield of C increased while the ferrite became progressively more and more reduced, which drove us to the obvious conclusion that shorter reduction periods might be desirable in order to minimize the accumulation of coke.

Therefore we decided to carry out complete cycles (reduction + re-oxidation with steam) of reaction using pure ethanol during the first step, and prolonging the latter for 20 min only. In this case, we show the integrated values of yield achieved for each product during each step, plotted in function of the number of cycles, in order to better highlight changes in products distribution.
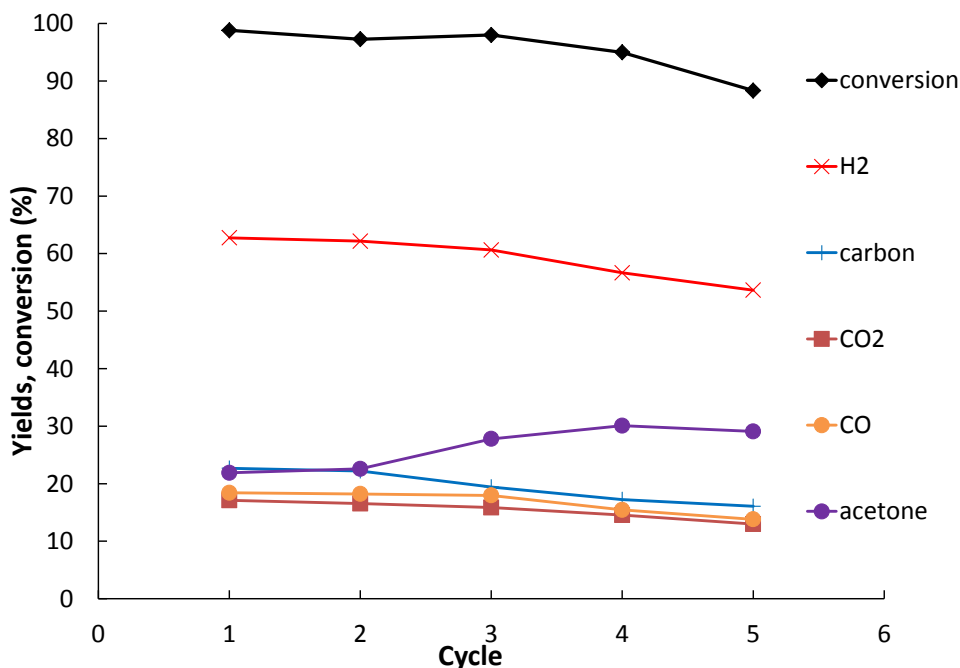
4.6.1.1. Fe$_3$O$_4$

Figure 4-37. Conversion and Yields in main products obtained during the 20 min-reduction steps running repeated cycles on Fe$_3$O$_4$ at 450°C (re-oxidation with steam at 450°C for 20 min)

Figure 4-37 plots the results obtained with magnetite over 5 complete cycles. Along with the increase of the number of cycles, the magnetite showed a decline in the conversion of ethanol, from initial values of 100% to values around 90% after 5 cycles. Hydrogen yield and carbon oxides yields both decreased, which means that during cycling the materials progressively lost its capacity to promote reactions of reforming and oxidation of ethanol. A positive fact is that the carbon yield showed a decreasing trend, and a correspondingly higher yield to acetone and other heavier products (not reported in figure). Acetone yield started from values around 20% in the first reduction and reached almost the 30% during reduction on the 5th cycle. We discussed before that the formation of acetone derives from acetaldehyde, which instead of decomposing gives acetates and acetone. In fact the acetaldehyde yield (not reported here because of its small amount) was zero at the beginning, but rose up to 5% in the reduction step of the 5th cycle, which confirms the

supposed pathway, and indicates that the material was losing its activity in the decomposition of ethanol and acetaldehyde.
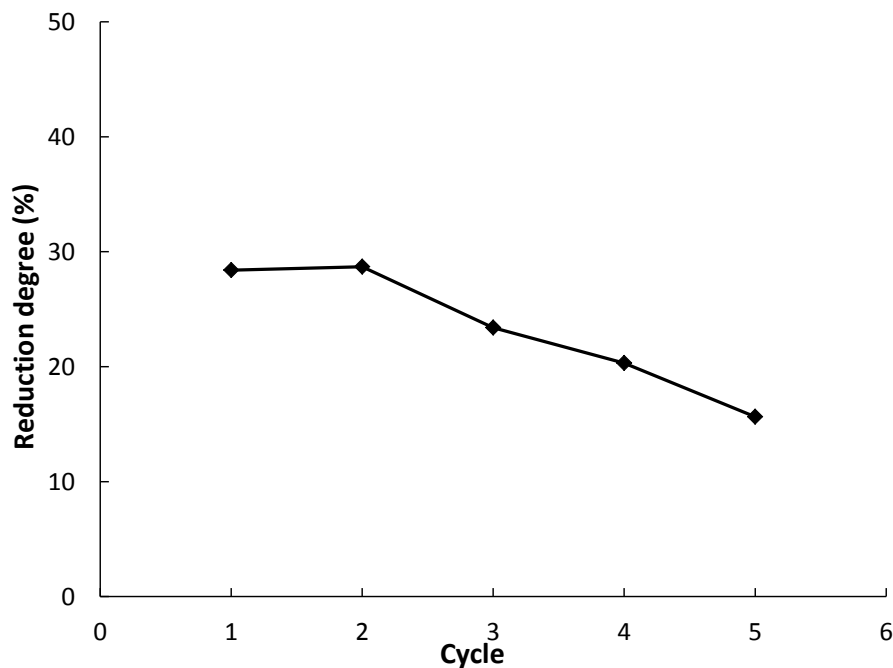
Figure 4-38. Reduction degree achieved by CoFe₃O₄ during the 20 min-reduction steps running repeated cycles at 450°C

From the results of the GC analysis and by means of the O and C balance it was possible to calculate the reduction degree achieved after each reduction step during cycling (Figure 4-38). In the first two cycles the reduction degree after feeding ethanol was around 30%, but at every cycle the material was more hardly reduced and at the 5th cycle its reduction degree was only 15%, which means that magnetite was less and less reduced. This also implies that the production of H_2 during the re-oxidation step will be likely decreasing.
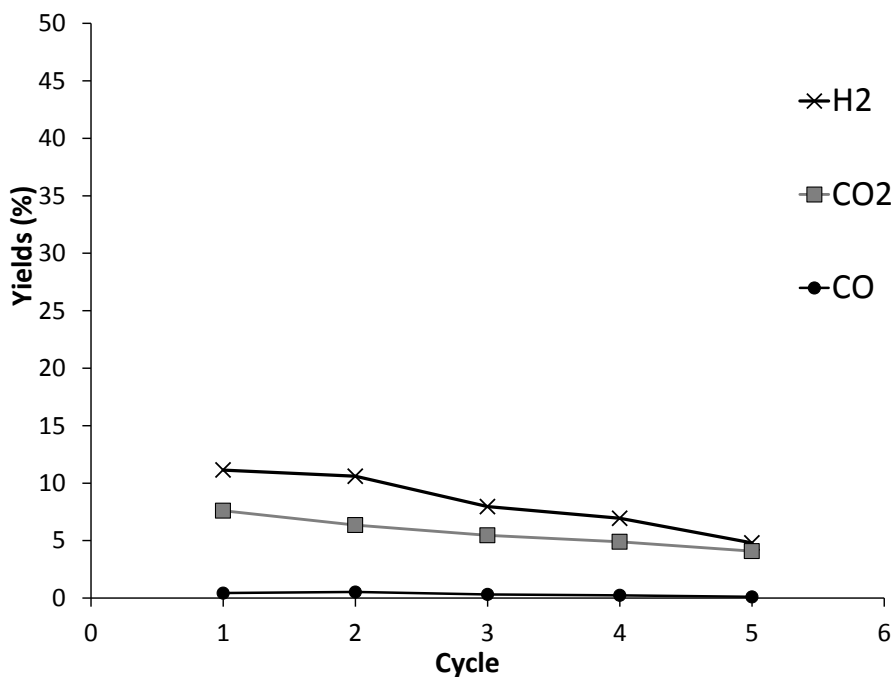
Figure 4-39. Integrated yields obtained during the re-oxidation step on repeated cycles tests on Fe$_3$O$_4$

As expected, Figure 4-39 shows that the H$_2$ yield was decreasing along with the increase of the cycle number. The hydrogen yield, obtained by integration of the instantaneous yields during the 20 minutes of each re-oxidation step, was 11% in the first cycle and then decreased down to 5% after 5 cycles. The carbon dioxide yield was 7% and decreased during cycling down to 4%. This could be explained either by a lower production of carbon during the first step, which corresponds to a lower production of carbon oxides in the second step, or by the formation of a more stable species of coke which is not removed during steaming. More characterization is needed in order to better explain this phenomenon. Carbon monoxide production was very low already at the beginning (< 1%) and decreased down to even smaller values during cycling.

4.6.1.2. $CoFe_2O_4$
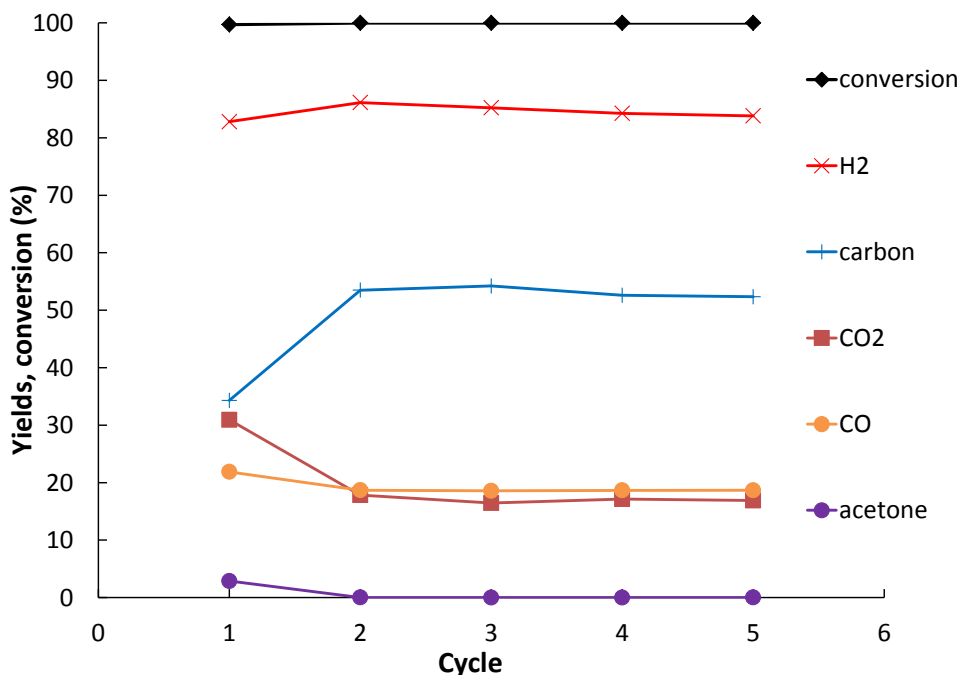
Figure 4-40. Conversion and Yields in main products obtained during the 20 min-reduction steps running repeated cycles on $CoFe_2O_4$ at 450°C (re-oxidation with steam at 450°C for 20 min)

The cobalt ferrite showed a more stable behavior compared to magnetite (Figure 4-40); in fact, in the first reduction ethanol conversion was complete and remained like this even after 5 cycles. Hydrogen yield was much higher than with magnetite (around 80-85%) and remained high during cycling. The drawback is the high amount of carbon produced, which started from 30% during the first reduction, but then increased from the 2nd cycle until values around 55%, thereafter remaining close to this value until the 5th cycle. This suggests that the amount of coke generated during reduction and that one removed during steaming were equivalent. Carbon oxides yield slightly declined during cycling, as in the case of magnetite, but in this case there was no increase of acetone yield.

Figure 4-41. Reduction degree achieved by CoFe$_2$O$_4$ during the 20 min-reduction steps running repeated cycles at 450°C

Despite the similar catalytic behavior shown during each reduction step, the reduction degree showed an important decrease during the first three cycles (Figure 4-41). In fact, the reduction was initially very high, around 75%, but then decreased down to 37% in the 2nd cycle and remained stable close to 25% after the 3rd cycle.

Figure 4-42. Maximum yields in main products obtained during the 20 min-re-oxidation steps running repeated cycles on CoFe$_2$O$_4$ at 450°C

The results of the re-oxidation steps are not easy to interpret, since the yields to all products showed a maximum value at the 3rd cycle (Figure 4-42). The result is surprising, because due to the decreasing reduction degree achieved during cycling, one would expect also a lower yield to H$_2$, which is the opposite of what experimentally observed.

4.6.1.3. NiFe$_2$O$_4$

Figure 4-43. Conversion and Yields in main products obtained during the 20 min-reduction steps running repeated cycles on NiFe$_2$O$_4$ at 450°C

Nickel ferrite (Figure 4-43) showed the most stable behavior during cycling. Ethanol conversion was complete during all tests. Hydrogen yield only slightly decreased from 80% down to 75% during reduction at the 5th cycle. Carbon production also slightly decreased during cycling, showing quite high values, from 52 to 46%. Yield to CO and CO$_2$ was around 20% and constant during cycling.
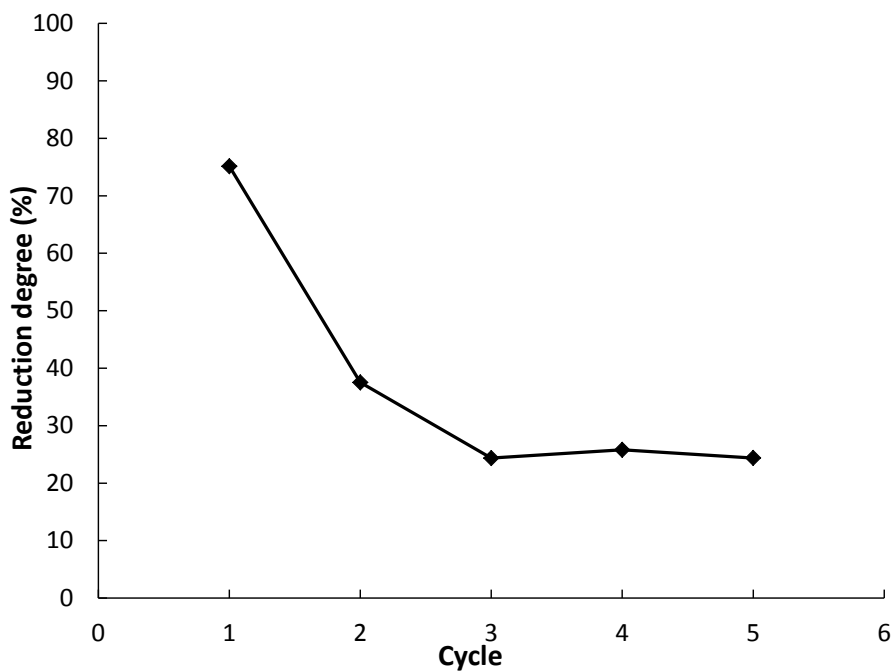
Figure 4-44. Reduction degree achieved by NiFe$_2$O$_4$ during the 20 min-reduction steps running repeated cycles at 450°C

In this case (Figure 4-44), the reduction degree achieved during the reduction steps decreased after the 1st cycle from 50% down to 30%, but then remained stable until the 5th cycle, which indicates that probably, as in the case of cobalt ferrite, an equilibrium was reached between the amount of carbon deposited and that steamed during re-oxidation.
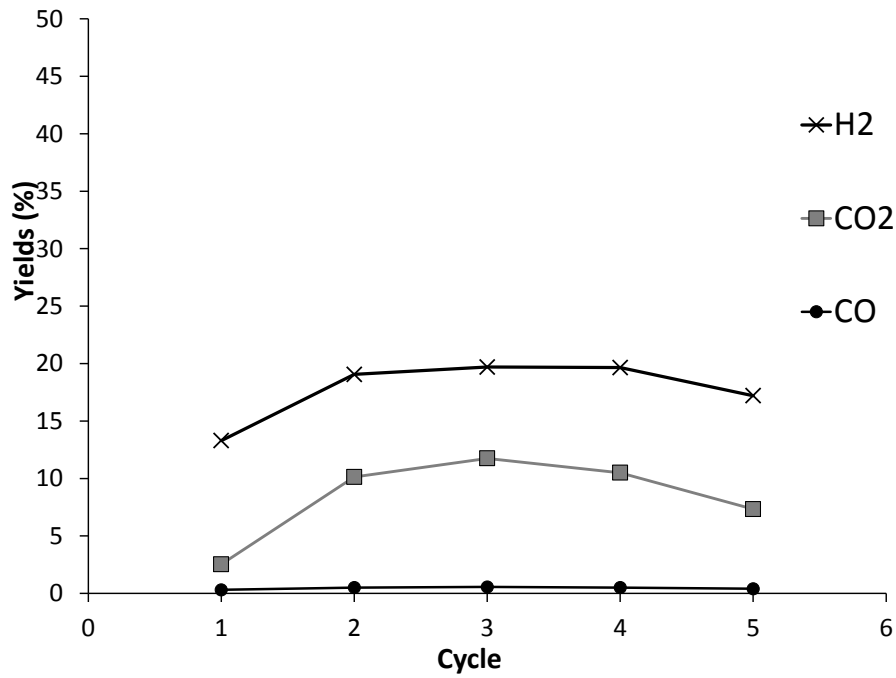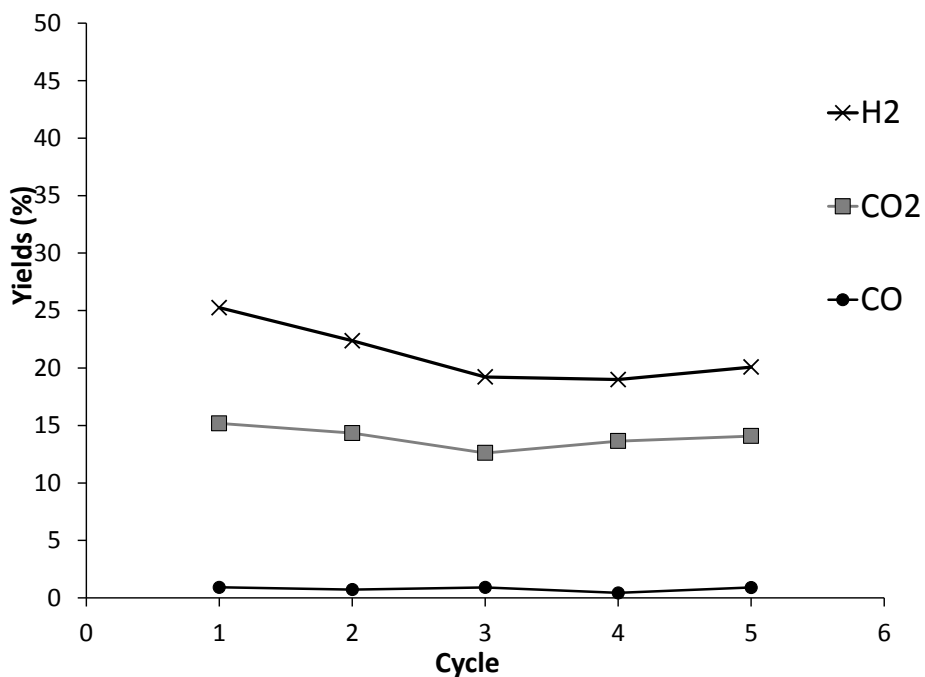
Figure 4-45. Maximum yields in main products obtained during the 20 min-re-oxidation steps running repeated cycles on NiFe$_2$O$_4$ at 450°C

The nickel ferrite confirmed its stability also during the re-oxidation steps (Figure 4-45). In fact, yield to hydrogen decreased, but the decline was smaller than that shown with the other ferrites (from an initial value of 25% down to 20% at the 5th cycle). The carbon dioxide yield also slightly decreased while CO yield was always smaller than 1%.
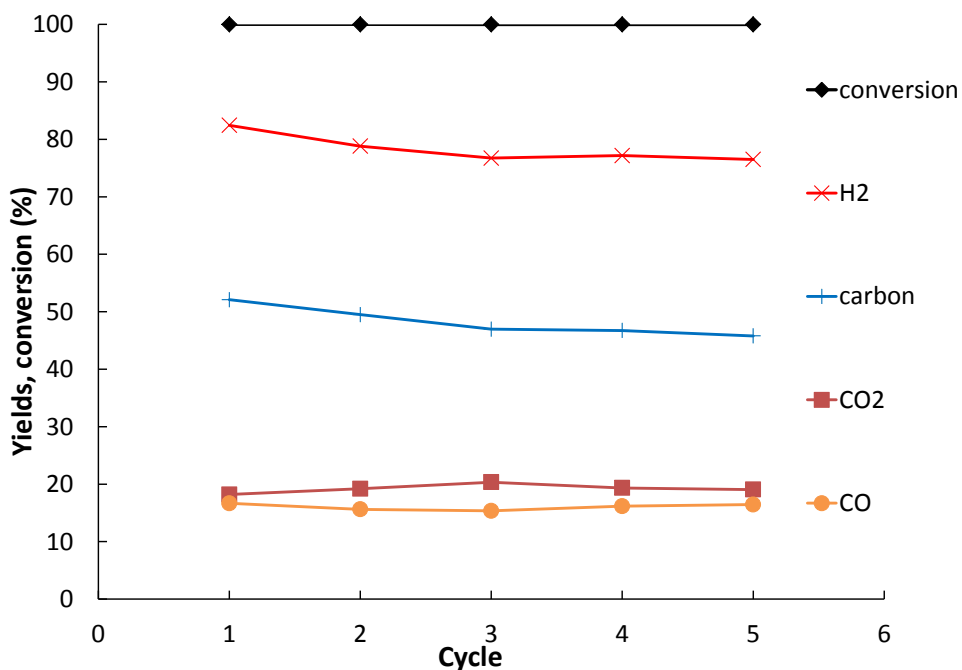
4.6.1.4. $CuFe_2O_4$
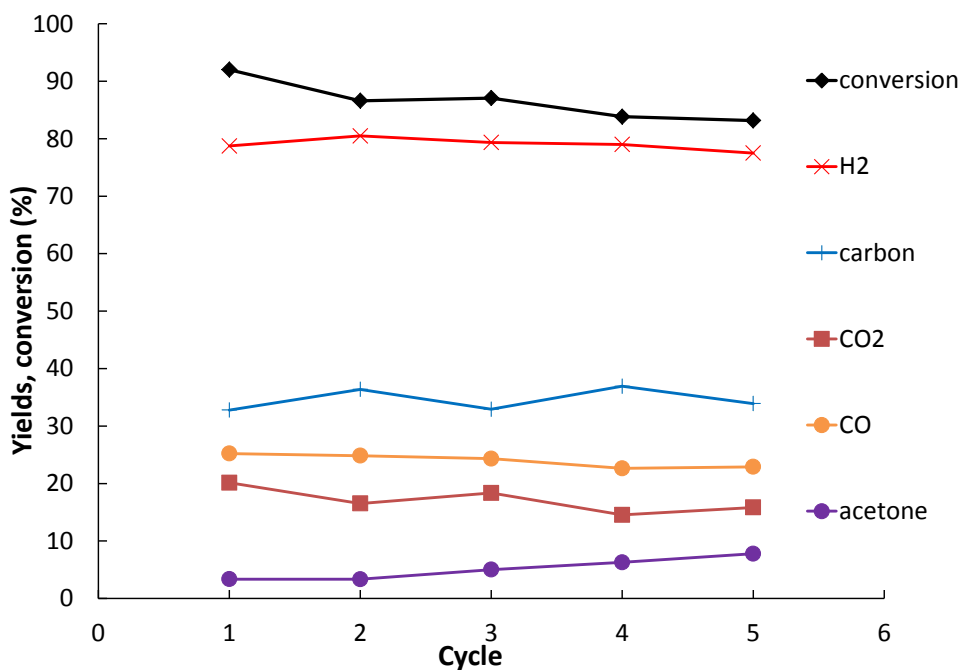
Figure 4-46. Conversion and Yields in main products obtained during the 20 min-reduction steps running repeated cycles on $CuFe_2O_4$ at 450°C

Copper ferrite (Figure 4-46) showed the lowest ethanol conversion amongst all ferrites, equal to 92% during the 1st cycle, down to 83% at the 5th cycle. Hydrogen yield reached values around 80%, similarly to the other ferrites. The catalyst showed good stability during cycling, and low carbon yield, about 30 - 40%, which is low if compared to values obtained with the other oxides. Yields to carbon oxides were also constant during cycling, with CO yield around 25% and CO_2 between 15 and 20%. As in the case of magnetite, the only yield which increased during cycling was that to acetone, from 3% at the 1st cycle to 8% at the 5th cycle.
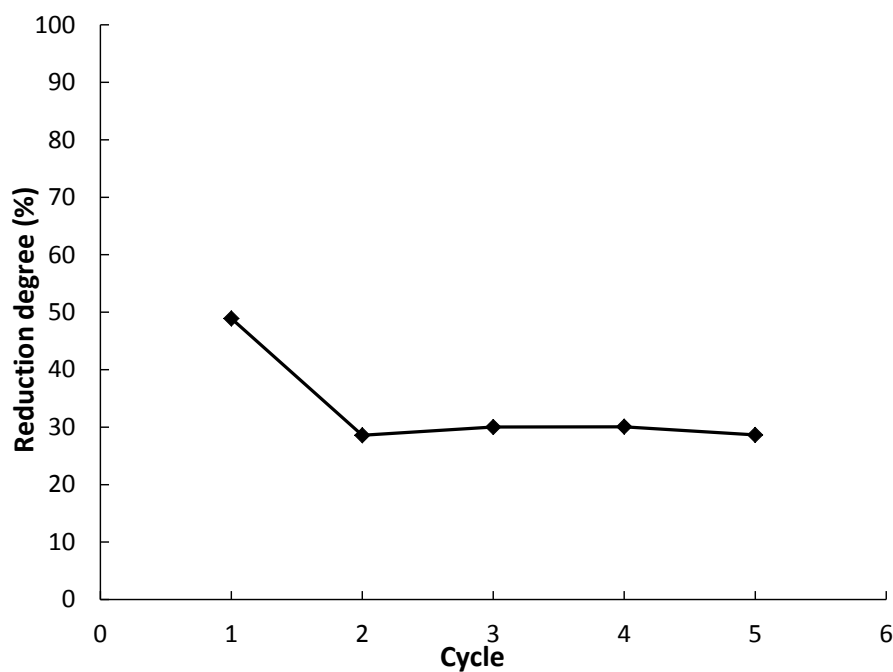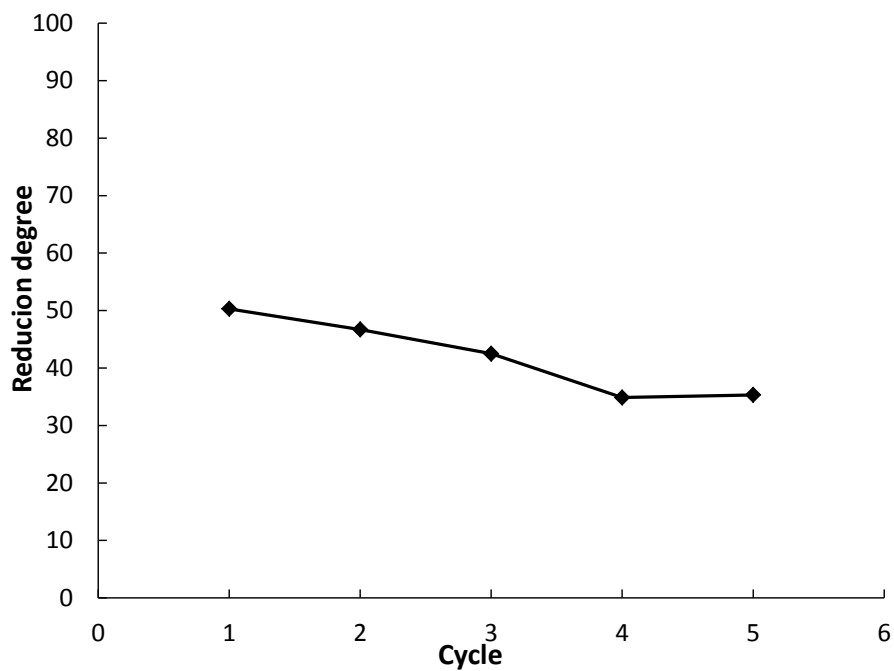
Figure 4-47. Reduction degree achieved by CuFe$_2$O$_4$ during the 20 min-reduction steps running repeated cycles at 450°C

The reduction degree achieved (Figure 4-47) during each reducing step decreased during cycling, from an initial value of 50% down to 35% after the reduction at the 4th and 5th cycle.
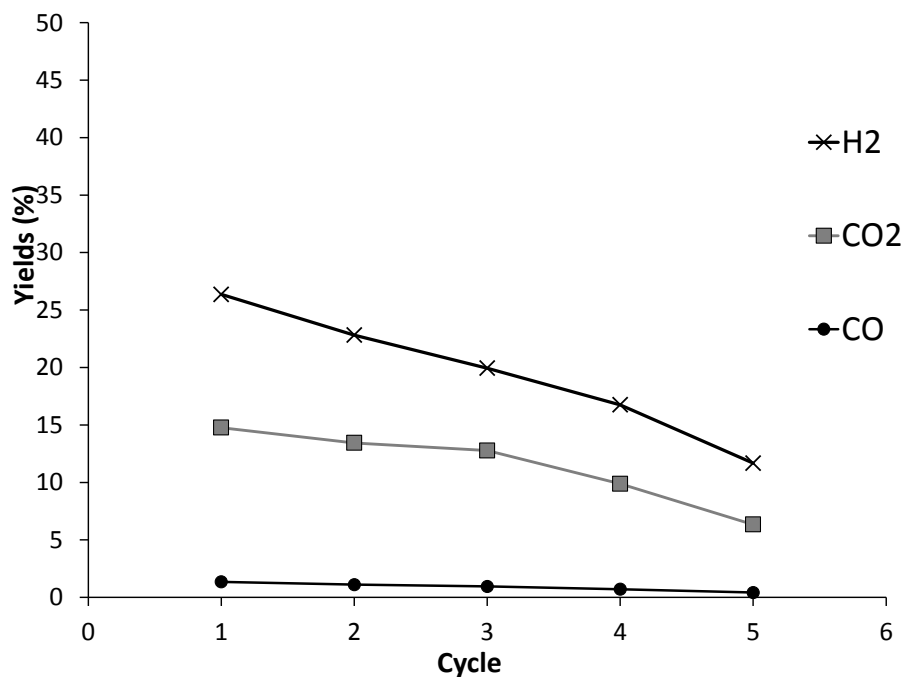
Figure 4-48. Integrated yields in main products obtained during the 20 min-re-oxidation steps running repeated cycles on CuFe$_2$O$_4$ at 450°C

Integrated yields to hydrogen (Figure 4-48) decreased along with cycles, from 26% down to 12% at the 5th cycle. The CO$_2$ yield was 15% at the beginning and decreased down to 6% at the 5th cycle; CO yield also showed a decreasing trend, but remained always less than 1%.

4.6.2. Characterization of samples after 20 minutes cycles

X-ray diffraction pattern of samples after (a) 20 min reduction with ethanol, (b) 1 complete cycle of 20 minutes per step (c) after 4 complete cycles plus 20 min more of reduction, and (d) after 5 complete cycles were recorded

Figure 4-49. X-Ray diffractograms of Fe$_3$O$_4$ collected after the different step of the 20 minutes step cycles at 450°C (X= Fe$_3$C; other peaks = magnetite)

Figure 4-49 shows the patters recorded for magnetite. After 20 min reduction, magnetite was in part reduced to carbides. The pattern went back to the one typical of magnetite when the cycle was completed by 20 min of re-oxidation, in fact no traces of carbides were left. After 4 complete cycles plus 20 min reduction, magnetite was again partially

reduced to carbides; however, in this case, the amount seemed to be much lower. This may mean that the material is less easily reduced with the increase of cycle number. The X-ray diffraction pattern obtained after the magnetite had completed 5 cycles demonstrate that even in this case the original spinel structure was completely recovered.
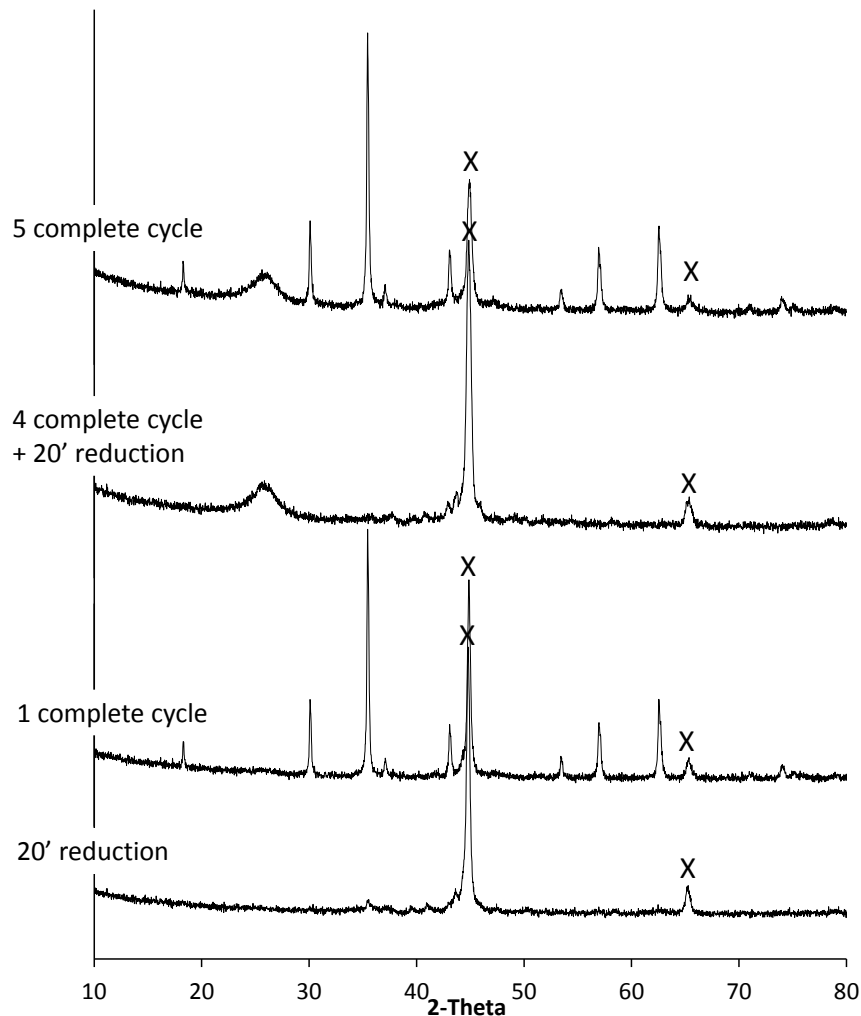
Figure 4-50. X-Ray diffractogram of CoFe$_2$O$_4$ collected after the different step of the 20 minutes step cycles at 450°C (X= Co$_3$Fe$_7$; other peaks = carbides in the reduced samples; magnetite in the reoxidized samples)

Differently from magnetite, with cobalt ferrite (Figure 4-50) 20 min under ethanol flow at 450°C were enough to fully reduce the material. Specifically, the ferrite was mainly reduced to Co$_3$Fe$_7$ alloy and, in minor amount, to iron carbides as shown by the

133

correspondingly weak reflections (Figure 4-50). After re-oxidation with water, the iron carbide disappeared, and the reflections attributable to the cobalt iron alloy also became less intense. Moreover, the pattern of the ferrite was shown again, which means that part of the reduced material had been restored to the ferrite phase. After 4 complete cycles plus 1 reduction, the material was again fully reduced to the cobalt-iron alloy and iron carbide. Moreover, in this case it was also possible to observe the presence of a broad reflection at 26° 2θ, which indicates the presence of coke. After the 5th re-oxidation, the material was partially re-oxidized to ferrite, but a part of it remained as reduced cobalt-iron alloy (Co_3Fe_7). No traces of carbide were found, however the peaks of coke were still present, which indicates that carbon was accumulating during cycling.
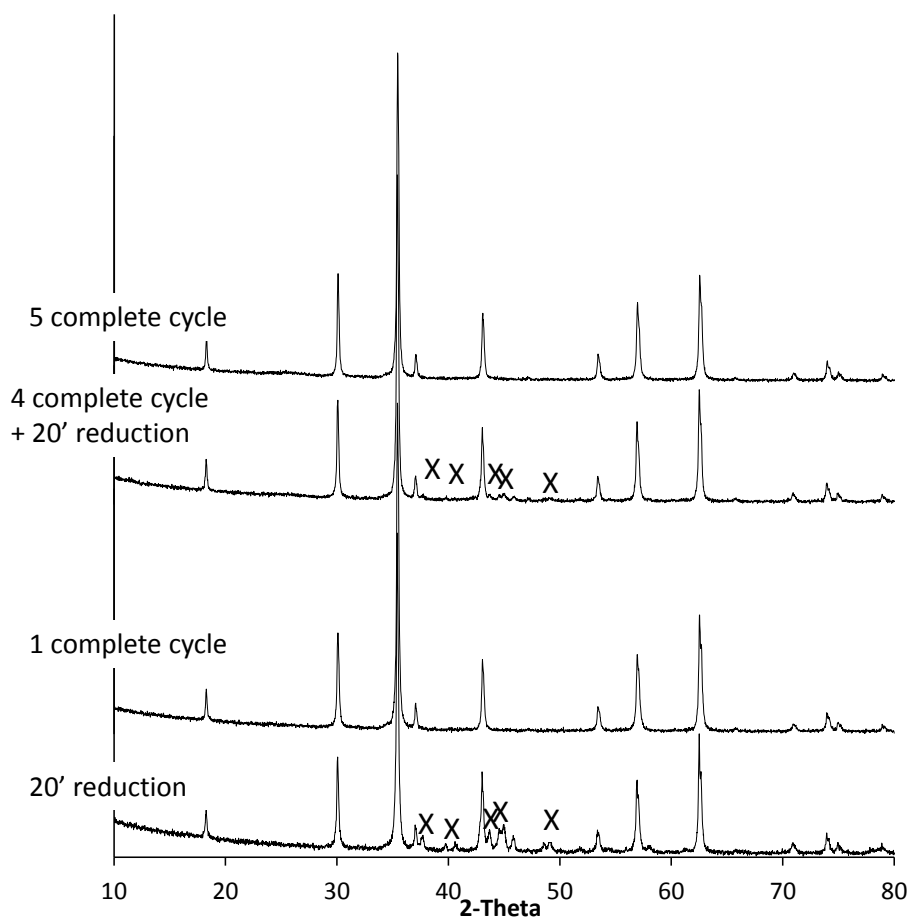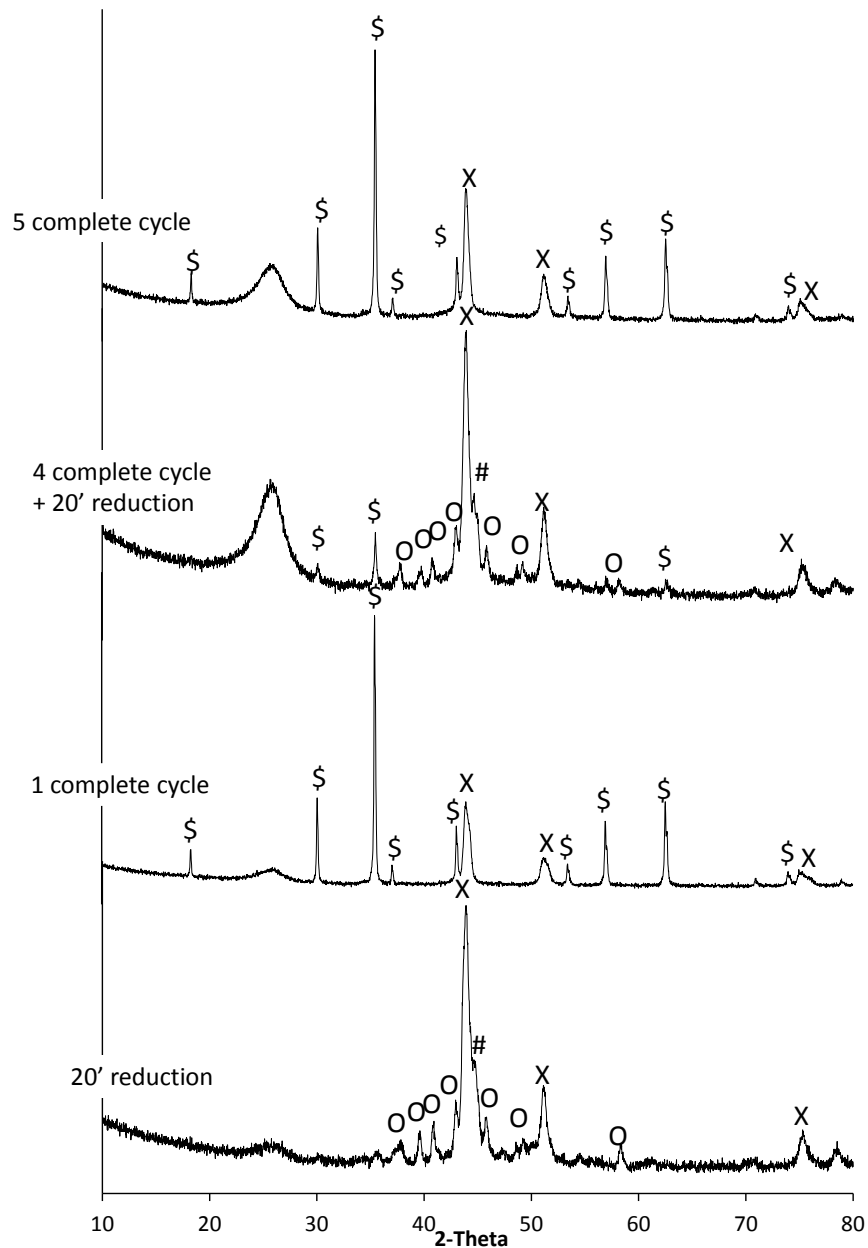
Figure 4-51. X-Ray diffractogram of NiFe$_2$O$_4$ collected after the different step of the 20 minutes step cycles at 450°C (X= Ni,Fe alloy; # = Ni^0; O = Fe$_3$C; $ = ferrite)

As previously observed during the 1h cycles, after contact with ethanol the nickel ferrite was reduced mainly to nickel, iron alloy, whereas a part of Ni is segregated as Ni^0 (Figure 4-51) Moreover, in this case it is possible to observe a relevant amount of Fe$_3$C and a small but broad reflection due to coke. After 20 min re-oxidation with water, the majority of the material had been re-oxidized to the ferrite, but a part remained reduced as Ni-Fe alloy.

The reflection of coke, although less intense, was still visible, which indicates coke accumulation during cycling. After 4 complete cycles plus 20 min reduction the material was again fully reduced to the iron-nickel alloy, iron carbide and metallic nickel. The amount of residual coke was relatively high in this case. After 5 complete cycles the sample was oxidized to ferrite, but a part of it remained reduced as Ni-Fe alloy. Finally, the peak of coke was still shown.

Table 4-4. Parameters used to fit the Mössbauer spectrum of the Fe_3O_4 sample after the different 20 minutes step with ethanol at 450°C, recorded at 25°C.

Sample	Fe^{3+}			$Fe^{2,5+}$			Fe_3C			Fe SPM[1]		
Fe_3O_4	IS	H	%	IS	H	%	IS	H	%	IS	QS	%
After 20' reduction	0.27	49.2	27.3	0.66	46.0	41.0	0.20	21.0	28.4	0.25	0.94	3.3
After 1 complete cycle	0.27	49.2	41.9	0.65	46.1	58.1	-	-	-	-	-	-
after 4 cycles and 20' reduction	0.26	49.0	36.6	0.65	45.9	53.9	0.11	20.9	9.5	-	-	-
After 5 cycles	0.27	49.0	41.4	0.65	45.8	58.6	-	-	-	-	-	-

[1] **Fe SPM indicates the doublet due to superparamagnetic species.**

The results of the Mössbauer characterization have been summarized in Table 4-4. It is possible to observe that after 20 min reduction the material was partially reduced to Fe_3C, as also previously observed by means of XRD analysis. The amount of iron carbide was the 28.4%, while the non-reduced species were present as the Fe^{3+} in tetrahedral sites (27.3%), the mixed value $Fe^{2,5+}$ (41.0%) in the octahedral sites and superparamagnetic

Fe^{3+}. As mentioned before the superparamagnetism is due to the small dimension of crystallites, where fast relaxations of the magnetic moments due to thermal excitation at temperatures below the Curie temperature or Néel temperature (at which materials are supposed to show magnetic behaviors) occur; as a result, a doublet is obtained. According to [13], the superparamagnetic species in that range of isomer shift and hyperfine fields are due to small particles of trivalent iron. The superparamagnetic iron represented the 3.3% of the sample. The ratio between the species Fe^{3+} : $Fe^{2,5+}$ was 40 : 60, which indicates that probably the carbide derived mainly from species sitting in the octahedral sites.

Results of the Mössbauer analysis on the other materials are not complete. The only results that may allow a comparison of ferrites are those obtained after the first 20 min of reduction. With the cobalt ferrite (which was only characterized after the first 20 minutes of reduction), it was possible to fit the resulting spectrum with two sextets and one doublet. The more important sextet was characterized by the typical parameters of Fe^0, having an isomer shift of 0.04mm/s and an internal hyperfine field of 35.5T. Its amount was the 57.7% of the total iron. The second sextet, representing the 28.3% of the overall iron content, was typical of the Fe_3C with an IS of 0.21mm/s and an H of 20.1T. The remaining 14% was represented by the doublet, due to the presence of superparamagnetic species. Also in this case the results of the Mössbauer characterization allowed us to precisely quantify the amount of the different Fe species.

Table 4-5. Parameters used to fit the Mössbauer spectrum of the NiFe$_2$O$_4$ sample after the different 20 minutes step with ethanol at 450°C, recorded at 25°C.

Sample	Fe^{3+}			Fe$^{2,5+}$			Fe$_3$C			Fe^0		
NiFe$_2$O$_4$	IS	H	%	IS	H	%	IS	H	%	IS	H	%
After 20' reduction	-	-	-	-	-	-	0.28	19.0	80.9	0.08	30.9	10.6
After 1 complete cycle	0.27	49.0	31.6	0.66	45.8	43.0	-	-	-	0.03	30.1	19.0

In the case of nickel ferrite, from the XRD pattern it was not possible to conclude if the prevailing reduced species was either the iron carbides or the nickel iron alloy. By means of the Mössbauer characterization (the results are only those from the first 20 min reduction and one complete 20 min cycle), it was possible to determine that the Fe$_3$C specie (IS = 0.28mm/s; H = 19.0T) was the 80.9% of the total Fe content after 20 min reduction, whereas the Fe^0 species (IS = 0.08mm/s; H = 30.9T) was the 10.6% (Table 4-5).

After completion of the 1st cycle, the material was in part re-oxidized to ferrite, but there was still the 19.0% of Fe^0 (IS = 0.03mm/s; H = 30.1T). As inferred from XRD pattern, this reduced species should be an iron nickel alloy; in fact it is possible to find in literature [14, 15] that these parameters are also characteristic of a large variety of Ni-Fe alloys. The magnetite signals were given, once again, by two sextets. The sextet characteristic of the Fe^{3+} species (IS = 0.27mm/s; H = 49.0T) was the 31.6% of the Fe content, while the sextet characteristic of Fe$^{2,5+}$ (IS = 0.66mm/s; H =45.8T) was the 43.0%. The ratio between Fe^{3+} : Fe$^{2,5+}$ was 42.4 : 57.6, which indicates an increase on the species Fe^{3+} after the cycle.

Table 4-6. Parameters used to fit the Mössbauer spectrum of the CuFe$_2$O$_4$ sample after the different 20 minutes step with ethanol at 450°C, recorded at 25°C.

Sample CuFe$_2$O$_4$	Fe^{3+}			Fe$^{2,5+}$			Fe$_3$C			Fe^0		
	IS (mm/s)	H (T)	%	IS (mm/s)	H (T)	%	IS (mm/s)	H (T)	%	IS (mm/s)	H (T)	%
After 20' reduction	0.30	50.1	4.9	-	-	-	0.23	20.9	79.3	0.08	30.9	15.8
After 1 complete cycle	0.30	48.7	40.4	0.65	45.4	56.6	-	-	-	-	-	-
after 4 cycles and 20' reduction	0.31	49.6	27.3	0.62	46.1	16.2	0.20	20.9	45.3	-	-	-
After 5 cycles	0.28	49.1	47.4	0.66	45.9	50.5	-	-	-	-	-	-

In the case of copper ferrite (Table 4-6), after 20 min reduction the majority of the sample (79.3%) was reduced to Fe$_3$C (IS = 0.23mm/S and H = 20.9T) and a 15.8% was due to Fe^0 (IS = 0.08mm/s; H = 30.9T). The remaining 4.9% was characterized by a non-defined sextet which was fitted using an isomer shift of 0.20 mm/s, a hyperfine magnetic field of 50.1T and a quadrupole splitting of 0.22mm/s. The latter has been attributed to an Fe^{3+} specie, however, according to literature [16], in the case of copper ferrite the Fe^{3+} is characterized by two sextets for the Fe^{3+} species sitting either in the octahedral or tetrahedral sites, both with larger hyperfine fields than magnetite. It is possible that in this case, because of its small amount, one of the two sextets was hidden by the bigger one, so both the sextets have been fitted with only a larger one. This was not observed on the fresh material, because its small particles gave a doublet due to superparamagnetism; however, it is possible that the sintering caused by the reduction with ethanol had rendered these species detectable by means of Mössbauer.

After completing the cycle, the material appeared to be fully re-oxidized. However in this case, the parameters were more similar to those of magnetite with hyperfine fields below 50T. This could indicate that copper had segregated, a point which would not be seen by means of XRD because the patterns of magnetite and copper ferrite are similar. In this case, the ratio Fe^{3+} : $Fe^{2,5+}$ was 41.6 : 58.4, that indicates an enrichment in Fe^{3+}. There was also a 3.0% amount of a superparamagnetic specie having IS = 0.11mm/s and QS = 0.59mm/s. After completing 4 cycles plus 20 min reduction, the material was not as strongly reduced as it was the after the first 20 min reduction. In fact the two sextets representing the ferrite specie contributed by the 43.5% (combined), and the carbide by the 45.3%. The remaining 11.2% was due to a superparamagnetic specie with IS = 0.46mm/s and QS = 1.22mm/s. The isomer shift and the quadrupole splitting of this doublet were relatively high for a Fe^{3+} species; however, the typical value of Fe^{2+} are even higher according to [13], but it could be possible that their presence has an influence on this deviation. Finally, after 5 complete cycles, the material was once again fully oxidized. The Fe^{3+} species (IS = 0.28mm/s; H = 49.1T) was the 47.4% and the $Fe^{2,5+}$ (IS = 0.66mm/s; H = 45.9T) was the 50.5%. Also in this case these parameters were typical of magnetite, which confirms the segregation of Cu from the ferrite. The ratio between the two species was even richer in the Fe^{3+} species, that could confirm the loss of copper from the octahedral sites and the inability of Fe^{3+} sitting in tetrahedral sites to occupy all vacancies.

Table 4-7. %C after the different steps of the 20 minutes cycles on the different ferrites

Sample	After 20' reduction (%)	After 1 cycle (%)	After 4 cycles + 20' reduction (%)	After 5 cycles (%)
Fe_3O_4	5.3	5.3	13.4	17.3
$CoFe_2O_4$	12.7	9.6	55.8	42.7
$NiFe_2O_4$	20.7	20.8	64.9	60.7
$CuFe_2O_4$	n.d.	n.d.	n.d.	n.d.

From the CHN analysis it was possible to determine the amount of carbon in samples (except for $CuFe_2O_4$), after the initial and final steps of the 20 min cycles (Table 4-7). In the case of magnetite, results were quite strange, since after the first 20 min reduction and after the complete cycle the amount of carbon was always equal to 5.3%, which, however, is a relatively good result compared to those obtained during the 1 hour cycles. After 4 complete cycles plus 20 min reduction the amount of carbon grew up to the 13.4%. This means that carbon was accumulating during the repeated cycles, and was not removed during re-oxidation with steam. Nevertheless, still it was a good result compared with results obtained during 1 hour reduction. After the 5th re-oxidation, the carbon content had raised again until the 17.3%. What is important to note is that in the amount of carbon was always less than 20%.

With the cobalt ferrite the C content was much higher; in fact after 20 min reduction the value obtained was of 12.7% and it decreased, as expected, down to the 9.6% after re-oxidation with water. The carbon went on accumulating on catalysts during cycles; in fact after 4 cycles plus one reduction, the carbon amount was the 55.8%, and after the 5th re-oxidation it was only in part consumed to the 42.7%. A similar trend was also shown with the nickel ferrite.

4.6.3. Conclusions on repeated cycles

4.6.3.1. Reactivity

The results reported in this paragraph can be divided in three groups:

a) The yields obtained during the repeated reduction steps showed relatively small differences between ferrites; however, these differences implied more important variations in the reduction degree achieved during each reduction step.

b) With all ferrites, the reduction degree decreased during cycling. In the case of magnetite the reduction degree went on decreasing after each cycle, while in the case of the other ferrites it seems that there was a point at which the material became "stable", and its reduction degree did not decrease any more during successive cycles. Surprisingly, this occurred with samples showing the greater amount of residual carbon accumulated on catalyst; in fact, one might expect that this hinders the reduction of the solid during contact with ethanol. Magnetite, which accumulated the smaller amount of carbon during cycles, was the sample showing the continuous decrease of reduction degree achieved during successive cycles.

c) During the re-oxidation step the yield to the main products (H_2, CO_2 and CO) decreased during cycling, but showed a more stable behavior with Ni and Co ferrites. The spinel showing the best performance was the nickel ferrite, which gave hydrogen yield always above the 20% and seemed not to decrease any more after the 3rd cycle.

Considering all these aspects, nickel ferrite seems to be the material more suitable for cycling, since its behavior seems to be more stable. On the other hand, it is also the material showing the highest yield to CO_2 during the re-oxidation steps, an aspect that once again highlights the need for limiting the carbon formation during the reduction step.

An advantage of shortening the reaction time during the reduction step is the considerable decrease of CO production during the re-oxidation step. With reduction

steps lasting 1 hour, the yield to CO was no less than 4-5%, whereas using 20 min reduction steps, CO yields lower than 1% were shown with all ferrites.

4.6.3.2.Characterizations

From the XRD characterization it was possible to identify the species that are produced during the different steps of the cycles. Particularly, the XRD analysis allowed us to find out that the segregated species are not reincorporated inside the ferrite structure during the re-oxidation step. The Mössbauer characterization has been important to quantify the amount of the different Fe species and compare the reduction levels achieved with the different ferrites. Finally, the CHN allowed to quantify the coke and carbides produced during cycling, which was not possible by means of the other techniques.

Particularly in the case of magnetite, it was shown by means of XRD and Mössbauer spectroscopy that it is the ferrite which is less reduced by ethanol, but also it is the more easily re-oxidized; moreover, it is also the sample that produced the lower amount of carbon.

The cobalt ferrite was more easily reduced by ethanol, however during the re-oxidation a part of the Co_3Fe_7 alloy remained in its reduced state. Moreover, through the CHN analysis, it was shown that the amount of carbon produced was greatly higher than that shown with magnetite.

The nickel ferrite once again showed a behavior similar to that of the cobalt ferrite. Even though from reactivity tests this ferrite seems to be the more suited to the chemical looping, it is characterized by several drawbacks. In fact, the amount of carbon produced was the highest, and the segregated species could not be reincorporated into the ferrite structure (probably because the presence of carbon hinders its reaction with steam). Despite this, it surprisingly showed the more stable behavior during repeated cycles,

The copper ferrite was characterized only by means of Mössbauer spectroscopy. Nevertheless, it was possible to observe that the prevailing reduced specie were iron carbides, which were produced in less quantities while increasing the number of cycles.

References:

[1]   K. Rintramee, K. Föttinger, G. Rupprechter, and J. Wittayakun, "Ethanol adsorption and oxidation on bimetallic catalysts containing platinum and base metal oxide supported on MCM-41," *Appl. Catal. B Environ.*, vol. 115, pp. 225–235, 2012.

[2]   S. M. de Lima, A. M. da Silva, L. O. O. da Costa, J. M. Assaf, G. Jacobs, B. H. Davis, L. V. Mattos, and F. B. Noronha, "Evaluation of the performance of Ni/La2O3 catalyst prepared from LaNiO3 perovskite-type oxides for the production of hydrogen through steam reforming and oxidative steam reforming of ethanol," *Appl. Catal. A Gen.*, vol. 377, no. 1, pp. 181–190, 2010.

[3]   J. Llorca, N. Homs, and P. Ramirez de la Piscina, "In situ DRIFT-mass spectrometry study of the ethanol steam-reforming reaction over carbonyl-derived Co/ZnO catalysts," *Journal of Catalysis*, vol. 227, no. 2. pp. 556–560, 2004.

[4]   J. V. Ochoa, C. Trevisanut, J.-M. M. Millet, G. Busca, and F. Cavani, "In Situ DRIFTS-MS Study of the Anaerobic Oxidation of Ethanol over Spinel Mixed Oxides," *J. Phys. Chem. C*, vol. 117, no. 45, pp. 23908–23918, Nov. 2013.

[5]   M. Dömök, M. Tóth, J. Raskó, and A. Erdőhelyi, "Adsorption and reactions of ethanol and ethanol–water mixture on alumina-supported Pt catalysts," *Appl. Catal. B Environ.*, vol. 69, no. 3, pp. 262–272, 2007.

[6]   G. Busca, "Infrared studies of the reactive adsorption of organic molecules over metal oxides and of the mechanisms of their heterogeneously-catalyzed oxidation," *Catal. Today*, vol. 27, no. 3, pp. 457–496, 1996.

[7]   S. M. de Lima, A. M. da Silva, L. O. O. da Costa, U. M. Graham, G. Jacobs, B. H. Davis, L. V. Mattos, and F. B. Noronha, "Study of catalyst deactivation and reaction mechanism of steam reforming, partial oxidation, and oxidative steam reforming of ethanol over Co/CeO2 catalyst," *J. Catal.*, vol. 268, no. 2, pp. 268–281, 2009.

[8]   H. Song and U. Ozkan, "Ethanol steam reforming over Co-based catalysts: Role of oxygen mobility," *J. Catal.*, vol. 261, no. 1, pp. 66–74, Jan. 2009.

[9]   R. Padilla, M. Benito, L. Rodríguez, a. Serrano, G. Muñoz, and L. Daza, "Nickel and cobalt as active phase on supported zirconia catalysts for bio-ethanol reforming: Influence of the reaction mechanism on catalysts performance," *Int. J. Hydrogen Energy*, vol. 35, no. 17, pp. 8921–8928, Sep. 2010.

[10]   S. M. de Lima, R. C. Colman, G. Jacobs, B. H. Davis, K. R. Souza, A. F. F. de Lima, L. G. Appel, L. V. Mattos, and F. B. Noronha, "Hydrogen production from ethanol for PEM fuel cells. An integrated fuel processor comprising ethanol steam reforming and preferential oxidation of CO," *Catal. Today*, vol. 146, no. 1–2, pp. 110–123, Aug. 2009.

[11]   S. Cocchi, "A chemical loop approach for methanol reforming," Università di Bologna, 2012.

[12]   G. A. Sawatzky, "Mössbauer Study of Electron Hopping in the Octahedral Sites of Fe3O4," *J. Appl. Phys.*, vol. 40, no. 3, p. 1402, Nov. 1969.

[13]   L. Moloto, S. Manzini, and E. Dikio, "Reduction of Magnetite in the Presence of Activated Carbon Using Mechanical Alloying," *J. Chem.*, vol. 2013, no. C, pp. 1–8, 2013.

[14]   A.-F. D. Lehlooh and S. H. Mahmood, "Mössbauer Spectroscopy Study of Iron Nickel Alloys," *Hyperfine Interact.*, vol. 139–140, no. 1–4, pp. 387–392, Mar. 2002.

[15]   J. Nishimura and K. Nomura, "57Fe conversion electron Mössbauer study of oxidized iron-nickel alloy pins," *Hyperfine Interact.*, vol. 207, no. 1–3, pp. 19–23, Dec. 2011.

[16]   J. Janicki, J. Pietrzak, A. Por??bska, and J. Suwalski, "Mössbauer Study of Copper Ferrites," *Phys. status solidi*, vol. 72, no. 1, pp. 95–98, Jul. 1982.

5. SHORT TIME TESTS

5.1. INTRODUCTION

In the previous chapters, we have shown that during the two looping steps, i.e. the ethanol oxidation and material re-oxidation by water, the samples were deeply transformed. For example in the first step magnetite was converted into metallic iron and iron carbide and in the second the cited phases were converted back to magnetite. It was important to try to understand how these transformations took place in order to control them. For this goal, the material transformations have been studied by in-situ XRD. The results obtained are presented and discussed in the first part of this chapter.

It was also shown in the previous chapters that coke was formed very early in the first step of the chemical loop and was only partially converted in the second step. Two strategies could be used to solve this problem. The first one was to run very short time looping steps and the second was to introduce a third step in the looping consisting in a treatment under oxygen or air to burn the coke remaining after the second step. These two possibilities have been studied and the results of the experiments are presented in the second part of this chapter.

5.2. IN-SITU XRD STUDY OF MAGNETITE DURING ETHANOL OXIDATION

X-ray diffraction patterns of the magnetite sample have been recorded under nitrogen flow at 450°C after successive period of time under ethanol feeding. For that, few mg of magnetite annealed at 450°C have been loaded in the heating chamber of the X-ray diffraction apparatus, described in Chapter 2.2.3. A first pattern has been recorded at 25°C under a N_2 flow of 30ml/min. At this point, the sample was heated to 450°C increasing temperature by 5°C/min and, after waiting 20 minutes for stabilization, a pattern was recorded. The two patterns were comparable except a variation of cell parameters related to the thermal expansion of the lattice cell. It was then started to feed ethanol for 1 minute with a flow of 0.52ml/h (11% in nitrogen). After this exposure, the flow was switch back to N_2 and a pattern was recorded. This procedure was repeated several times but increasing the feeding time. The obtained diffractograms have been analyzed using the Rietveld method. The various phases have been identified and for each phase, crystallites sizes, lattice parameters and relative weight percentage in the sample have been calculated. These results are presented in Figures 5-1 to 5-10. Each of the calculated parameters have been plotted as a function of the cumulative amount of ethanol to which the sample was exposed.

5.2.1. 1st stage of the study: magnetite evolution during the first ten minutes under ethanol stream.

The evolution of the phase composition of the magnetite sample has been plotted in Figure 5-1 versus the cumulative amount of ethanol to which the sample was exposed at 450°C.
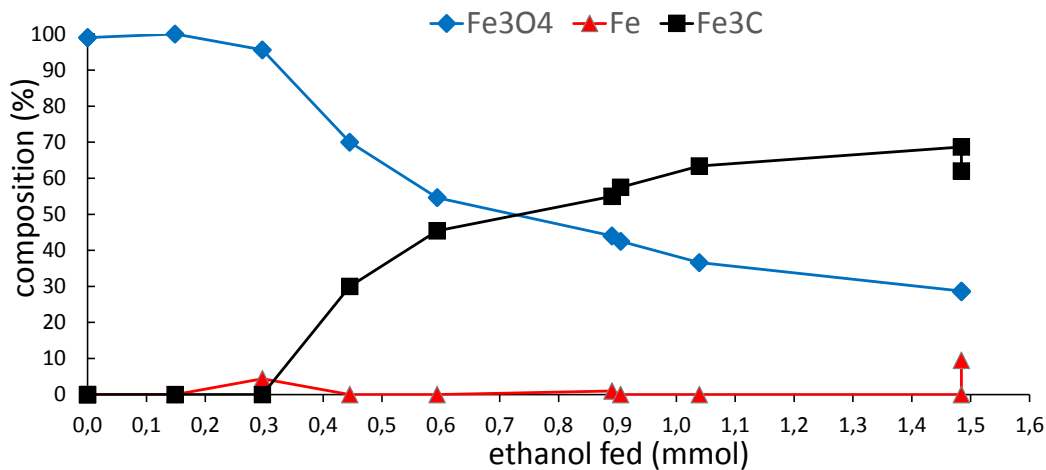
Figure 5-1. Composition of the sample versus the cumulative amount of ethanol to which the sample was exposed at 450°C during the in-situ XRD experiment. The last point (a) corresponds to the results of the diffractogram collected at 450°C after cooling down the apparatus for one night

No change of phase composition was observed after feeding 0.15mmol of ethanol (which, in this experiment conditions corresponds to 1 minute of feeding). The magnetite should only be reduced at the surface or transformed in very small amount. It should be recall that X-ray diffraction is not extremely sensitive and 1 or 2% of a new phase could easily not be detected. Furthermore at the beginning a small part of ethanol could be adsorbed on the walls of the in-situ cell and could not pass through the powdered sample. After feeding 0.30mmol of ethanol a change was observed, with the formation of metallic iron αFe (ICSD 00-003-1050) representing 4 weight % of the sample. The composition drastically changed when 0,45mmol of ethanol were fed. At this point, the amount of magnetite decreased to 70%, while a new phase Fe_3C was formed. In fact, Fe^0 seen before has disappeared. This clearly show that the reduction of the ferrite to iron carbides passes through the formation of metallic iron, which further reacts with ethanol to form Fe_3C. This is in accordance with what was suggested by Bonnet et al. [1].

After this point the magnetite relative ratio continued decreasing whereas that of the iron carbide increased without the appearance of other phases. When more than 0.7mmol of ethanol were fed, which corresponds to about 5 minutes of total feeding, the iron carbide

became the major phase. After 10 minutes of total feeding (about 1.5mmol) the experiment was stopped and the chamber containing the sample cooled down to room temperature under N_2 flow, for the night. The day after the apparatus have been turned on, the temperature was increased again by 5°C/min up to 450°C, and a pattern was recorded again. It was expected to obtain the pattern of the day before, however the composition of the phases was slightly changed ((a) in Figure 5-1). The percentage of the magnetite was the same however, the percentage of the carbide phase decreased and a small amount of metallic iron appeared.

It can be possible that during the process the carbide decomposed to iron and C

Fe3C → 3Fe + C
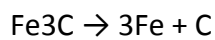
No peaks of C were found, but this can be due to the low crystallinity of the coke formed which avoids to obtain a good reflection.
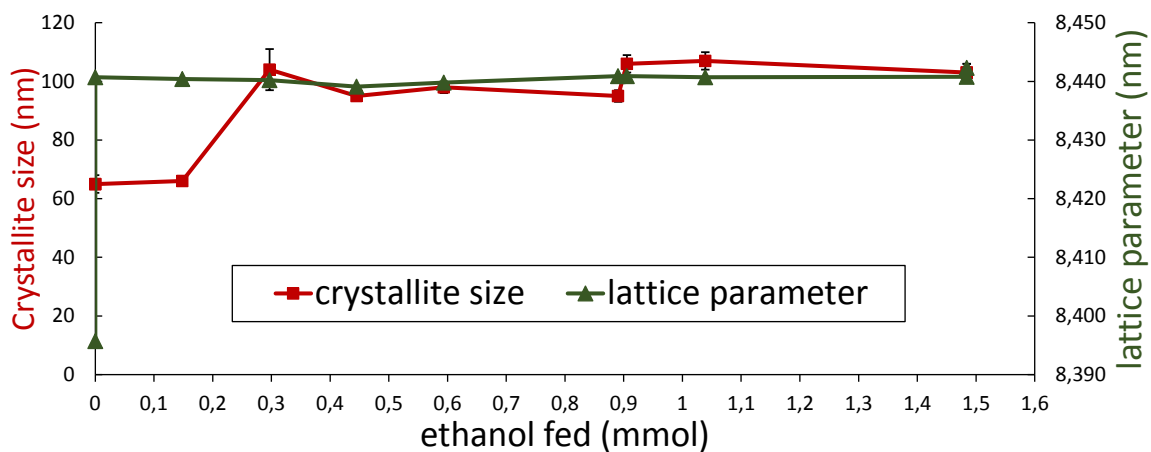

Figure 5-2. Crystallite size and cell parameter of the phase Fe₃O₄ during the in-situ XRD test

The trend of the crystallite size of the magnetite phase and its cell parameter is plotted as a function of the cumulative amount of ethanol in Figure 5-2. It is possible to see that as soon as the magnetite starts to be reduces its crystallite size increases from 66 to about

100 nm, which means that along with the reduction, a sintering of the magnetite phase took place. The size of the crystallite remains stable around 100nm continuing feeding the ethanol. The size of the crystallite increases from 95nm to 106nm and then remain at values above 100nm. The lattice parameter of magnetite (which is cubic and can be represented by only one parameter) remained stable with values between 8.4391 and 8.4423 during the feeding of ethanol.

5.2.2. 2nd stage of the study: re-oxidation of the magnetite sample evolution during the first two minutes of water feeding

It was interesting to study the re-oxidation of the reduced magnetite sample by water. Thus A after a total feeding of 10 minutes of ethanol, a flow of water was sent on the sample. The experimental parameters remained the same, with a temperature of 450°C, a flow of N_2 of 30ml/min and the liquid was fed at a rate of 0.52ml/h which in the case of water corresponds to 29% of the gas composition.
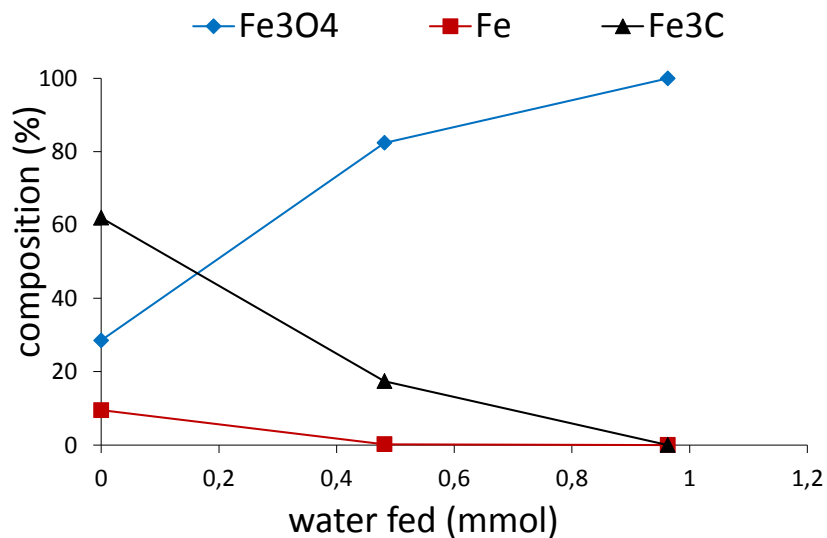
Figure 5-3. . Composition of the sample versus the cumulative amount of water to which the sample was exposed at 450°C during the in-situ XRD experiment

After only two minutes of water feeding, i.e. about 1.0mmol, the material changes completely its composition. The metallic iron and the carbide produced during the reduction are totally re-oxidized leading to pure magnetite.
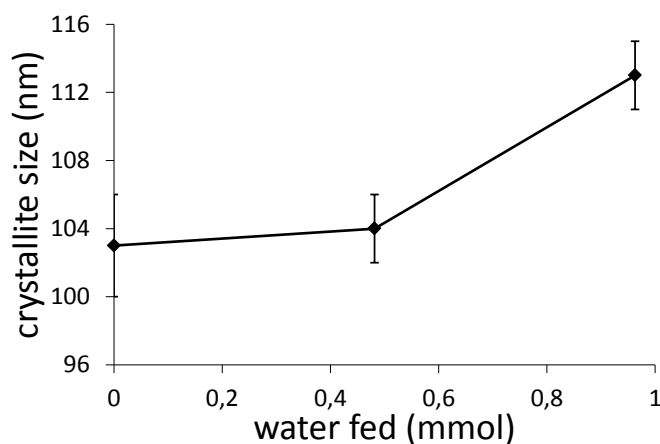

Figure 5-4. Crystallite size of the phase Fe$_3$O$_4$ during the in-situ XRD experiment feeding water for two minutes on the pre-reduced sample

The size of the crystallites of magnetite is further increasing during this part of the experiment. The value at the beginning is of about 104nm and rise up to 113 nm after 1mmol of water fed. This indicated that the water plays also a sintering role on the material.

5.2.3. 3rd part: one hour of ethanol feeding

Once the material was oxidized again to magnetite the experiment has been continued feeding ethanol again.
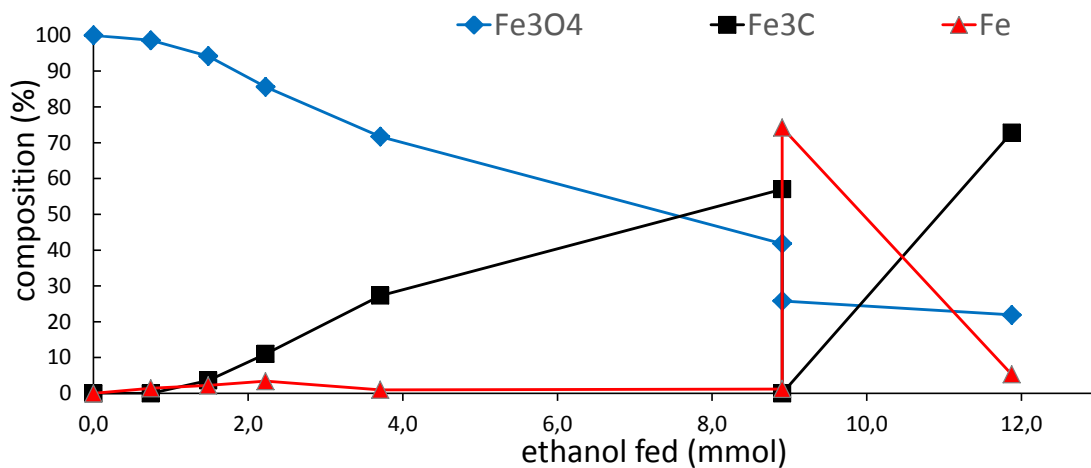

Figure 5-5. Composition of the sample versus the moles of ethanol fed at 450°C during the in-situ XRD experiment

Initially ethanol has been sent on the sample for 5 minutes, which corresponds to 0.7mmol of ethanol, and the x-ray pattern was recorded. However, in this case the material did not reach the same composition as in the first part of the experiment at the same amount of ethanol. In fact, in the first part of the experiment, when 0.7mmol of ethanol were fed the composition was about 50% of magnetite for 50% of iron carbide. In this experimental stage the composition was 98 % of magnetite and 2 % of iron, that means that the material has been only slightly reduced. It was possible that the ethanol

did not reach the sample because of some instrumental issue, and so the test has been repeated for five more minutes. At that point the magnetite was reduced to 94 %, and the amount of iron increased to 2 %. In the same time Fe_3C started to be produced (4 %). This means that the ethanol war reaching properly the sample even in the first five minutes, but another problem could have occurred. Either the material was not anymore active, less probable because the effect is very strong; either the water fed has remained into the apparatus and avoids the reduction of the sample, which is most probable. At this point, this stage of the experiment cannot be compared to the first one, however, the presence of water and the inhibition of the reducing effect of ethanol allowed changing the material more gradually and better observing the structural changes.

In fact in this case iron was better observed for a longer time, and was also observed when the iron carbide started to be produced, it started to decrease. This is in agreement on what was observed in the first experimental stage and confirm the main pathway of formation of the carbides pass through the formation of metallic iron. In this case, the tests were conducted up to a total feeding of 9 mmol of ethanol. The sample was then cooled down to room temperature under the N_2 flow and the phase composition at that point was: 57 % of Fe_3C, 42 % of Fe_3O_4 and 1 % of iron.

After a pause for the night during which the temperature had to be lowered to room temperature, the material has been heated back at 450°C at a constant rate of 5°C/min and the X-ray diffraction pattern was recorded. The composition of the sample was drastically changed: a small part of the magnetite has been further reduced and its composition decreased from 42 % to 26 %; the Fe_3C pattern was not found anymore, while the iron phase represented now the 74 % of the sample.

The reduction of the magnetite can be due to the presence of ethanol in the chamber atmosphere even after the end of the experiment. It is probable that at that point, since the apparatus was not equipped with an opportune venting system, both the water and the ethanol were not able to degas completely from the lines.

The transformation of the carbide into metallic iron could take place in the presence of excess of C at the surface of cementite which decomposed according to the following reaction:

$Fe_3C \rightarrow 3Fe + C$
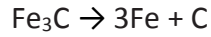
To check if it was possible to obtain again a majority of carbide, 3mmol of ethanol have been fed. At this point the composition of the sample was 73 % of carbide, 22 % of magnetite and 5 % of metallic iron. Moreover, the values seem to be those obtainable by continuing the trends at the same rate than before the interruption for the night.
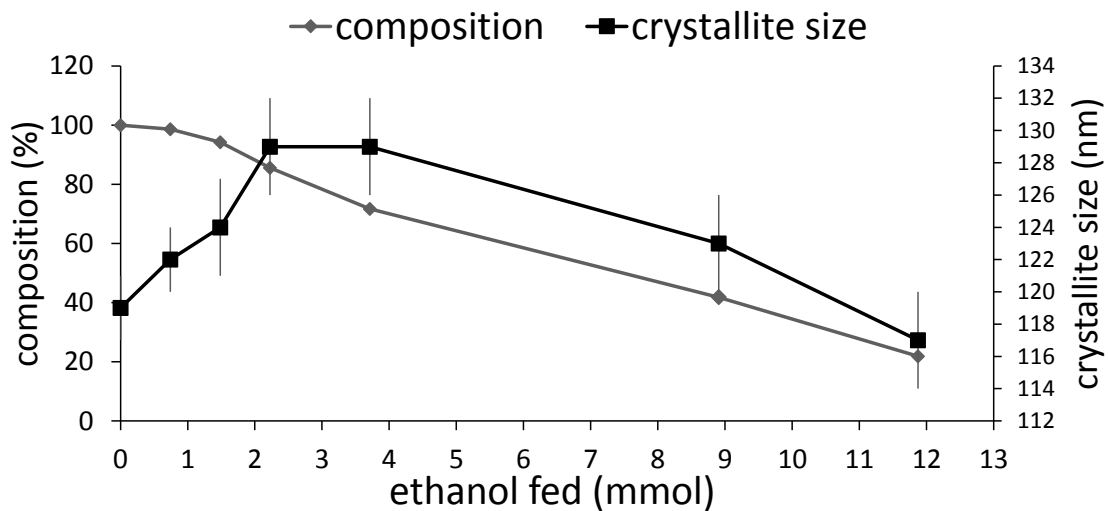

Figure 5-6. Composition and crystallite size of the phase Fe₃O₄ during ethanol feeding obtained from the in-situ XRD experiment

Observing the trend of the crystallite size at the changing of the composition of the sample it is possible to see that it was not significantly affected by the ethanol feeding, since its values were always between 117nm and 129nm. Such value should represent an equilibrium value for magnetite at 450°C.
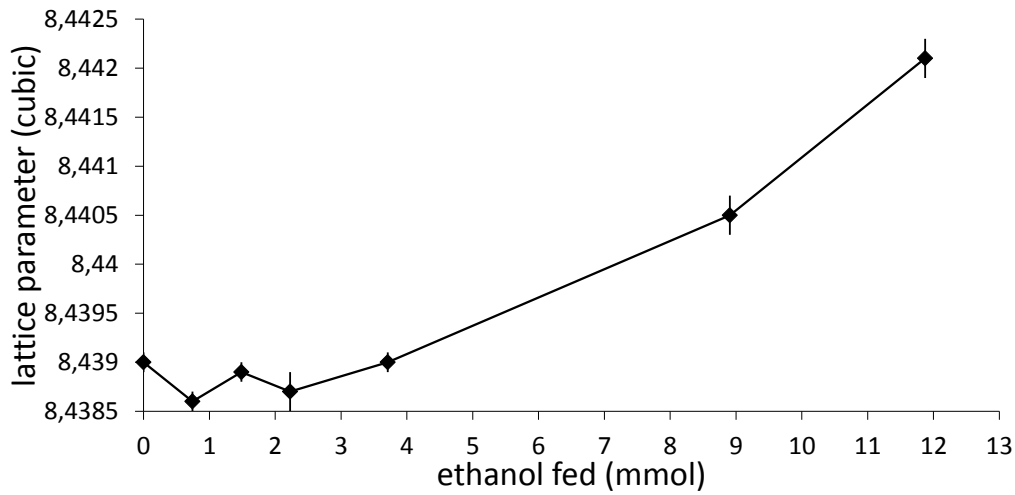
Figure 5-7. Trend of the lattice parameters of Fe₃O₄ during feeding ethanol at 450°C obtained from the in-situ XRD experiment

The lattice parameter of magnetite change slightly during the experiment, however it is possible to observe an increasing trend with ethanol feeding.
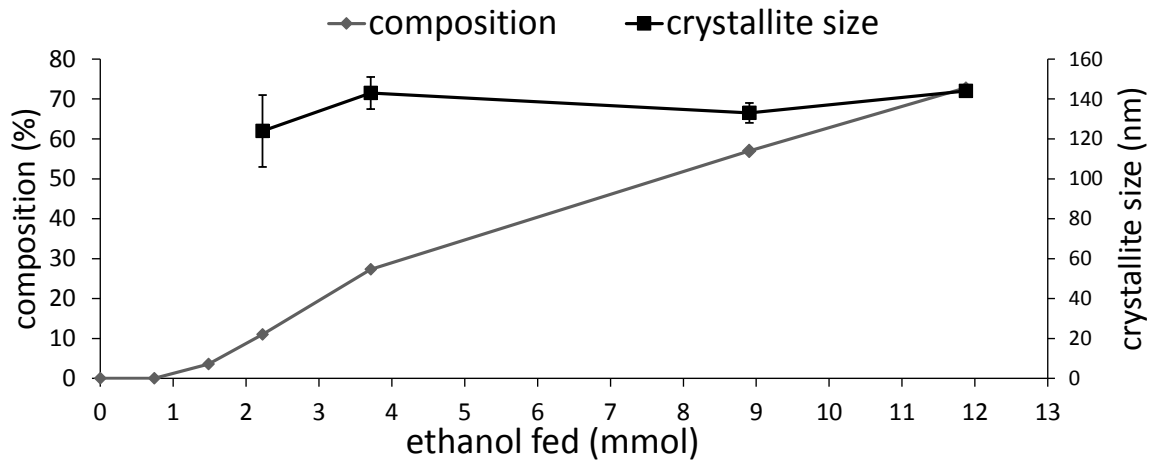

Figure 5-8. Composition and crystallite size of the phase Fe₃C during feeding ethanol at 450°C obtained from the in-situ XRD experiment

The crystallites size trend of the carbide produced from the reduction of the magnetite is characterized by a small initial increase from 124nm to 143nm at the beginning and then a stabilization.

5.2.4. 4th stage of the study: re-oxidation through ten minutes of water feeding

To conclude the experiment, water was fed again on the magnetite sample after the second reduction with ethanol.
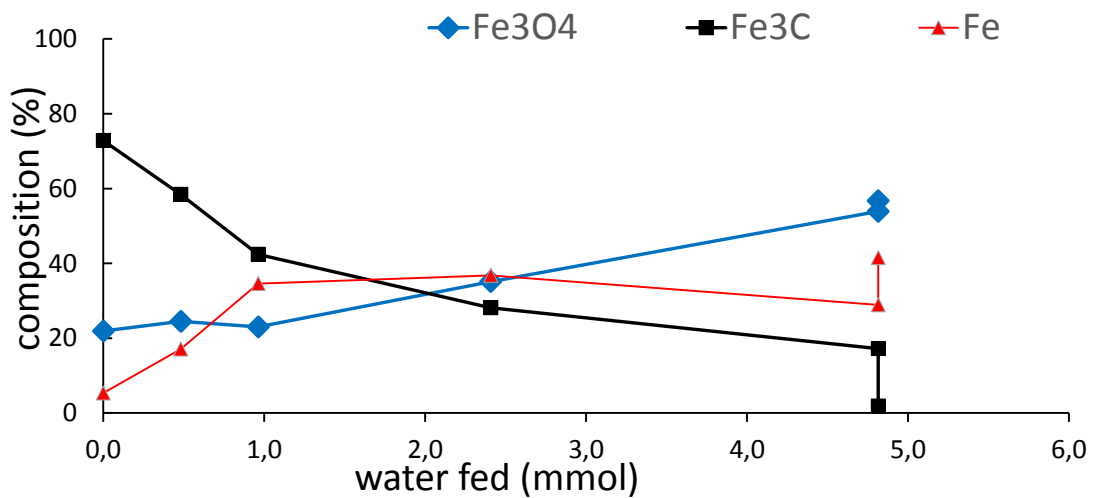

Figure 5-9. Composition of the sample versus the cumulative amount of water to which the sample was exposed at 450°C during the fourth stage of the in-situ XRD experiment.

As in the previous stage, the re-oxidation was not as rapid as in the first cycle, because, probably, of the feeding system that could not be purged anymore. However, as before, this slowed down the modification of the oxide and allowed to better observe the phenomena happening.

In the previous re-oxidation only one mmol of water was needed to completely restore the magnetite. In this case, the re-oxidation was much slower and did not reach 100%

even after about 5mmol of water that corresponds to a 10 minutes feeding. At the beginning whereas the carbide amount decreased, the magnetite was not varied, but the amount of iron increased. The composition started to be enriched in magnetite only after 1mmol of water fed. The iron content was remaining stable and decreased only when more than 3mmol of water were fed. These results clearly showed that iron is an intermediate in the conversion of iron carbide into magnetite. A previous study of reaction of cementite with water showed that the reactions occurring were the following [2]:

$Fe_3C + H_2O \rightarrow 3Fe + CO + H_2$

$Fe_3C + 2H_2O \rightarrow 3Fe + CO_2 + 2H_2$

$3Fe + 4H_2O \rightarrow Fe_3O_4 + 4H_2$
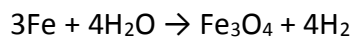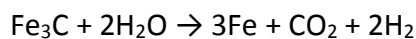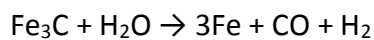
From Gibbs free energies these reactions should be favored only above 600°C, but they were found to take place at temperature of 300°C.

The results obtained in the fourth stage of the in-situ study confirmed totally those of this previous study and the re-oxidation of cementite by water should proceed the same way.

5.2.5. Conclusions on the in-situ XRD study

The results obtained in the in-situ XRD study show that at the beginning the magnetite is reduced in metallic iron, which is then converted into carbide:

Magnetite (Fe_3O_4) $\rightarrow$ Wûstite (FeO) $\rightarrow$ Iron (Fe) $\rightarrow$ Cementite (Fe_3C)
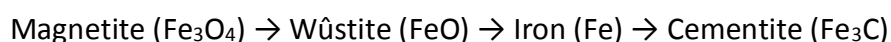
However it can be noted that the metallic iron is only detected at the beginning of the reduction process and in very small amount. Furthermore Würstite (Fe_xO), which is normally formed during the reduction of magnetite in metallic iron, is not detected. These

results bring us to not discard completely the existence of a second pathway corresponding to a direct conversion of the iron oxide into carbide in a reducing and carburizing atmosphere without the formation of metallic iron as proposed earlier. The reduction in this case should probably proceed through the formation of oxi-carbide species, certainly amorphous and hardly differentiated from cementite by Mössbauer spectroscopy:

Magnetite (Fe_3O_4) $\rightarrow$ $Fe_xO_yC_z$ $\rightarrow$ Cementite (Fe_3C)
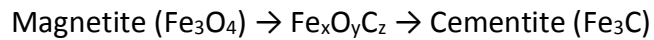
However the results of the second stage of the in-situ XRD study tend to confirm that the main pathway, taking place should well be the first one. If we consider such pathway with the first rapid reduction of magnetite into metallic iron, ethanol should interact directly with ethanol in the gas mixture. Adsorbed ethanol should dissociate at the metal surface and a supersaturation of the metallic phase with dissolved carbon should occur. When the carbon activity in the metal is higher than the carbon activity for cementite (Fe_3C) formation of cementite particles nucleate and grow at the metal surface and at the grain boundaries. Carbon diffusion is very slow through cementite and the later should act as a barrier for further carbon transfer from the gas phase to the metal, which should lead to the formation of graphite at the cementite surface. The carbon activity increases at the graphite/cementite interface, which becomes unstable and starts to decompose according to the following reaction: $Fe_3C \rightarrow 3Fe + C$. The formed metallic particles, which should not be present in large amount can be carburized but more important act again as catalyst for further carbon deposition.

This process explains the unavoidable formation of coke, which takes place. It also explains why the coke formed has a tendency to growth as graphitic filaments. Indeed when formed by decomposition of carbide the iron particles are small and favor thus the formation of filaments when re-carburized.

The analysis of the crystallite size of the different phases has shown that during the overall redox and transformation processes all the phase crystallite sizes increased. The sintering process in the case of magnetite appears independent of the reduction and

transformation process since it occurs in parallel to it in the first ethanol decomposition step where tit increases from 65 to 103nm.

During the re-oxidation process by water the magnetite is firstly transformed into metallic iron and then further oxidized to magnetite. The particle size of the formed magnetite continues increasing but gently and do not overpass 120nm. Probably the sample reaches a sintering degree that is stable continuing cycling.

One of the major conclusions that can be drawn for the drawing of a clean cycling process (without formation of coke) could be that formation of cementite should be avoided. Nevertheless it seems that this is impossible. It can however be observed that the formation of cementite at the very beginning of the step is lower. It was thus interesting to run the looping process with short cycling time.

5.3. SHORT TIME LOOPING STEPS PROCESS

5.3.1. Analysis of the products

In order to try to avoid the formation of coke in the first step of the chemical loop, we have experimented short time looping steps. To simulate a potential use of such approach for the production of hydrogen, a multi-cycles processes with steps of 5 and 2 min have been run on the magnetite at 450 °C. Additional this study allowed to test the behavior the looping process in a long time, with continuous switching of the feeding. Magnetite has been chosen as looping material because it gave good results during the longer tests and because it led to complete recovery after a complete cycle (no segregation). With such short cycling times it was only possible to follow the production of hydrogen by mass spectroscopy.
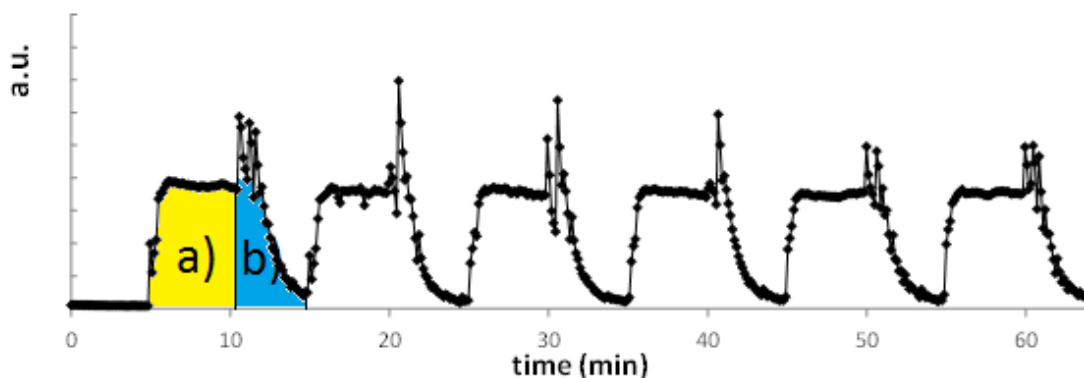
Figure 5-10. Trend of the hydrogen production obtained through mass spectrometry analysis during repeated cycling of 5 min steps with ethanol and water feedings (450°C; 30ml/min N_2; a) 15.6% vol. ethanol; b) 29.3% vol. H_2O)

The feeding was switched from ethanol/N_2 to water/N_2 whereas the mass spectrometer was recorded continuously In the example reported in the figure, the first part of the repeated signal (in yellow), represents the trend of H_2 obtained from ethanol, while the second part (in blue) represents that of H_2 obtained from water.

It was not possible to quantify the amount of hydrogen produced in each step since no calibration have been made, however it was possible to obtain important informations on the cycling. To better understand this complicated pattern, the areas below the profile curve for each step of each cycle have been integrated using the trapezoidal equation of the type:

$$A = \sum (x_n - x_{n-1}) \left[\frac{y_n + y_{n-1}}{2} \right]$$

The resulting areas measured for the reduction and oxidation steps have been plotted for the successive cycles (Figure 5-11).

Figure 5-11. Trend of the integrated values of hydrogen mass spectrometry signal during the reduction and oxidation steps of successive cycles on Fe$_3$O$_4$ at 450°C

Several observations can be made for the results obtained:

a) During the first 6 reduction steps, run for 5 minutes each, the hydrogen production decreased over the first one, but remained stable over the subsequent;

b) During the first 6 oxidation steps, run for 5 minutes each, the hydrogen production remained high over the first steps but decreased then to stabilize over the last ones.
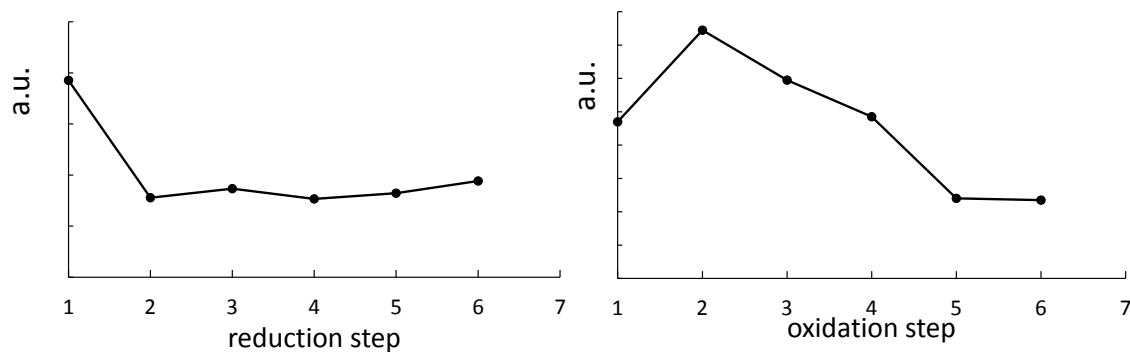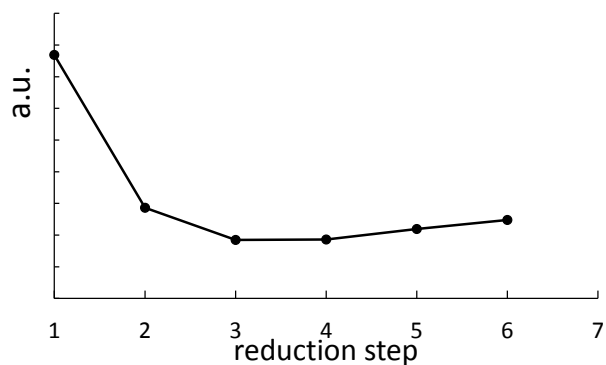
Figure 5-12. Trend of the integrated values of ethanol mass spectrometry signal obtained during the reduction steps of successive cycles on Fe$_3$O$_4$ at 450°C

The trend of conversion of ethanol during the reductions steps has been studied by following the signal corresponding to unconverted ethanol over the successive reduction steps (Figure 5-12). It can be observed that the ethanol conversion rapidly increased over the first three cycles to remain then constant.

Figure 5-13. Trends of the integrated values of water mass spectrometry signal obtained during the reduction steps of successive cycles on Fe$_3$O$_4$ at 450°C

The productions of water, carbon dioxide and carbon monoxide have also been followed during the reduction steps of successive cycles. Their trends are respectively plotted in Figure 5-13Figure 5-14. The production of water during the reduction step has a maximum

obtained during the 2nd cycle and then decreases progressively. In the oxidation step, the signal of water represents its conversion and it is possible to see that its trend is quite constant during cycling.

Figure 5-14. Trends of the integrated values of CO$_2$ mass spectrometry signal obtained during the reduction steps of successive cycles on Fe$_3$O$_4$ at 450°C

The amount of carbon dioxide produced during the reduction steps is decreasing at the beginning, but seems to reach a stable trend continuing cycling as well as during the oxidation step.
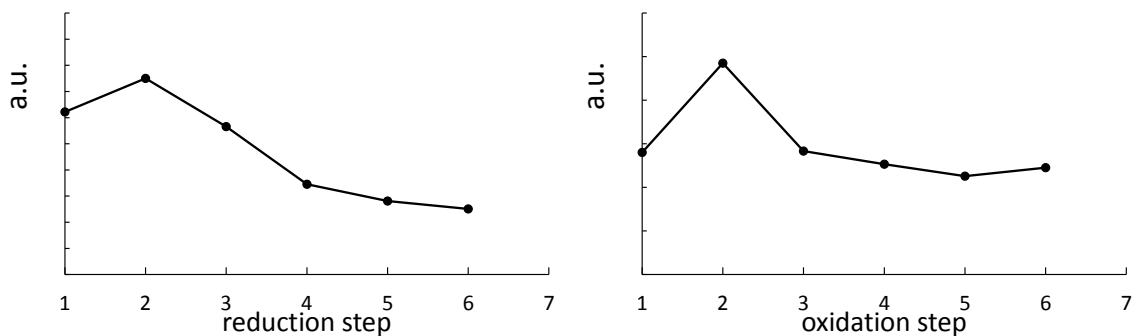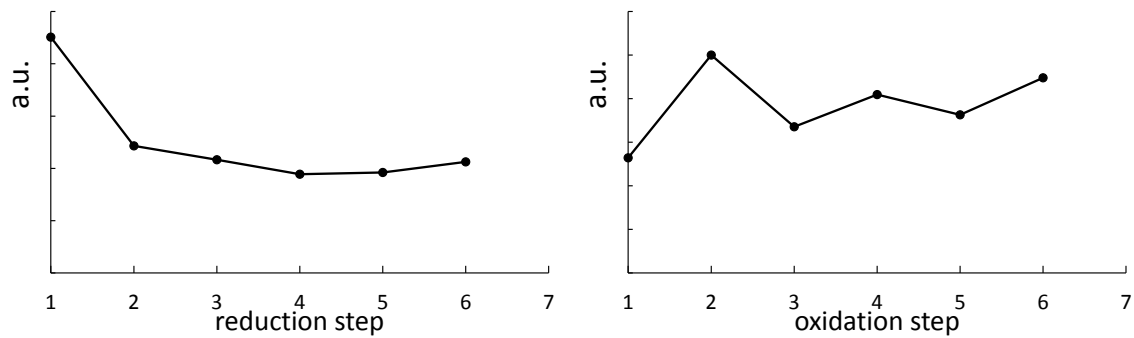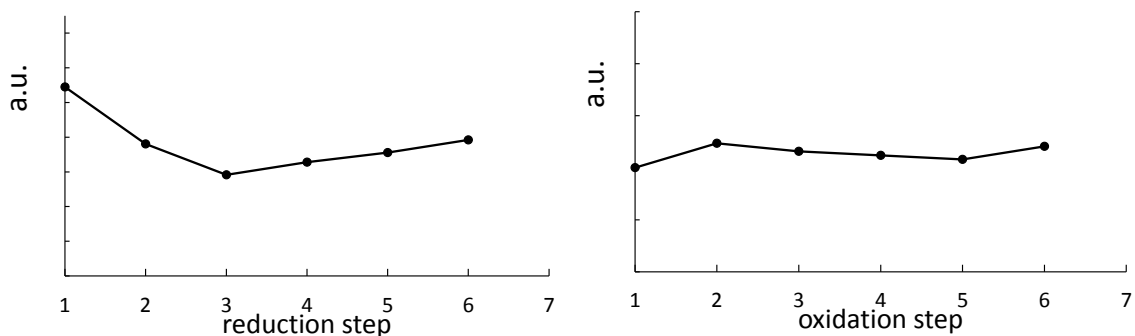
Figure 5-15. Trends of the integrated values of CO mass spectrometry signal obtained during the reduction steps of successive cycles on Fe$_3$O$_4$ at 450°C

The analysis of CO formed was made following the trend of mass 28 on the mass spectra, but that mass corresponds also to that of nitrogen, which is the gas carrier of the reaction. However, the amount of nitrogen used in the two steps of the process was the same, so it was possible to consider the modifications of the signal as due to the production of the carbon monoxide. The trend of CO seems to follow more or less that of CO$_2$.

5.3.2. Analysis of the material

In order to understand the modification happening on the material during repeated short cycles, other tests similar to those showed before have been made. In this case, however, the mass spectrometer connected at the exit of the reactor was less sensitive than the one used in the previous case, so it was not possible to obtain the trend of hydrogen. However, these new tests have been made mainly to characterize the magnetite at different stage of the cycling. Characterization through XRD, Mössbauer, spectroscopy and carbon analyses have been performed on the magnetite sample. Before reporting the results of this characterization it was important to verify the proper functioning of the cycling process and ethanol conversion.

Ethanol conversion

The conversion of ethanol during the 5min step cycling process has been followed by mass spectrometry (Figure 5-16).

Figure 5-16. Trend of the ethanol consumption in the composition of the outgassed stream as observed from the mass analysis during repeated cycles of 5 minute per step.

The reduction steps are those were the ethanol is observed in higher quantities. It is possible to note that the amount of ethanol in the outgassed stream increases during about the first 120 minutes of cycling i.e. 15 steps of 5 minute before stabilization. This means that the ethanol conversion is decreasing at the beginning before reaching a state. To understand if this characteristic depends exclusively from the material or from the duration of the steps, another test switching the feeding between ethanol and water every two minutes has been performed.
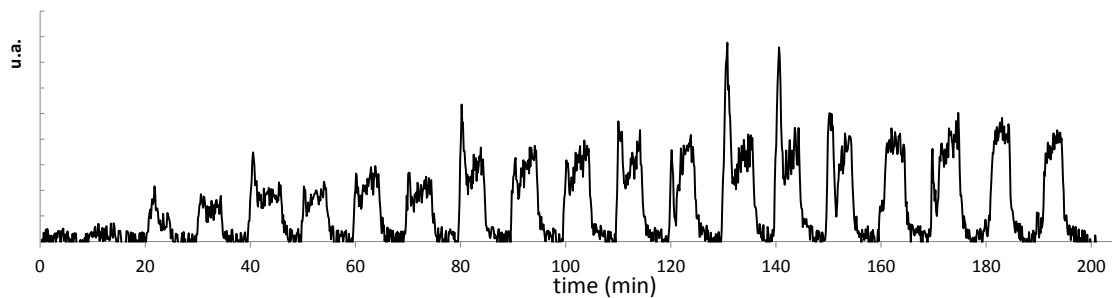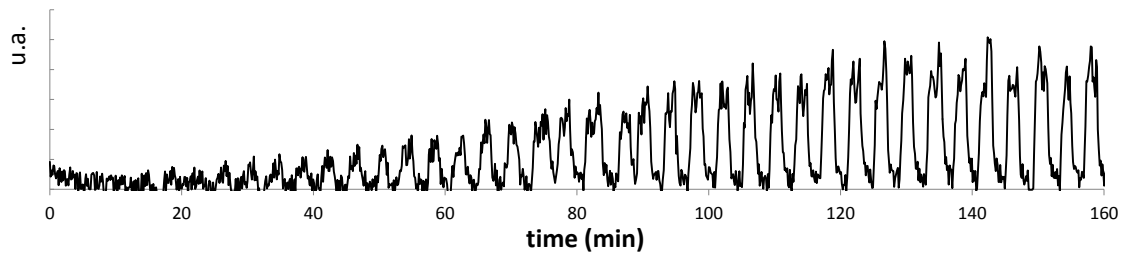
Figure 5-17. Trend of the ethanol in the composition of the outgassed stream as observed from the mass analysis during repeated cycles of 2 minute per step.

As it is possible to observe in Figure 5-17, the same behavior of ethanol conversion was observed for the lower time cycling.

5.3.2.1.   Characterization of the magnetite during cycling

It was important ti verify if the material was changing radically in the short cycles process as in the longer one. Characterization by XRD and Mössbauer spectroscopy have been made first at the beginning of and the end of the reduction re-oxidation step of the first short time cycle and secondly at the beginning and the end of the re-oxidation of the twentieth short time cycle, which corresponds to a total time of 3h20 (longer than the 2h hours of a 1h-step cycle).

Figure 5-18. Comparison of the X-ray diffraction patterns of Fe₃O₄ at the beginning (in red) of and the end (in black) of the re-oxidation step of a 5 minutes cycle

The X-ray diffraction patterns show that after 5 minutes of reduction the material is slightly reduced (Figure 5-18). In fact there is only one small peak at 45° 2θ, corresponding to iron. When completed the cycle this peak disappears and the pattern is the typical one of magnetite. In both the cases, the peaks are relatively narrow which indicates that sintering already took place during the reduction step of the material.
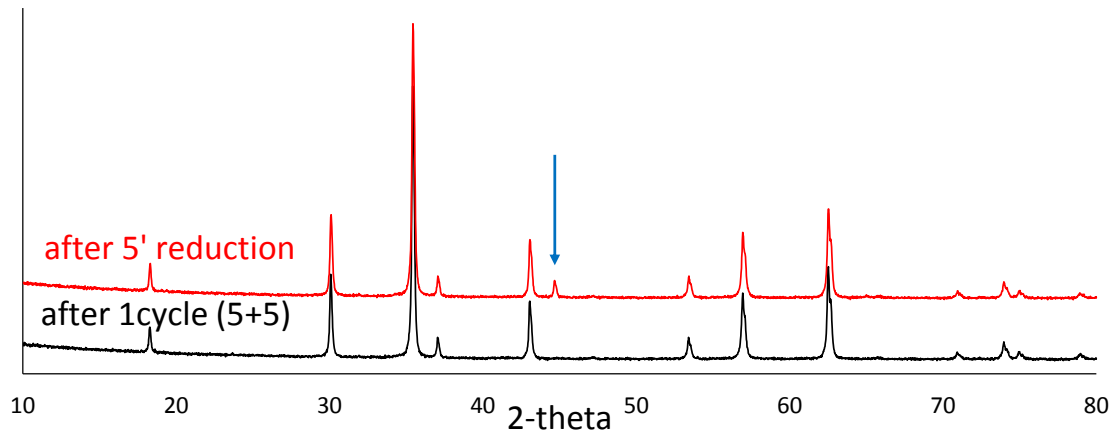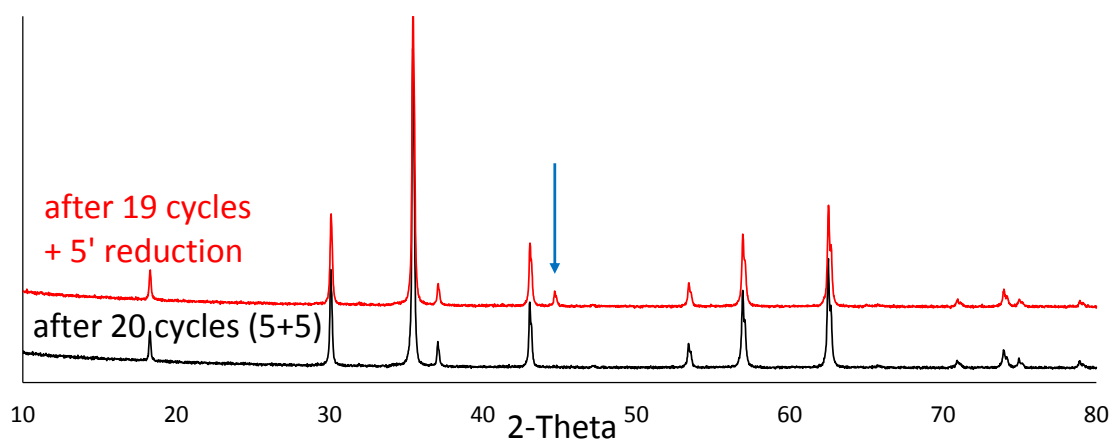

Figure 5-19. Comparison of the X-ray diffraction patterns of Fe₃O₄ at the beginning (in red) of and the end (in black) of the re-oxidation step of the twentieth short time cycle of a 5 minutes cycle

The X-ray diffraction patterns of the material at the beginning and the end of the re-oxidation of the twentieth short time cycle shows are similar to those recorded during first cycle. No coke and no carbide are detected. In order to better quantify the phases and detect the presence of minimal amounts of carbide or a coke, Mössbauer analyses and carbon analyses have been performed.

Table 5-1. Mössbauer parameters computed from the spectra of Fe$_3$O$_4$ after the different steps of the repeated cycles, recorded at 25°C; IS: isomer shift; H: internal magnetic field.

SAMPLE		%	IS (MM/S)	H (T)
Fe$_3$O$_4$ after 5 minutes reduction	Fe^{3+}	35	0.26	48.8
	Fe$^{2,5+}$	63	0.65	45.8
	Fe^0	2	-0.16	32.5
Fe$_3$O$_4$ after 1 complete cycle (5/5minutes)	Fe^{3+}	35	0.26	49.2
	Fe$^{2,5+}$	65	0.65	46.1
Fe$_3$O$_4$ after 19 complete cycles + 5 minutes reduction	Fe^{3+}	33	0.26	49.1
	Fe$^{2,5+}$	63	0.65	46.0
	Fe^0	4	-0.04	32.6
Fe$_3$O$_4$ after 20 complete cycles	Fe^{3+}	37	0.24	49.0
	Fe$^{2,5+}$	63	0.66	46.1

Through the Mössbauer analysis it has been possible to quantify the amount of the different species of iron at the same stages as those studied by XRD. After the first 5 min of reduction a metallic iron phase characterized by an average magnetic hyperfine field of 32.5T and an isomer shift of -0.10mm/s is formed and represents 2% of the iron species in the sample. After the re-oxidation only the sextet characteristic of magnetite are observed.

For the twentieth cycle, the Mössbauer analysis is similar except that the relative amount of iron formed is slightly higher with 4%.

The carbon content of the samples have been measured through the CHN analysis. The results are presented in Table 5-2

Table 5-2. Amount of carbon present in the sample after the various step of the repeated cycle as obtained from the CHN analysis

SAMPLE	% OF CARBON IN WEIGHT
Fe_3O_4 after 5 minutes reduction	0.3
Fe_3O_4 after 1 complete cycle (5/5minutes)	0.2
Fe_3O_4 after 19 complete cycles + 5 minutes reduction	1.3
Fe_3O_4 after 20 complete cycles	1.0

At the beginning of the re-oxidation step of the first 5 min cycle, the analyses show the presence of a small amount of coke of 0.3% in weight. After the re-oxidation step the value slightly decreases to 0.2%. The coke has thus been only partially oxidized during the re-oxidation step.

At the beginning of the re-oxidation step of the twentieth 5 min cycle, the analyses show that the amount of carbon has increased with 1.3% which is a very good results considering that the overall time of cycling at this point is 195 minutes.

Finally, it has measured that after 20 complete cycles of 5 minutes (200 minutes totally) per step the C% is only 1.0%.

5.3.3. Conclusion on the characterization of repeated cycles

From the test repeating cycles for long time it has been possible to observe through the mass analyses that the conversion of ethanol decreases during the first 2h of cycling and remains then stable independently from how long each step of the cycle is run. It is possible to suppose that the magnetite requires this amount of time to be stable during cycling and probably it will remain so even at much longer time of cycling.

From the analysis of the other products of the reaction it has been shown that during the reduction steps of repeated cycles there is an initial decrease of the compounds but they are reaching a stable trend after the first 2-3 cycles. On the re-oxidation steps, however, the carbon oxides seem not to change their trend during cycling. The CO is produced in very low amount and since its signal is the same of nitrogen is also hard to recognize its trend. The CO_2, as well, has a trend, which is not well defined so it is not possible to say if it increases or decreases during cycling. The hydrogen after an initial increase at the 2nd cycle start decreasing progressively at each cycle and seems not to reach an equilibrium. It would be interesting to calibrate the instrument in order to understand if the productivity of the hydrogen in a long cycling time is the same independently from how long each step is run.

The study of the magnetite material during 5 min cycle by X-ray diffraction, Mössbauer spectroscopy and carbon analysis showed that the formation of cementite could be avoid

with short cycling time. However the formation of coke, which is slow down (only 1.3 weight % after twenty cycles) cannot be completely avoided. Water alone is not able to complete oxidize the carbon and it seems necessary add a third step where the material would be further oxidized in air to completely remove it.

This type of test has been run after the complete cycle of 1h step, feeding 20ml/min of air added to 30ml/min of nitrogen. The carbon oxides production has been monitored through the micro-GC analysis and the reaction was stopped after 90 minutes were no more carbon oxides were produced. The CHN test on the material after this step revealed that the amount of carbon remained from the 28.6% produced in the 2nd step was only 0.3% which means that the air is able to oxidized the coke produced more efficiently than water. It is possible to suggest that in that case the duration of the third step had to be kept high since a high quantity of carbon was present on the surface, however, probably, in the case of short step cycles the time of an hypothetical third step could be of some seconds and should not dramatically decrease the productivity keeping the solid clean from coke.

References:

[1]   F. Bonnet, F. Ropital, P. Lecour, D. Espinat, Y. Huiban, L. Gengembre, Y. Berthier, and P. Marcus, "Study of the oxide/carbide transition on iron surfaces during catalytic coke formation," *Surf. Interface Anal.*, vol. 34, no. 1, pp. 418–422, Aug. 2002.

[2]   T. Akiyama, "Thermal and gas analyses of the reaction between iron carbide and steam with hydrogen generation at 573 K," *Int. J. Hydrogen Energy*, vol. 29, no. 7, pp. 721–724, Jul. 2004.

6. CONCLUSIONS AND PERSPECTIVES

This thesis deals with a study on the feasibility of the Steam-Iron process (Chemical-Loop Reforming) using different mixed ferrites as looping materials and ethanol as the reducing fuel. The aim of this process is the production of high-purity hydrogen, without the need of expensive separation units.

The study was first focused on the chemical and physical properties of the materials synthesized. Characterization showed that the synthesis method chosen, the co-precipitation technique, was suitable to obtain the mixed ferrites, with the exception of $CuFe_2O_4$, in which part of the copper was not incorporated in the spinel structure, but remained segregated as CuO. Moreover, the various techniques used for the physical-chemical characterization of samples allowed to draw a complete picture of the main features of materials synthesized, and also to predict the behavior of the materials.

The DRIFT spectroscopy study allowed to detect the species adsorbed on the ferrites surface after interaction with ethanol and the nature of the interaction. By combining this information of the nature of alcohol interaction with the ferrite with the qualitative identification of the products desorbed during thermal-programmed-heating, it was possible to propose different reaction pathways for the anaerobic oxidation of ethanol over the various mixed ferrites. These pathways were also confirmed by results obtained during reactivity tests in the continuous-flow reactor.

Preliminary experiments in the laboratory-scale allowed us to see that the feeding ethanol leads to the production of a large variety of compounds, and that the temperature required to achieve the reduction of the ferrites in a reasonable time frame is 450°C. This temperature was used in both steps of the chemical loop.

Comparing the results of the reduction tests (the first step of the cycle, during which ethanol is made react with the metal oxide) obtained with the different materials showed that the composition of the ferrite affects, although at a limited extent, the products distribution. Particularly, it was found that magnetite and copper ferrite were producing

more hydrogen and CO than cobalt and nickel ferrites; the latter produced a greater quantity of acetaldehyde and, in the case of nickel ferrite, of methane. The common drawback observed during these experiments was the high production of carbons shown during the reduction step, which during the re-oxidation step (the second step of the loop, during which the pre-reduced ferrite is contacted with steam) led to the production of CO_2 (which would not be a problem for a fuel cell purpose) and a relevant amount of CO, which is undesired because it is a poison for the PEM fuel cells electrodes, and clearly makes the principal aim of the chemical-loop approach not reached.

The study of the second step, in which steam was fed on the pre-reduced materials, showed that high yield to hydrogen could be obtained. This confirmed that carrying out the steam-iron process with these materials and ethanol as the reducing fuel is chemically feasible, provided the problem of carbon accumulation during the reduction step is solved.

The characterization of materials after the two steps showed that all ferrites reached a high reduction degree. However, in the case of the mixed ferrites the segregation of Co, Ni, and Cu metal oxides was shown. In the case of copper, segregation occurred already during the thermal treatment, in the case of nickel started with the reduction step, while in the case of cobalt it occurred during the re-oxidation step.

The use of the azeotrope ethanol/water mixture instead of pure ethanol was investigated, in order to reduce the amount of coke accumulated during the reduction step. The results showed that water slowed down the reduction process, which implied a lower hydrogen production during the second step, but the amount of carbon accumulated during the reduction step was only slightly decreased.

The study was then aimed at defining conditions at which the accumulation of carbon during the reduction step might be decreased. In this aim, we decreased the reduction time, from 1 h to 20 min, and carried out repeated cycles. In fact, after 20 min all materials studied had already reached their higher reduction degree.

The materials showed similar behaviors, however with some notable differences: magnetite produced a lower amount of carbon, but on the other hand did not achieve high reduction degrees, and its properties were decreasing along with the increase of the cycle number. Cobalt and nickel ferrites performed better because the behavior was constant during the repeated cycles, but produced the higher amount of carbon, besides showing the segregation of Co and Ni.

Magnetite was also used to carry out in-situ XRD tests and repeated shorter cycles. During contact with ethanol, magnetite formed first metallic iron and then iron carbide, with the reverse situation shown during re-oxidation with water. The calculation of the crystallite size allowed understanding that the segregation of the material is relevant during the first minutes of the first reduction step, and becomes less important during the following repeated cycles.

Finally, tests carried out by performing short-time reduction steps along several cycles indicated that the influence of the time at which each step is carried out plays an important role on the carbon accumulation and on the nature of the phase formed in the reduced state. These experiments allowed us to design the optimal conditions for the cycle reforming of ethanol.

ACKNOWLEDGMENTS

I would like to acknowledge the Tuck foundation, which through the Enerbio project has given the grants for the thesis and allowed me to make this interesting experience.

Vorrei inoltre ringraziare il Prof. Fabrizio Cavani per avermi dato la possibilità di compiere quest'ennesima impresa e di avermi aiutato in ogni occasione.

Mes remerciements vont également au Dr. Jean-Marc Millet pour m'avoir accueilli dans le laboratoire de Lyon et pour m'avoir appris tant des choses précieuses.

Du laboratoire de l'IRCELYON je dois aussi remercier Chantal Lorentz pour la patience de m'avoir fait plein des CHN et Françoise Bosselet et Yoann Aizac pour les manips XRD.

In the laboratory in Lyon I also have found a very wonderful atmosphere and I met very nice people who helped me and made me feel like home. In most cases they did not limit being colleagues, but they became good friends and travel mates… a big thank to all of them! (I will not make any names up to now, because I am sure to forget someone!)

Grazie anche a tutti I colleghi del laboratorio di Bologna, vecchi e presenti, per i caffè presi insieme e per l'arricchimento culturale derivato dai discorsi durante i pranzi in bibliotechina. Anche qui, oltre a dei colleghi ho trovato molti amici coi quali spero di rimanere in contatto a lungo. Tra loro un ringraziamento speciale a Stefano, Max, Juliana e Sigrid per avermi aiutato con le prove qui riportate. E grazie anche ai "grandi" del laboratorio per avermi aiutato in tante occasioni, anche se non vi ripagherò mai producendo elettricità con la cyclette come vorrebbe IL Direttore…

Thanks to all the 17 "official" flat-mates and the uncountable unofficial I had in 9 years to have been my family- surrogate and always supporting me.

Grazie anche ai compagni della sempre quarta P.P. on Fire che tra partite, pizze e spalle rotte mi hanno spesso distratto dall'università (in bene…) e per avermi insegnato che spesso essere i primi degli ultimi è più divertente che essere gli ultimi dei primi (non cercate un significato filosofico, non c'è).

Ringrazio anche i miei amici di sempre di Matelica per riuscire a farmi divertire a tutte le ore del giorno anche a distanza e per farmi sentire come se non fossi mai partito ogni volta che torno a casa.

Ultimo, ma non per importanza un enorme grazie a tutta la mia famiglia, compresi nonni, zii, cugini e Holly per avermi sempre supportato e tifato per me.

…and thank you all for your attention…